MICROMIXING EFFECTS IN ATMOSPHERIC REACTING FLOWS

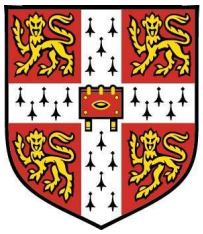

University of Cambridge

Department of Engineering

This dissertation is submitted for the degree of

Doctor of Philosophy

by:

Andrew Garmory

Fitzwilliam College

Thursday, 27^{th} of September, 2007

"Was it ever?"

Mike Stephenson, passim.

...

Declaration

This dissertation is the result of my own work and includes nothing which is the outcome of work done in collaboration except where specifically indicated in the text. The dissertation contains approximately **42,000** words, **67** figures and **9** tables.

Andrew Garmory
Hopkinson Laboratory, Cambridge.
Thursday, 27^{th} of September, 2007

Acknowledgements

The work presented in this thesis could not have been carried out without the help of many people. While there is not space here to mention them all, a special mention must be made of several people. Most importantly my supervisor, Dr E. Mastorakos, for his support, guidence and relentless optimism in the face of my frequent negativity. I also thank him for his excellent proof-reading. Prof R. E. Britter has on many occasions provided an invaluable insight into the subject of atmopsheric pollution. Dr L. Valiño (LITEC, Zaragoza) and Prof W. P. Jones (Imperial College London) have both provided highly useful advice on the development of the Stochastic Fields code used here. Funding from the EPSRC and a scholarship from The Worshipful Company of Leathersellers have enabled me to complete this work free from financial worry.

I am most grateful to all the members of Dr Mastorakos' research group past and present whose time here has coincided with my own for all their help. In particular I. S. Kim, C.N. Markides, G. De Paola, E. S. Richardon, C-W. Lee and T. Løvås for passing on their hard won knowledge. It is no understatement to say that without P. Benie and his computing expertise non of the work presented here would have happened, I have yet to ask him a technical question that he couldn't answer immediately. I must also thank my friends and fellow students in the searing heat of the Hopkinson Lab, A. Triantafyllidis, S. Bennett, R. Kavanagh, P. Kumar and R. C. Payne for providing such interesting and enlightening discussion. Very occasionally about work.

Finally I would like to thank my parents, Neil and Patricia, and my sisters, Rachel and Sarah, for their support and for believing that I have spent the last three years doing something worthwhile and not just avoiding getting a proper job. I dedicate this thesis to them, and expect them to read it in full.

Publications

Preliminary work for this thesis has been published in the following articles:

- Simulation of the evolution of aircraft exhaust plumes including detailed chemistry and segregation [1].
- Micromixing effects in a reacting plume by the Stochastic Fields method [2].

and in the following conference papers:

- Simulations of the dispersion of reactive pollutants in a street canyon, considering different chemical mechanisms and micromixing [3].
- Micromixing effects in air pollution modelling [4].

Abstract

This thesis describes the application of the Stochastic Fields (SF) transported Probability Density Function computational method to atmospheric reacting flows. This allows the effect of turbulent fluctuating quantities (segregation) on reaction rates to be studied directly.

The SF method and its implementation in both its Ito and Stratonovich forms is discussed. The equivalence of the two methods, provided the stochastic integrals are correctly evaluated, is demonstrated for a one-dimensional diffusion problem and also in the simulation of a laboratory reacting plume. The Ito implementation was found to result in a more robust method numerically and was used for all subsequent calculations. The SF method was able to predict the mean and RMS of an inert scalar in a laboratory reacting plume with high accuracy when compared with experimental data. Reactive scalar quantities were also predicted accurately and it was demonstrated that neglecting segregation led to an overprediction of the mean by around 30%.

The simulation of pollutant reactions in a jet engine exhaust plume and in a street canyon has been carried out using the SF method. Both simulations used complex chemical mechanisms containing 24 and 28 species respectively. The results revealed a strong correlation between species Damköhler number, Da, and segregation effect. Only when the species Da was greater than 5 did segregation significantly affect the predicted concentration.

The SF method has been extended to the calculation of nucleation and growth

of aerosols in a jet. In agreement with previous work it was found that ignoring the effect of turbulence of nucleation rate can lead to overpredicting the particle number flux by approximately 25%. Both particle number density and mean particle diameter were found to be close to experimental data for the same conditions. Including the effect of turbulence was found to decrease mean particle size at the centre of the jet and increase it at the outside.

Contents

List of Figures

List of Tables

Chapter 1

Introduction

1.1 The Micromixing Problem in Atmospheric Reacting Flows

As increasing numbers of people live in urban areas there is an increasing drive to understand and model the dispersion of pollutants in these areas. Britter and Hanna [11] describe four scales of dispersion. The largest is the regional scale (up to 100 - 200km). The city scale is of the order of the diameter of a large urban area (around 10-20km), at this scale it is usual to think of the buildings as providing a 'surface roughness,' which affects the flow rather than as individual buildings. Next is the neighbourhood scale (up to 1-2km) where, depending on the desired information, buildings may still be averaged into a roughness or be treated as individual obstacles. The smallest scale is the street scale (less than 100-200m) where the actual flow may be considered.

When considering the level of pollution that humans are actually exposed to, rather than longer term averages, it is the smallest of these scales that is important. It is here that humans and pollution sources such as vehicular traffic are in close proximity. The flows at this scale will be turbulent. In addition to sources such as thermal production there will also be traffic produced turbulence (TPT). If this last

factor is not considered it can lead to overprediction of pollution levels at low wind speeds [11]. As will be discussed further in Section 4.2.1, another area of concern is pollution emitted at airports as aircraft go through landing and take-off cycles. This is of great interest at the present time and is the subject of much debate and legislation.

In addition to dispersion, some pollutants will also undergo reaction in the atmosphere. At the street and neighbourhood scales it may be necessary to consider the interaction of turbulence and chemistry, as at this fine scale the effect of reactant segregation cannot necessarily be neglected. *Segregation* is the presence of reactant fluctuations from the mean in space and time and the decay of these fluctuations is governed by *micromixing* [12].

Consider the advection-diffusion equation describing the evolution of the instantaneous concentration ϕ of a pollutant ignoring deposition and emissions, but including chemical reaction. Solutions to this equation would virtually always use some sort of averaging, e.g. time averaging in a statistically-steady problem. For unsteady problems, we could think of the averaging as an ensemble or even as a volume average over, say, an Eulerian Grid cell or a cell in an LES calculation. After Reynolds decomposition and averaging, denoted by an overbar, we obtain

$$\frac{\partial \overline{\phi}}{\partial t} + \overline{U}_i \frac{\partial \overline{\phi}}{\partial x_i} = D \frac{\partial^2 \overline{\phi}}{\partial x_i^2} - \frac{\partial (\overline{u_i' \phi'})}{\partial x_i} + \overline{\dot{w}} \tag{1.1}$$

where $\dot{w}$ is the chemical source term for ϕ and primed quantities represent the turbulent fluctuations. $\overline{U}_i$ is the mean gas velocity and D the molecular diffusivity. It is evident that the Reynolds averaging procedure brings in a new term, $\overline{u_i' \phi'}$, which represents turbulent diffusion and requires modelling, as for example by the so-called "K-theory," whereby turbulent diffusion is assumed to occur in the same way as molecular diffusion but with a turbulent diffusivity, K, derived from the length and velocity scales of the turbulence [13]. The mean wind speed $\overline{U}_i$ can come from a Grid Model or LES or any other calculation solving (modelled) fluid mechanics

equations. Understanding the nature of the micromixing problem for the evolution of the chemical reaction can be achieved by examination of the mean reaction rate $\overline{\dot{w}}$. Take for example the chemical reaction $A+B \rightarrow C$, then $\dot{w} = \beta\phi_A\phi_B exp\,(-T_{act}/T)$, where T_{act} is the activation temperature. Performing a Reynolds decomposition, we obtain

$$\dot{w} = \overline{\dot{w}} + \dot{w}' = \beta(\overline{\phi}_A + \phi'_A)(\overline{\phi}_B + \phi'_B)exp\left(-\frac{T_{act}}{\overline{T} + T'}\right) \tag{1.2}$$

If for simplicity we ignore for the moment fluctuations in temperature, we can group the exponential and the pre-exponential constant β to give the reaction rate constant k, and then only a product between the species concentration fluctuations appears:

$$\overline{\dot{w}} = k\left(\overline{\phi}_A\overline{\phi}_B + \overline{\phi'_A\phi'_B}\right) \tag{1.3}$$

Therefore, to calculate the mean reaction rate, one needs to take account of $\overline{\phi'_A\phi'_B}$. If temperature fluctuations were included the mean reaction would become an even more complex function of fluctuating quantities. Hilst [12] shows the effects of segregation on a bi-molecular reaction by considering an analytical solution for the reaction rate alone. It can clearly be seen that when the reactant covariance, $\overline{\phi'_A\phi'_B}$, is negative the reaction rate is retarded. Liang and Jacobson [14] consider a more complex problem of ozone production over several different land-use types. They find that by assuming that parcels of air from two types of land are perfectly mixed, rather than segregated, ozone production can be overpredicted by as much as 60%.

Common practice in Air Quality Modelling has been to completely neglect $\overline{\phi'_A\phi'_B}$. As discussed by [5, 14–16], this is acceptable if the chemistry is very slow compared to the turbulent timescales, since turbulence is the process by which the fluctuations ϕ'_A and ϕ'_B decay due to mixing. For illustration of this concept, consider a problem where the mean concentrations are constant in space, but with small-scale fluctuations (i.e. segregation) present. It can be shown that the equation for the variance $\sigma^2 = \overline{\phi'^2}$ of the scalar is then given simply by [12, 17]

$$\frac{d\sigma^2}{dt} = -2\frac{\sigma^2}{T_{eddy}} + 2\overline{\dot{w}'\phi'} \tag{1.4}$$

The first term in the r.h.s. of Eq. (1.4) represents the rate of decay of the fluctuations. It is called the scalar dissipation and has been modelled here following the conventional model that uses a large-eddy timescale T_{eddy}, which is equivalent to assuming that the scalar fluctuations decay at the same rate as the turbulence kinetic energy. The second term is due to the chemistry. For the first-order reaction $A \rightarrow B + C$, the chemical source term is $\dot{w}_A = -k\phi_A$, hence $\overline{\dot{w}'\phi'} = -k\sigma^2$. At this stage the Damköhler number is introduced. This is a non-dimensional number that represents the rate of the chemical reaction processes in the flow relative to the rate at which scalar fluctuations decay due to physical mixing.

$$Da = T_{phys}/T_{chem} \tag{1.5}$$

T_{phys} is here set equal to T_{eddy}, although other definitions can be used. Equation (1.4) can be integrated, using Da, to give $\sigma^2(t) = \sigma_0^2 exp\,[-2(1+Da)t/T_{eddy}]$, where the Damköhler number $Da = kT_{eddy}$. Hence, if $Da \ll 1$, turbulence is given enough time to kill the scalar fluctuations before the chemistry becomes important. In the general case where the chemistry in *not* linear, third-order correlations also appear in Eq. (1.4). Still, however, it can be argued that if the chemistry is very slow ($Da \ll 1$), the species will be well-mixed (i.e. $\sigma_{A,B}^2 \rightarrow 0$, $\overline{\phi'_A\phi'_B} \rightarrow 0$) before the reaction proceeds appreciably and hence neglecting segregation is not a problem.

When attention is focused on faster chemical phenomena at length scales close to the pollution sources, Da may not be low and the well-mixed assumption, typical of urban Box Models, Eulerian Grid or Lagrangian codes, is flawed. Examples are the initial, fast conversion of NO to NO_2 and the reactions between VOC radicals and NO_x. Reactions with the hydroxyl radical are also considered to be fast [18, 19]. If $Da = O(1)$ or if $Da \gg 1$, the chemistry-turbulence interaction is important. The mean reaction rate calculated by ignoring segregation can then be out by orders of

magnitude [12, 14, 16].

Vinuesa and de Arellano [20] show the effect of segregation and Da on a convective boundary layer (CBL). They compare results from a LES where mixing is considered in detail with a model that assumes perfect mixing within the CBL. They show results for reactant concentration with time at Damköhler numbers ranging from 0.1 to 1.9 (Where Da is defined using a timescale based on the scale of turbulence rather than the size of the CBL). They found that at the lower Da the prediction assuming perfect mixing is in good agreement with the LES at long times, but at shorter times even for low Da the perfect mixing case overpredicts the reaction. For the higher Da perfect mixing overpredicts the reaction to some extent at all times and significantly at shorter times.

Meeder and Nieuwstadt [21], performing simulations of an atmospheric boundary layer, shows that while LES offers improved predictions compared to assuming perfectly mixed reactants, there are still effects due to segregation at the sub-grid scale. These effects occur particularly at regions of high scalar gradient. This is to be expected as segregation is likely to be more pronounced where the gradients are larger. [16] shows similar results.

Srivastana et al [22] present some results for a reacting plume using an adaptive grid. Despite the good resolution achieved by systematic grid refinements, this problem persists even at the smallest cell. To predict such phenomena accurately, the mean reaction rate needs to take account of the species small-scale inhomogeneities.

Also considered in this thesis is the influence of turbulence on aerosol processes. Aerosols are small particles of liquid or solid suspended in a carrier gas. These particles can be produced by a variety of sources, details of which are given in [15, 23]. Human exposure to aerosols has been linked to lung disease and cardiovascular problems [24]. In particular, recent evidence suggests that it is ultrafine particles, i.e. those with diameter less than 50nm, that are the cause of most of the health problems associated with particulate matter due to their ability to penetrate deep in to the lungs [25, 26]. Samet et al [27] found consistent evidence linking cardiovascular

and respiratory illness and death with exposure to fine particulates, and that this evidence was stronger than that linking exposure to gas phase pollutants such as O_3, CO, SO_2 and NO_2 to death rates. As it is the number concentration of the smallest particles that plays an important role, it is important to understand and to be able to predict the processes affecting these particles [28]. Aerosol concentrations also have an important effect on visibility, with aerosols responsible for up to 99% of the optical properties of the atmosphere in the urban environment [29].

Liquid aerosol particles, of the ultrafine size, can be produced by condensation from the gas phase. Once nucleated these particles can then grow and coagulate with other particles. The physical processes by which this happens and the mathematical models used to predict this behaviour are discussed in detail in Chapter 5. These processes are highly non-linear and hence the effect of turbulent fluctuations of quantities on mean nucleation, growth and coagulation processes can be pronounced [30]. Hence techniques for the treatment of turbulent flows with aerosol processes need to be addressed. The next section considers some turbulent reacting flow methods, while Chapter 5 considers the application of these to aerosol processes.

1.2 Approaches to Modelling Turbulent Reacting Flows

1.2.1 Moment Methods

Methods for turbulence-chemistry interactions are numerous, but have not been used extensively yet in atmospheric dispersion. Moment methods aim to provide a direct closure for $\overline{\phi'_A \phi'_B}$. Baldyga and Bourne [31] and Fox [32] present various models for this correlation for simple reactions from the chemical engineering community. Hilst [12] also gives models for multiple reactions and contains a good review from the atmospheric community. Results are presented showing the effect of closure at different levels from first order (which assumes perfect mixing) to using an ap-

proximation for the third order moments. The higher order closures give significant improvements over first order.

Meeder and Nieuwstadt [21] and de Arellano et al [16] attempt closure models in the context of LES. The species reaction term is split into a part dependent on concentrations averaged over the resolved grid scale and a part representing the effects of fluctuations below the smallest resolved grid scale. Following Sykes et al [33], Meeder and Nieuwstadt [21] used a prognostic equation for these sub-grid fluctuations using closures for third moments. It is worth noting that such closure equations require greater computing resources in order to calculate new derivatives of higher moment terms. The authors report good agreement for their model with experimental data at low Da and use their results at higher Da to show that sub-grid scale segregation is important (as discussed above).

Vinuesa and de Arellano [20] attempt to use an effective reaction rate model which still appears to overpredict the reaction but not to as great an extent as neglecting segregation altogether. Moment methods with detailed chemistry have only recently been attempted [16]. The main problem in using moment methods for complex chemistry is the fact that transport equations for $\overline{\phi'_A\phi'_B}$ contain extra unclosed terms that are not easy to model. An additional problem is that in non-isothermal situations the strong non-linearity due to the exponential dependence of the reaction rate on the temperature makes the higher order correlations as important as the lower-order ones and hence modelling these becomes crucial.

1.2.2 Conditional Moment Closure

Another method for micromixing which by-passes the need to model the difficult $\overline{\phi'_A\phi'_B}$, is the Conditional Moment Closure model (CMC) that has been applied successfully both to turbulent combustion and to atmospheric problems. The method was developed independently by Bilger and Klimenko and a comprehensive overview of their derivations and the method is given in [34]. The CMC approach is a

conserved-scalar method, which means that the reactive scalars (i.e. the species participating in the chemical reactions) are related to a non-reactive (conserved) scalar (i.e. a compound scalar that has no source term in its governing equation). In the high Damköhler number limit, these relations are supplied by assuming infinitely fast chemistry [35]. In CMC, these relations are conditional averages of the concentrations given a value of the conserved scalar and are calculated with modelled transport equations that can include finite-rate chemistry. The mean species concentrations at a point are found by integrating the conditional averages over the conserved scalar PDF (usually of a presumed shape).

Crudely speaking, macromixing is included in the turbulent large-scale transport of the conserved scalar, which affects the conserved scalar PDF. This conserved scalar is often the mixture fraction in two-stream problems. The conserved scalar field can be calculated using a separate computer package, possibly a commercial CFD package, which can supply both mean and variance of conserved scalar from which a presumed PDF is derived. Micromixing is included in the CMC equations through the conditionally-averaged scalar dissipation rate. Closures are needed for the conditional velocity, conditional turbulent flux and for the conditional reaction rate. The usual treatment for the last of these is to assume that the conditional reaction rate depends only on conditional species averages, not on conditional fluctuations. This is called first order CMC and the reasoning behind the approach is that the fluctuation of concentration (i.e. segregation) is due mainly to fluctuations of mixture fraction. In this way the effect of $\overline{\phi'_A \phi'_B}$ is considered. The final closure needed is for the conditional scalar dissipation. Scalar dissipation is the decay of scalar fluctuations and hence this term represents micromixing. Klimenko and Bilger [34] discuss the importance of this term and suggest closures for it.

Brown and Bilger [6] successfully developed a formulation of CMC for the NO-NO_2-O_3 system in a wind-tunnel plume. The use of CMC with more realistic chemistry, the CBM-IV mechanism, has been described by Mastorakos [17]. It was shown that segregation is important for power station plume problems in the first 30 min-

utes or so of their evolution. In particular, it was found that micromixing affects certain species only, such as the OH and other radicals of the CBM-IV mechanism. Separate analysis of this chemistry was performed with the Computational Singular Perturbation (CSP) method. The CSP method in Neophytou et al [19] is used to reduce the CBM-IV method by identifying, systematically, species which undergo 'fast' reactions relative to the rest of the mechanism. These 'fast' species are then assumed to be in quasi-steady state and hence their reaction rate does not have to be calculated in the usual manner. A mechanism reduction technique becomes vital if complex real world problems are to be rendered tractable with existing computing resources. The results of Ref [19] confirmed that the species affected by micromixing were those with the fastest chemical timescales. Very slow species, such as CO and some VOC's, are predicted accurately by the conventional method of neglecting fluctuations [17].

1.2.3 Transported PDF Methods

A method applicable to all turbulent reacting flows is the PDF approach [36], where a transport equation for the joint probability density function of the reacting scalars is considered. Fox [32] gives a very good description of the PDF method including its derivation. The transport equation is:

$$\begin{aligned} \frac{\partial f_\phi}{\partial t} &+ \langle U_i \rangle \frac{\partial f_\phi}{\partial x_i} + \frac{\partial}{\partial x_i}[\langle u_i | \boldsymbol{\psi} \rangle f_\phi] \\ &= -\frac{\partial}{\partial \psi_i}[\langle \Gamma_i \nabla^2 \phi_i' | \boldsymbol{\psi} \rangle f_\phi] - \frac{\partial}{\partial \psi_i}[(\Gamma_i \nabla^2 \langle \phi_i \rangle + \dot{w}_i(\boldsymbol{\psi})) f_\phi] \end{aligned} \tag{1.6}$$

The main attraction of the PDF method is that the effects of concentration fluctuations on the reaction rate are considered directly. However a closure must be supplied for the first term on the right hand side of Eq. (1.6) which is the conditional molecular diffusion or micromixing term.

To solve Eq. (1.6) for any practical purpose using finite volume or finite differ-

ence methods would be impractical and so its numerical implementation very often involves particle based Monte Carlo approaches. Very crudely, in the Monte Carlo simulation the fluid is thought to be comprised of (virtual) particles. This can be done using an Eulerian or a Lagrangian method. In the former, the particles belong to a cell in the flow but their position within that cell is undefined; rather the particles have different compositions and the ensemble of particles in a cell represents the PDF. Using information about the velocity and turbulence fields, effective flow rates between cells are defined and these are used to advect a given number of particles from one cell to an adjoining one. The particles so transfered are chosen at random from those in the cell and in this way the PDF properties are advected. This method is used by Gonzalez [37] to model a reactive plume and a heated boundary layer. In Lagrangian methods the particles have a composition and an exact position in the flow. Their motion is governed by stochastic equations chosen to correspond to Eq. (1.6). The PDF is then found from the ensemble of particles in a locality. This is the more widely used method and has recently been used in atmospheric problems by Cassiani et al [38]. The relative merits of the two methods are discussed in [39] and [32]. Principally these are that Eulerian methods are cheaper, but suffer from discretisation errors due to dividing the flow into cells. The Lagrangian method involves a compromise between discretisation errors due to taking a local average over a finite region and statistical errors due to taking averages over a small number of particles [40]. This leads to the need for a large number of Monte Carlo particles.

In the atmospheric community the dispersion of inert rather than reacting pollutants has been widely investigated using Lagrangian Stochastic models. These use a random walk to track the motion of inert particles. Baerentsen and Berkowicz [41] and Luhar and Britter [42] develop a model to predict vertical dispersion in a convective boundary layer by combining two Gaussian random walks from both the large area slow down drafts and small area fast up drafts. In doing this they are able to correctly predict the downward drift of the plume centre-line in these conditions. More recently, Ermak and Nasstrom [43] use a random walk model based on eddy, or

turbulent, diffusivity. Srinivas and Venkatesan [44] use a random walk model based on the Langevin equation to investigate the dispersion of radionuclides. This last model also takes account of radioactive decay which is akin to the reaction term in reacting flow PDF methods. However, these models take no account of micromixing.

In either the Eulerian or the Lagrangian reacting flow PDF approach there are also intra-particle effects in addition to the particle motion. Firstly, the composition of a particle will change due to reaction and in this way the effects of fluctuations from the mean on the reaction are considered directly. Secondly, the composition will change in a way governed by interaction with nearby particles; this is to simulate the effects of micromixing. This chemistry and diffusion step is the key difference between the implementation of the PDF method for reacting flows and the Lagrangian Stochastic models for atmospheric turbulent dispersion. Incidentally, including micromixing even in inert scalar mixing seems to be important for predicting accurately the correct dispersion and scalar fluctuations [38].

The choice of micromixing model for PDF methods is an area of active research. Gonzalez [37] uses the Interaction by Exchange with the Mean (IEM) model, whereby particle compositions are relaxed back to the mean using a characteristic scalar timescale T_{eddy}, thereby reducing segregation. Using this method, the governing equation for the effect of micromixing on particle composition is:

$$d\phi_i^* = -\frac{\phi_i^* - \overline{\phi}_i}{T_{eddy}} dt \tag{1.7}$$

The main disadvantage of this model is that it assumes that the same timescale can be used for each scalar and that this timescale is the turbulence integral timescale. In reality the reaction will affect the local scalar gradients and this can effect each of the reacting scalars differently. Cha and Trouillet [45] discuss a method of finding different timescales for each scalar and hence improving the treatment of micromixing. Cassiani et al [38] use a model called "Interaction by Exchange with the Conditional Mean" (IECM), where the scalar values relax back to a mean concentration condi-

tioned over velocity. The argument for this is that the scalar mixing is only thought to occur between fluid elements in the same eddy.

More complicated models can be employed that use a stochastic equation for diffusion in composition space [46]. At the expense of greater complexity, these give improved behaviour of PDF development. The PDF method has found some use in idealised atmospheric dispersion problems of reacting scalars [37, 47]. The computational cost of this method with detailed chemistry is quite high [37] due to the large number of Monte Carlo samples needed to achieve statistical convergence. However, the PDF approach is a theoretically-sound method by which micromixing can be included to atmospheric dispersion codes at any spatial resolution, including LES [48]. There is no limitation on the Damköhler number and chemistry to any level of complexity can be used within the limits of the computing resources available.

This Chapter has attempted to describe the problem of micromixing effects in reacting flows, together with an overview of current methods of modelling such effects. Powerful numerical techniques already exist to solve partial differential equations in an Eulerian formulation. If these could be combined with accurate predictions, such as those possible with Lagrangian PDF methods, it would be highly desirable. A method which has the potential to do this is the Stochastic Fields method, and this is the subject of the next Chapter.

1.3 Objectives

The object of this work is to investigate numerically the effect of turbulence on reacting flows in the atmosphere at the local or urban scale. The reacting flows considered are firstly those involving the reaction of gaseous pollutants and secondly flows involving the conversion of gas to liquid aerosol droplets. In both cases it is thought that turbulent fluctuations in the quantities that these processes depend on, also known as segregation, will have an influence on the mean reaction rate. This work attempts to quantify this influence.

The method used for this is the Stochastic Fields or Field Monte Carlo method, which is described in detail in Chapter 2. This is an Eulerian transported PDF method. The use of a PDF allows direct consideration of the effect of segregation on the reaction rate. The Eulerian Stochastic Fields method is thought to have some advantages in implementation over other PDF methods and another objective of this work is to develop a practical Stochastic Fields code which can be applied to situations of practical interest and consider its advantages and disadvantages as a method.

The next chapter describes the Stochastic Fields method and its implementation and Chapter 3 describes its use to model a well characterised laboratory reacting plume. This is done in order to validate the method and its implementation used here. In Chapter 4 the code is coupled with a commercial CFD solver and used to model both a jet engine exhaust plume and also a polluted street canyon. Chapter 5 considers aerosol processes and the application of PDF methods in general and the Stochastic Fields method specifically to this. Each chapter contains a review of the relevant literature.

Chapter 2

The Stochastic Fields Method and its Implementation

2.1 The Stochastic Fields Method

The Stochastic Fields method has been developed as an alternative method of implementing the transported PDF equation (Eq. (1.6)). The method was derived independently by Valiño [49] and Sabel'nikov [50]. It is also known as Field Monte Carlo (FMC) [49] and Eulerian Monte Carlo (ECM) [51, 52], however it will be referred to in this work as the Stochastic Fields or SF method. The Stochastic Fields method has similarities with an earlier method for simulating reacting flow, namely Spalding's multi-fluid method which was applied to turbulent combustion [53] and also to water treatment reactions in turbulent flow [54]. The multi-fluid method solves for the transport of several 'fluids' through the flow, each fluid is associated with a particular range of values of some characteristic quantity of the flow, such as mixture fraction. The ensemble of these fluids can approximate the PDF of this quantity throughout the flow, which enables the effect of imperfect micromixing to be considered.

Rather than simulating the evolution of the joint scalar PDF by tracking the

stochastic motion of notional particles moving through the domain of the flow (as in traditional Lagrangian Monte Carlo methods), the SF method uses a number of Eulerian 'stochastic fields' each of which extend over the whole spatial domain of the flow. Each field contains a value for each scalar at each spatial node, these fields then evolve according to a governing stochastic partial differential equation (spde). This spde is chosen such that the ensemble of values for the scalars across all fields at a point are statistically equivalent to the one-point joint PDF at that point. It is then straightforward to extract means, variances, co-variances and higher moments from the ensemble of fields at each node. The ease with which this can be done is one of the advantages of this method. Valiño and Sabel'nikov take different approaches resulting in governing spde's that differ because Valiño's spde is interpreted using Ito calculus whereas Sabel'nikov derives an equation that must be interpreted in the Stratonovich sense [55]. The two different equations, if properly implemented, will give identical results. A short discussion of Ito and Stratonovich calculus for stochastic differential equations is given in the next subsection followed by the two derivations and their spde's in the subsequent sections.

2.1.1 Ito and Stratonovich Calculus

Unlike a deterministic differential equation, stochastic differential equations (sde's) can be integrated according to different rules of calculus with differing outcomes. For an sde consisting of a deterministic and random part, if dW is the increment of a Wiener process, i.e. a random process with zero mean and variance equal to the time elapsed [55] then:

$$dx = a(x,t)dt + b(x,t)dW(t) \tag{2.1}$$

If this equation is to be integrated in the Ito sense then the increment of the stochastic part $b(x_i,t_i)\Delta W_i$ must be evaluated such that x_i is statistically independent of ΔW_i [55]. In practice when integrating numerically this implies that the integrand

of the stochastic term, i.e. $b(x_i, t_i)$, must be evaluated only once per timestep [56]. If the sde is to be integrated in the Stratonovich sense it is written as:

$$dx = a(x,t)dt + b(x,t) \circ dW(t) \tag{2.2}$$

where $\circ$ implies Stratonovich calculus. The stochastic part of this integral is defined as [55, 57]:

$$b(x,t) \circ \Delta W = b\big[\frac{x(t_i) + x(t_{i-1})}{2}, t_{i-1}\big][W(t_i) - W(t_{i-1})] \tag{2.3}$$

hence the integrand of the Wiener term must in this case by evaluated at the midpoint of the timestep [58]. Eqs.(2.1 & 2.2) correspond to different Fokker-Planck equations; that is the PDF's produced by the two equations will be different. Conversely, any individual Fokker-Planck equation will give spde's with different coefficients for Ito and Stratonovich calculus. It can be shown [55] that a Stratonovich sde can be found to give statistically identical results to an Ito sde. The Stratonovich spde Eq. (2.2) is the same as the Ito spde

$$dx = [a + \frac{1}{2}b\frac{\partial b}{\partial x}]dt + bdW \tag{2.4}$$

hence it is possible to derive two different spde's which will give identical results provided they are implemented correctly. Pope [59] shows a method of integrating Ito sde's in a Monte Carlo simulation where the sde is transformed into one which has a strictly linear stochastic part. By reference to Eq. (2.2) and Eq. (2.4) it can be seen that when this is the case the two forms are identical and hence a midpoint integration scheme can be used.

2.1.2 Ito Formulation of the SF Equation

Valiño [49] starts from Eq. (1.6) [36] and closes the conditional velocity fluctuation and molecular diffusion terms at this stage. The gradient approximation is used

for the conditional velocity fluctuation term $\langle u_i|\psi\rangle f_\phi$ [36] and the Interaction by Exchange with the Mean (IEM) (also known as Linear Mean Square Estimation) is used for the molecular diffusion. Neither of these closures are new and both have known deficiencies [60], however they were not the main subject of Valiño's work, rather they are used because of their simplicity to implement and their use in other work [61–63]. The modelled transport equation for the joint scalar PDF, f_ϕ, thus takes the form:

$$\begin{aligned} \frac{\partial f_\phi}{\partial t} + U_k \frac{\partial f_\phi}{\partial x_k} &- \frac{\partial}{\partial x_k}\left(K \frac{\partial f_\phi}{\partial x_k}\right) \\ &= -\frac{\partial}{\partial \psi_i}\left[\frac{\psi_i - \overline{\phi}_i}{T_{eddy}}\right] - \frac{\partial}{\partial \psi_i}[\dot{w}_i(\boldsymbol{\psi}) f_\phi] \end{aligned} \tag{2.5}$$

where U_k is the mean velocity, K is the combined molecular and turbulent diffusivity, T_{eddy} is a characteristic timescale of turbulent scalar mixing and $\overline{\phi}_i$ is the local mean of scalar i. The PDF is then represented by N stochastic fields τ^n which contain values for each scalar at each point throughout the flow. So, $f_\phi(\psi; \boldsymbol{x}, t) = \frac{1}{N}\sum_{n=1}^{N} \delta[\psi - \tau^n(\boldsymbol{x}, t)]$. These fields are defined by Valiño [49] as being twice differentiable in space. Using this definition and applying the chain rule (see [49] for details) Eq. (2.5) is converted into a pde where each term is expressed as a derivative, or second derivative, of composition ψ. Hence it has been converted into a Fokker-Planck equation describing the evolution of the Eulerian composition PDF. A Fokker-Planck equation has an equivalent spde [55] describing the evolution of the N stochastic fields that represent f_ϕ. If interpreted in an Ito sense, as discussed below, this takes the form:

$$\begin{aligned} d\tau_i^n &= -U_k \frac{\partial \tau_i^n}{\partial x_k} dt + \frac{\partial}{\partial x_k}\left(K \frac{\partial \tau_i^n}{\partial x_k}\right) dt \\ &+ \dot{w}\left(\tau_1^n, \tau_2^n, \ldots, \tau_I^n\right) dt + (2K)^{1/2} \frac{\partial \tau_i^n}{\partial x_k} dW_k^n - \frac{\tau_i^n - \overline{\phi}_i}{T_{eddy}} dt \end{aligned} \tag{2.6}$$

where τ_i^n is the concentration of species i in field n. $\overline{\phi}_i$ is the mean concentration of

the scalar, calculated as an average over the fields. As Eq. (2.6) was derived from a transport equation for the one-point joint PDF, the ensemble of the scalar values at a particular point in space and time across all fields is statistically equivalent to the one-point joint PDF at that point. However no two-point statistics should be inferred from the scalar fields and the individual fields should not be thought of as actual instantaneous representations of the flow.

The first two terms on the right-hand-side of Eq. (2.6) represent transport of the scalars. The third term is the chemistry source term; we can see that it is evaluated for τ_i^n using scalar values from field n. In this way the effect of fluctuations from the mean on the reaction rate is considered directly, i.e. the need to find a closure for reactant co-variances such as $\overline{\phi'_A \phi'_B}$ is avoided.

The fourth term is the random or 'Wiener' term and can be thought of as representing random advection, on the scale of the spatial grid, caused by the turbulence field. The size of the random advection or scalar fluctuation will be determined by the strength of the turbulence, provided via K (and hence a local turbulent velocity and length scale), and the local scalar gradient. This is as should be expected as variance is produced only where scalar gradients are present. An independent value of dW is needed for each spatial component in each field, within a field the same values of dW_k^n are used for all scalars. As Eq. (2.6) is derived to be used in the Ito sense the integrand of the Wiener term must be independent of dW_k^n.

The final term represents the effects of micromixing or molecular diffusion which causes scalar fluctuations to decay. As mentioned previously the closure used here is the IEM model. The scalar mixing timescale used in this model is the large scale turbulent scalar timescale, as it is this which determines the rate at which fluctuations are passed down to the smallest scales where they are destroyed by the action of molecular diffusion [64]. In Eq. (2.6) the assumption is made that the scalar mixing timescale is the same for all scalars and equal to the velocity timescale [32, 60]. The latter assumption allows the timescale to be found from the fluid mechanics of the flow. The assumption that the timescale should be equal for

all species is open to question, particularly when considering passive and reactive scalars as reaction can produce gradients which in turn affect mixing [45]. The closure assumptions behind Eq. (2.6) are equivalent to those in the modelled one-point PDF equation and are discussed at length in the literature [32, 36, 38, 47, 49]. We can safely argue that these assumptions are quite mild and we hence expect the Stochastic Fields model to be applicable to a wide range of turbulent reacting flows.

If the final two terms on the r.h.s. of Eq. (2.6) are ignored we are left with a simple advection-diffusion-reaction equation using the same velocity and turbulence field,

$$d\tau_i = -U_k \frac{\partial \tau_i}{\partial x_k} dt + \frac{\partial}{\partial x_k} \left(K \frac{\partial \tau_i}{\partial x_k} \right) dt + \dot{w} \left(\tau_1, \tau_2, \ldots, \tau_I \right) dt \tag{2.7}$$

which is equivalent to assuming perfect or infinitely fast micromixing. Hence by using only one field and dropping the final two terms we can provide a direct measure of the effect of imperfect micromixing in a reacting flow. Also the Wiener term in Eq. (2.6) should not affect first scalar moments other than through the chemistry term, so for passive scalars the mean distribution found from Eq. (2.6) should be the same as found with Eq. (2.7).

As the Stochastic Fields method is derived from the joint-scalar PDF equation rather than the joint-velocity-scalar PDF, information about the velocity and turbulence must be provided from an external source via U_k, K and T_{eddy} for each spatial node, either from measured data or by modelling. If the reactions involved in the flow give off a significant amount of heat (especially those involved in combustion) then this will affect the density of the flow and with it the flow field. In this case one of the scalars in the SF calculation will be temperature or enthalpy and at each timestep this must be used to update the flow field which will then return new values of U_k, K and T_{eddy} to the SF code. This is known as two-way coupling. On the other hand, most atmospheric reactions do not release sufficient heat to affect the density of the flow. If this is so then information about the flow field needs to be passed

to the SF calculation, but enthalpy or temperature information does not need to be passed the other way. This is one-way coupling. Temperature will usually need to be carried as a scalar in the SF calculation even for one-way coupling as the reaction rate will be dependent on temperature fluctuations. This means that the PDF of temperature will be found but, in the absence of a chemistry source term, the mean will be unaffected.

2.1.3 Stratonovich Formulation of the SF Equation

Sabel'nikov and Soulard [50] also derive their spde from the modelled PDF transport equation, Eq. (2.5). They do not at this stage specify the IEM model as the closure for micromixing although they do use this model in their subsequent calculations. They start with an spde for the stochastic fields which splits the velocity into a deterministic part and a Gaussian random part for which the correlation time tends to zero, they chose to take this limit in the Stratonovich sense. The coefficients of the deterministic and random parts of the spde are then chosen so that the PDF of the fields is identical to Eq. (2.5). For a constant density flow Sabel'nikov and Soulard's resulting governing spde for the stochastic fields is:

$$d\tau_i^n = \left[\left(-U_k + \frac{1}{2}\frac{\partial K}{\partial x_k}\right)\frac{\partial \tau_i^n}{\partial x_k} - \frac{\tau_i^n - \overline{\phi}_i}{T_{eddy}} + \dot{w}(\tau_1^n, \ldots, \tau_I^n)\right]dt + \sqrt{2K}\frac{\partial \tau_i^n}{\partial x_k} \circ dW_k \quad (2.8)$$

Eq. (2.8) is not the same as Eq. (2.6), despite both having the same modelled PDF transport equation, Eq. (2.5), due to the different calculus used for the Wiener term. In fact it can be shown [50] that if Eq. (2.8) is compared to Eqs.(2.2 & 2.4) a term of

$$\frac{\partial}{\partial x_k}\left(K\frac{\partial \tau_i^n}{\partial x_k}\right) - \frac{1}{2}\frac{\partial K}{\partial x_k}\frac{\partial \tau_i^n}{\partial x_k}$$

must be added to the deterministic part to convert from Stratonovich to Ito spde and that this gives the same governing equation as derived by Valiño in Eq. (2.6).

Sabel'nikov and Soulard [50] claim an advantage of this derivation is that no restriction needs to be placed on the differentiability of the fields. They also point out that using the Stratonovich method allows the normal rules of calculus to apply, i.e. those for deterministic pde's. This will affect the way the Stochastic Fields method is implemented. However, as we have seen, Eq. (2.6) and Eq. (2.8) are equivalent and providing they are each implemented correctly they will give identical results. As such it seems valid to use Sabel'nikov and Soulard's less restrictive derivation as an alternative method of deriving Valiño's Ito spde. Either method can, therefore, be chosen as required with the decision made depending on the practicalities of implementation.

Sabel'nikov and Soulard [50] state that Eq. (2.6) should be thought of as an advection-reaction equation rather than an advection-reaction-diffusion equation with the second order spatial term acting with the Wiener term to give advective rather than diffusive behaviour in individual fields in the absence of micromixing or chemistry. This behaviour is shown in Section 2.2 but Eq. (2.6) must still be implemented numerically in the same way as an advection-diffusion-reaction equation. The modelling of turbulent diffusion as being the cumulative effect of many advective processes is analogous to the true physical process of turbulent diffusion. But when using either of Eqs.(2.6 & 2.8) the stochastic advection in individual fields will be on the scale of the spatial grid and therefore cannot be true instantaneous realisations of the flow. We should also note that while the Stochastic Fields equations may be advection-reaction equations, they have been derived from Eq. (2.5) in which the assumption is made that turbulent mixing can be modelled by the use of a diffusivity.

2.2 Implementation of the Stochastic Fields Method

As the Stochastic Fields method is a relatively new method of carrying out Monte Carlo simulations of reacting flows there are only a small number of examples of its use. The Ito based method has been validated against a particle based Monte Carlo simulation for the case of a single reactive scalar [49]. It is has recently been used by Mustata et al to model a turbulent piloted diffusion flame with flow-field data provided by a Large Eddy Simulation (LES) [51]. When used with LES much of the turbulent velocity is resolved and the stochastic Wiener term only models those turbulent fluctuations at the sub-grid scale. These fluctuations will be small compared to those found when using a RANS code to provide the flow-field as this will only provide mean velocities.

Sabel'nikov and Soulard have applied their Stratonovich method to a series of numerical test cases [50] in order to demonstrate properties of the method. They have also applied their method to a turbulent premixed flame over a backwards facing step [52, 58], which they did by coupling their code with a RANS solver. As yet the SF method has only been used with simple chemistries; Mustata et al [51] use a mechanism with four reactions between six species and temperature, while Sabel'nikov and Soulard [58] use a single step mechanism with five species and temperature. In this work we have performed calculations using both Eqs.(2.6 & 2.8) and attempted to assess the advantages of each and suitability to certain situations. For both methods an operator-splitting technique has been used whereby the terms in the governing spde's are integrated in turn rather than simultaneously. The next section contains a discussion of the implementation of the transport terms in both the Ito and Stratonovich senses, while subsequent sections detail the extension to include micromixing and chemistry.

2.2.1 Transport in Ito Implementation

In the absence of micromixing and chemistry Eq. (2.6) becomes:

$$d\tau_i^n = -U_k \frac{\partial \tau_i^n}{\partial x_k} dt + \frac{\partial}{\partial x_k}\left(K \frac{\partial \tau_i^n}{\partial x_k}\right) dt + (2K)^{1/2} \frac{\partial \tau_i^n}{\partial x_k} dW_k^n \tag{2.9}$$

To implement this Ito spde correctly the integrand of the Wiener term must be evaluated only once per timestep in order to preserve its independence from dW. Because of this iterative methods should not be used. There are significant advantages to the use of iterative procedures for the integration of the other terms. In fact, as discussed in Section 2.2.6, complex chemistries cannot be integrated using a single-step explicit method. Because of this we chose to make the Wiener term a separate fractional step. The advection and spatial second order 'diffusion' term are solved first for each scalar in each field:

$$\frac{\partial \tau_i^n}{\partial t} = -U_k \frac{\partial \tau_i^n}{\partial x_k} + \frac{\partial}{\partial x_k}\left(K \frac{\partial \tau_i^n}{\partial x_k}\right) \tag{2.10}$$

This equation is solved using either the VODPK solver [65] or using the User Defined Scalar option in the commercial CFD package FLUENT [10]. The former uses the 'Method of Lines' to transform the pde's into a large set of ode's. The choice of VODPK is motivated by the use of this solver for similar advection-diffusion-reaction problems in combustion [66] as the chemistry term will be added to this step. FLUENT solves Eq. (2.10) using an iterative, implicit method. Both methods should ensure stability of the advection-diffusion scheme.

The outcome from this first step, $\tau_i^n(t^*)$, is updated for the random forcing term by a simple Euler method, which constitutes the second step in the fractional step procedure. This is equivalent to using the Euler-Maruyama approximation of an Ito process [67] which converges with order 0.5 w.r.t. timestep in the path-wise sense, but 1.0 in the averaged sense. Kloeden and Platen [67] give alternative schemes with better convergence, but at the expense of greater complexity and computing resources. Again from [67] and [55], the Wiener step is found by:

$$\Delta W_k^n = \xi_k^n (\Delta t)^{1/2} \tag{2.11}$$

where ξ_k^n is a Gaussian random number with zero mean and variance of 1, independent for each spatial dimension and field. This gives the properties required of ΔW as described above. The same values of ξ_k^n have been used for each scalar in a given field. Hence, the second and final fractional step is:

$$\tau_i^n(t + \Delta t) = \tau_i^n(t^*) + (2K)^{1/2} \frac{\partial \tau_i^n(t^*)}{\partial x_k} \xi_k^n (\Delta t)^{1/2} \tag{2.12}$$

which was solved for each scalar i and for every field n at every point in space. The scalar gradient is found using a central difference approximation. Eq. (2.12) is an explicit Euler approximation to an advection process which by itself would be unstable. However we have found this method to be stable when used with Eq. (2.10) as a separate step. With this method there is a danger of unbounded scalars if the timestep is too large. While this can be avoided by carefully limiting the timestep, we have found that placing a limit on the maximum size of the 'jump' produced by the Wiener term gives a more robust numerical scheme which prevents unbounded scalars. The maximum size of the Wiener step is limited to the difference between the current scalar value and its upper or lower physical limit, see Fig. 2.1. This is done rather than bound the scalar after the step as this would lead to the term being biased towards values that move away from the limit. This is shown in Fig. 2.2; at the smaller timestep there is little difference between bounding the scalar after the timestep and placing a limit on the size of the Wiener term, indicating that with small timesteps the problem of unbounded scalars diminishes.

2.2.2 Transport in Stratonovich Implementation

The use of Stratonovich calculus allows the usual rules of calculus to apply and as such iterative numerical schemes for advection can be used. Sabel'nikov and Soulard [50, 58] implement Eq. (2.8) using a two-step method Heun scheme. It

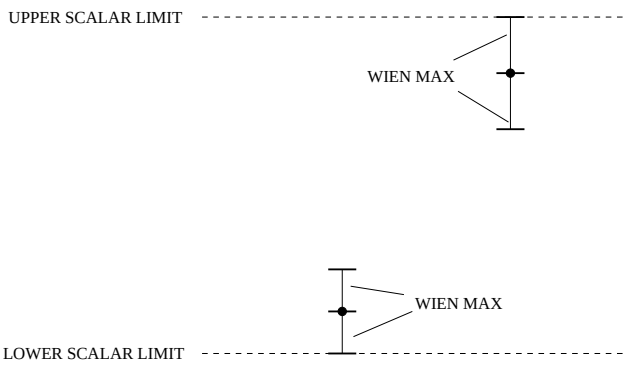

Figure 2.1: The maximum size of the Wiener step is limited so that its magnitude is less than or equal to the difference between the current value of the scalar and the nearest physical bound on the scalar.

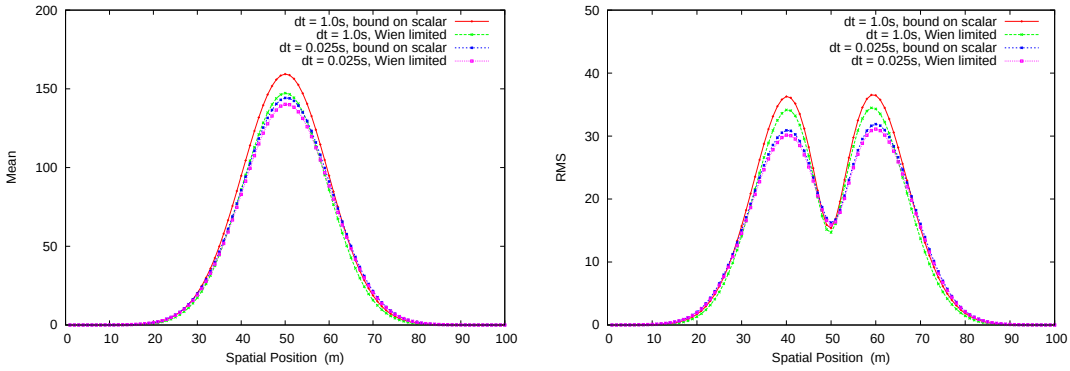

(a) (b)

Figure 2.2: Mean and RMS of an arbitrary scalar diffusing from a line source with $K = 2.0\text{m}^2\text{s}^{-1}$, results at 25s using 100 fields. Calculations performed using Ito method by replacing negative values with 1.0×10^{-30} and by limiting the magnitude of the Wiener step.

has been implemented here using a two-step method and also a three-step Runge-Kutta method [68] which provides greater stability. In the absence of chemistry and micromixing this takes the form:

$$\begin{aligned}
\tau_i^n(1) &= \tau_i^n(t) + L\{\tau_i^n(t)\} \\
\tau_i^n(2) &= \frac{3}{4}\tau_i^n(t) + \frac{1}{4}\tau_i^n(1) + \frac{1}{4}L\{\tau_i^n(1)\} \\
\tau_i^n(t+\Delta T) &= \frac{1}{3}\tau_i^n(t) + \frac{2}{3}\tau_i^n(2) + \frac{2}{3}L\{\tau_i^n(2)\} \\
L\{\tau_i^n(t^*)\} &= \left(-U_k + \frac{1}{2}\frac{\partial K}{\partial x_k}\right)\frac{\partial \tau_i^n(t^*)}{\partial x_k}\Delta t + (2K)^{1/2}\frac{\partial \tau_i^n(t^*)}{\partial x_k}\xi_k^n(\Delta t)^{1/2} \quad (2.13)
\end{aligned}$$

where the random number ξ_i^n is held constant throughout the three steps. The scalar gradient is found using a central difference approximation. Provided the initial profile of the fields is smooth this method will preserve the boundedness of the scalars without the need for limiting them after the timestep. However physical limits can still be violated if sharp initial gradients are used such as 'top-hat' profiles.

An alternative method is to use a fractional-step method where the deterministic parts of Eq. (2.8) are integrated together using the VODPK solver as a first step. The second step is to calculate the Wiener term alone using a predictor corrector method.

$$\begin{aligned}
\tau_i^n(1/2) &= \tau_i^n(t^*) + \frac{1}{2}(2K)^{1/2}\frac{\partial \tau_i^n(t^*)}{\partial x_k}\xi_k^n(\Delta t)^{1/2} \\
\tau_i^n(t+\Delta t) &= \tau_i^n(t^*) + (2K)^{1/2}\frac{\partial \tau_i^n(1/2)}{\partial x_k}\xi_k^n(\Delta t)^{1/2} \quad (2.14)
\end{aligned}$$

Again ξ_k^n is held the same for both steps. There seems to be some confusion in Chapter 7 of [32] that this predictor-corrector scheme will give better convergence compared to a simple Euler method, as indeed is true for ode's. However, as will be shown later, this is not the case for stochastic equations where it gives different results. The motivation for using this scheme was that the two-step scheme is a true mid-point scheme and has been used by Sabel'nikov and Soulard to calculate

Stratonovich integrals, while the operator-splitting procedure was necessary to calculate chemistry terms successfully. It was found that the scheme in Eq. (2.13) gave results equal to those of Eq. (2.14), thus showing that the third order Runge-Kutta scheme is appropriate. The Runge-Kutta scheme was also more stable.

2.2.3 Micromixing

The closure adopted for the micromixing or molecular diffusion term is the IEM model:

$$\frac{d\tau_i^n}{dt} = -\frac{\tau_i^n - \overline{\phi}_i}{T_{eddy}} \tag{2.15}$$

where $\overline{\phi}_i$ is the local mean value of scalar i. In the SF method this will be found by taking at each grid node for each scalar the mean of the value in each field. For the Ito method Eq. (2.15) can be added as an extra term in Eq. (2.10) where it will be solved according to the method of lines simultaneously with the deterministic spatial operators. Similarly it can be added to the deterministic part of each Runge-Kutta stage in Eq. (2.13) as $-\frac{\tau_i^n - \overline{\phi}_i}{T_{eddy}}\Delta t$. In each case a decision must be made as to when the means are evaluated; the most accurate method is to re-calculate the means at each Runge-Kutta stage or each time the derivative subroutine is required by VODPK, this will require the whole set of scalars from each field to be passed to the solver at the same time (Method 1). This will be particularly expensive if VODPK is used as it must invert an $M \times M$ matrix where M is the product of scalars x grid resolution x fields passed to solver. The alternative is to calculate the mean before the step and calculate a field at a time using the same mean value throughout (Method 2), this will lead to errors if the other terms cause scalars to change significantly during the step.

Another method is to solve Eq. (2.15) as a separate fractional-step with the mean calculated immediately prior to this. This method can be speeded up because Eq. (2.15) has an analytical solution:

$$\tau_i^n(t+\Delta t) = \overline{\phi}_i + (\tau_i^n(t) - \overline{\phi}_i) exp\left(-\frac{\Delta t}{T_{eddy}}\right) \tag{2.16}$$

Thus it can be applied as a single, separate, step. The IEM model itself does not change the mean and performing it as a separate step will therefore avoid errors due to using an incorrect mean. On the other hand there will be greater operator-splitting errors. The second and third approaches described here have been employed. In practice it has been found that when fast chemistries are used the second approach is one of the largest sources of error. By using both Methods 2 & 3 it is possible to check that this error is being kept to a minimum, by keeping the timestep sufficiently small.

2.2.4 Boundary Conditions

One of the advantages of the Stochastic Fields method is that ordinary Eulerian boundary conditions can be used at the edge of the fields. These will be Dirichlet (fixed value) or Von Neumann (fixed gradient). It is usual for scalar values to be specified at inlets to the domain and outlets to be taken sufficiently far downstream of the region of interest that the gradient can be assumed to be zero. Walls, which can cause some difficulty if particle Monte Carlo methods are used [60], can simply be treated as having zero gradient when using the Stochastic Fields formulation.

Sabel'nikov and Soulard [50] discuss the effect of the Wiener term on boundary conditions. They point out that it will lead to a boundary switching between being an inflow and an outflow depending on the sign of ξ^n. They further point out that this will lead to losing the original information in the field as it is replaced by the value at either end of the domain until the field will eventually be a step. If there is a large mean velocity, i.e. greater than the Wiener term, this will serve to ensure that information is only advected into the field from one direction.

It has, so far, not been possible to implement the SF method in a symmetric or axisymmetric formulation. While it is possible to use Eq. (2.7) in this way, it is not

clear what boundary condition should be employed for the SF method on the plane or axis of symmetry. While the mean and higher moments may be symmetrically distributed there is no reason why an individual field should be so and therefore no reason to use a zero gradient condition on the axis. This may represent the observation that a turbulent field will *only* be symmetric on average. This problem can also be thought of as an extension to Sabel'nikov's boundary condition problem discussed above. Take for example a symmetric plume taking a high value in the centre dropping to zero away from the centre, see Fig. 2.3. Wiener steps directed towards the centre will cause the lower, outer values to be advected towards the centre whilst the original, higher, central values are advected out of the domain. Hence this information is effectively lost from the domain. If the direction of the Wiener term subsequently reverses then the (lower) value currently at the axis will be advected into the domain if a zero gradient boundary is used. Therefore, in this thesis, axisymmetric grids have not been used to avoid this problem.

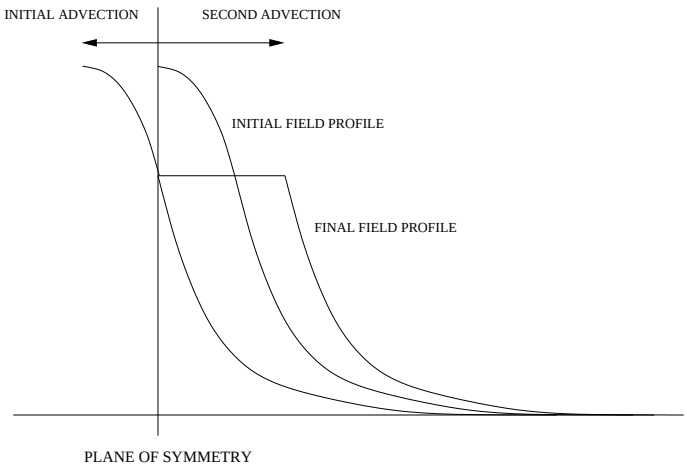

Figure 2.3: Loss of information from fields when a symmetry boundary condition is used with the Stochastic Fields method.

2.2.5 Comparison of Inert Transport Using Ito and Stratonovich Methods

This section presents results obtained for the one-dimensional turbulent diffusion of an inert scalar using the two formulations of the Stochastic Fields method, Eqs.(2.6 & 2.8). The results obtained are then compared and discussed. A constant turbulent diffusivity of $K = 2.0\text{m}^2\text{s}^{-1}$ was used for the entire domain. Hence in the Ito case Eq. (2.6) becomes:

$$d\tau_i^n = \frac{\partial}{\partial x_k}\left(K\frac{\partial \tau_i^n}{\partial x_k}\right)dt + (2K)^{1/2}\frac{\partial \tau_i^n}{\partial x_k}dW_k^n - \frac{\tau_i^n - \overline{\phi}_i}{T_{eddy}}dt \tag{2.17}$$

and in the Stratonovich, case Eq. (2.8) becomes:

$$d\tau_i^n = -\frac{\tau_i^n - \overline{\phi}_i}{T_{eddy}}dt + \sqrt{2K}\frac{\partial \tau_i^n}{\partial x_k} \circ dW_k \tag{2.18}$$

Both Eqs.(2.17 & 2.18) were solved using a 1D grid extending 100m with 1m grid spacing, zero gradient boundary conditions were applied at either end of the grid. An initial Gaussian profile was used, centred at 50m, the peak of which takes an arbitrary value of 1000 (as shown in Fig. 2.4). For the results using the Ito method, the operator splitting procedure of Section 2.2.1 was employed with the IEM model for micromixing added to the deterministic part of the code solved by VODPK. For the Stratonovich method the Runge-Kutta method described in Section 2.2.2 is used, again with the IEM model added to the deterministic part. Results were also found using Eq. (2.7) by employing the Ito formulation with only a single field and the Wiener term switched off. This last method will obviously only give the mean whereas the other two methods will give a PDF at each point, these results will be presented by calculating the moments of the PDF. In all cases the initial profile was allowed to diffuse outwards for a total of 25s using timesteps of $\Delta t = 0.025$s.

In Fig. 2.4 the initial profile and the final profile after 25s can be seen. The final profile is, as expected, still a Gaussian shape. If there is no chemical reaction the Wiener and IEM terms should not affect the first moment of the PDF and hence

the mean SF solution after 25s should agree with this profile. Also shown is a single field shown after 25s using both the Stratonovich and Ito methods in the absence of micromixing. In the absence of micromixing (and chemistry) it can clearly be seen that, as the integral must here obey the ordinary rules of calculus, Eq. (2.8) will be a pure advection process in this situation. This is indeed the case in Fig. 2.4 where we see that the Stratonovich field is essentially the original profile shifted some distance to the right with a small amount of numerical diffusion.

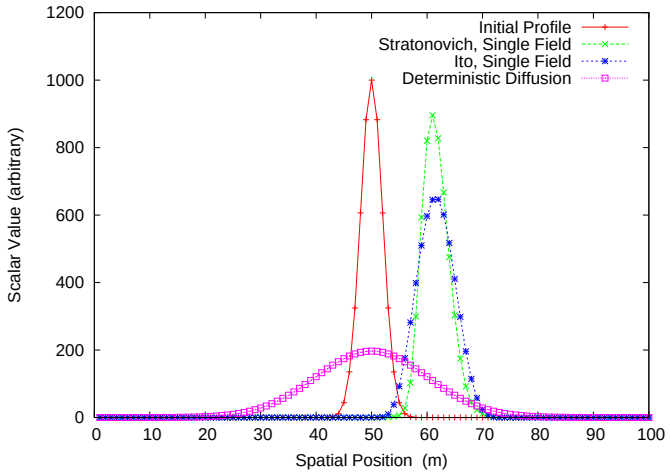

Figure 2.4: Turbulent transport of inert scalar. Results shown are from simple 1D deterministic diffusion code and also evolution of a single field from the Ito and Stratonovich methods in the absence of micromixing.

If we consider the evolution of a single field according to the Ito calculus, using the same random number sequence as for the Stratonovich case, we can see that the field does not behave as if subject to a diffusive process. The field is much closer to the advected Stratonovich field than the deterministic diffusion. This demonstrates the point made by Sabel'nikov and Soulard [50] that Eq. (2.6) is an advection-reaction process for the individual field rather than an advection-diffusion-reaction process as the presence of the second-order spatial operator might suggest. This term in combination with the Wiener term produces advective behaviour when Ito

integration is used, this is due to Ito calculus not obeying the usual rules of calculus [55]. The difference from the Stratonovich field in Fig. 2.4 is due to increased numerical diffusion.

The inclusion of the IEM micromixing term causes the pure advection behaviour for the field to be lost. This is because the mean, which will have a diffused shape, will now affect individual fields. Fig. 2.5 shows the effect of micromixing on individual fields using both methods, also shown are the mean profiles (using 100 fields) that the individual fields are relaxing back to. With $T_{eddy} = 100$s the micromixing is relatively slow and this is reflected in the fields being similar to those in Fig. 2.4 although we can see that region where the field is at zero has been reduced. When T_{eddy} is reduced to 5s the effect of increasing the rate of micromixing can clearly be seen as the individual field is much closer to the mean field. The fields obtained using the different methods are also much closer together with this faster mixing timescale and it can be seen that the two equations, Eqs.(2.6 & 2.8), do indeed lead to identical results.

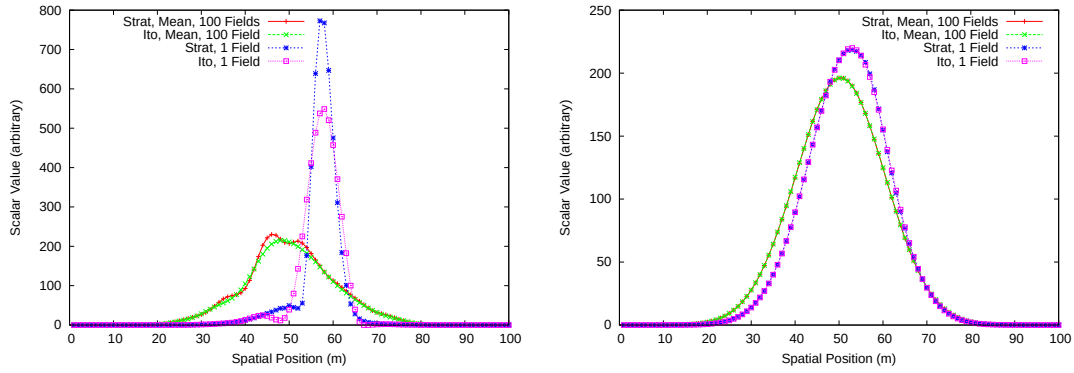

(a) (b)

Figure 2.5: Evolution of individual fields using Ito and Stratonovich methods with micromixing present. $T_{eddy} = 100$s for (a) and $T_{eddy} = 5$s for (b).

The mean and RMS of fluctuations from the mean using (a) the Ito method and (b) the Stratonovich are shown in Fig. 2.6. The mixing timescale used here

is 5s. For both methods the mean result is very close to that produced from a 1D diffusion code (Eq. (2.7)) as they should be. This shows the ability of the two numerical methods used to correctly find the mean. The effect of using the wrong stochastic integration method for a particular spde can also be seen here. Eq. (2.6) has been implemented here using the Runge-Kutta method, which integrates in the Stratonovich sense. When this is done the second-order spatial term does act as a diffusion term for the individual fields in addition to the diffusion in the mean caused by the stochastic advection term. The outcome of this is to give excessive diffusion in the mean.

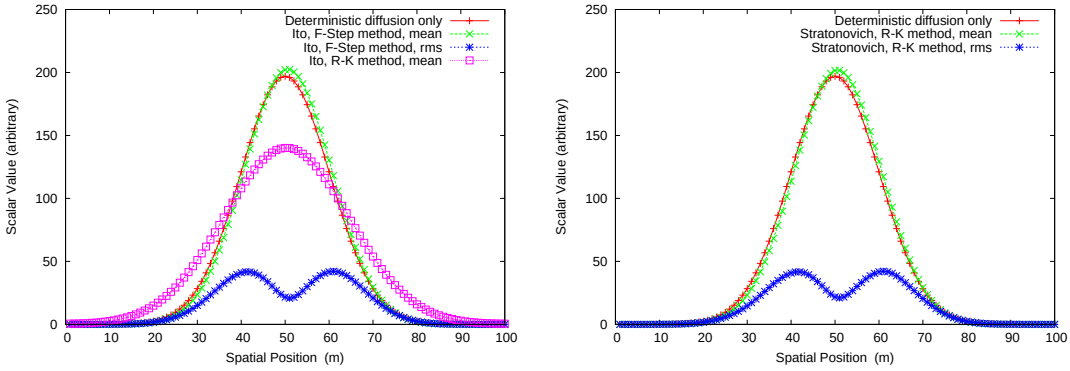

(a) (b)

Figure 2.6: Mean and RMS of inert scalar after 25s using (a) Ito and (b) Stratonovich methods using 100 fields with $T_{eddy} = 5$s, along with the mean as found using 1D diffusion Eq. (2.7). Also shown is the result of integrating Eq. (2.6) in the Stratonovich sense.

Further evidence of the equivalence of the Ito and Stratonovich methods, as well as a demonstration of the ability of the Stochastic Fields method's ability to produce higher statistical moments, can be seen in Fig. 2.7. Here we see variance, skewness and kurtosis excess for the case with $T_{eddy} = 5$s. It can be seen that for all three higher moments the two methods give virtually identical results when the same random number sequence is used. Given that the results using the fractional-

step, Euler Wiener term method for the Ito spde are identical to those found using a Runge-Kutta method for the Stratonovich, which should give stable advection behaviour, it seems safe to conclude that this method for the Ito spde is acceptable in terms of both stability and accuracy.

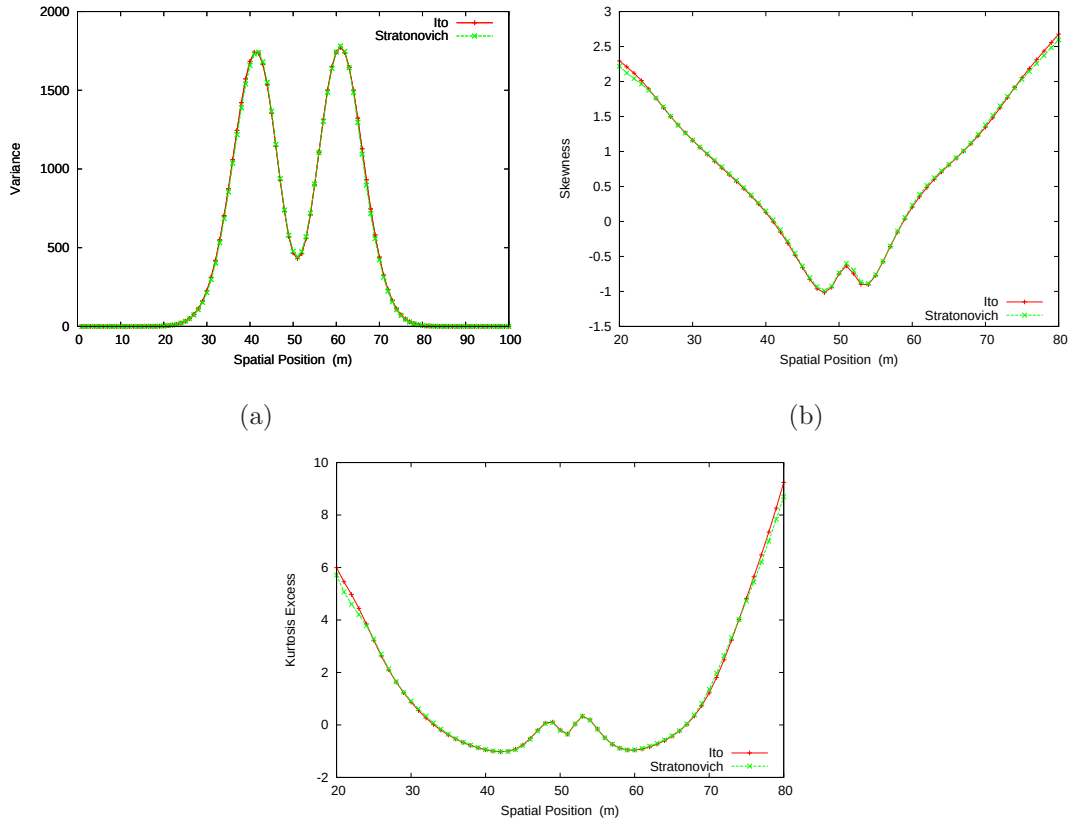

(a) (b)

(c)

Figure 2.7: Higher statistical moments of inert scalar after 25s using Ito and Stratonovich methods with $T_{eddy} = 5$s. Same random number sequence used in each case with 100 fields. (a) Variance; (b) skewness and (c) kurtosis excess.

It was seen in Fig. 2.5 that the use of a smaller T_{eddy} leads to fields that are closer to the mean, this will obviously lead to a smaller variance. It will also lead to an increase in the statistical accuracy of the results for a given number of fields. As with all Monte Carlo calculations the standard deviation of the statistical error

in calculating mean quantities from from a sample of N realisations is, according to the central limit theorem [69]:

$$E_s = \frac{\sigma}{\sqrt{N}} \tag{2.19}$$

where σ is the standard deviation, or rms, of the measured quantity. Hence, as more fields are used the error will decrease as the inverse of the square root of the number of fields and will increase with the rms of the quantity under consideration. This is illustrated in Fig. 2.8 in which it can be seen that using the larger T_{eddy} gives means that are less smooth and further from the true mean values. The reduced smoothness is even more apparent in the variance plot. The Ito method seems to give smoother results for the $T_{eddy} = 100$s case perhaps due to the increased numerical diffusion in the method used here. This consideration could be useful when the code is used with stiff chemistries, as will be discussed in the next section.

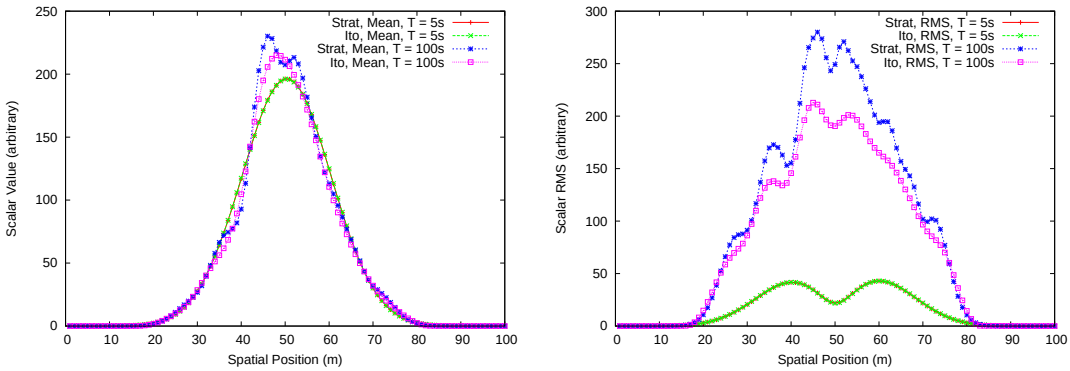

(a) (b)

Figure 2.8: Mean (a) and RMS (b) of inert scalar after 25s using Ito and Stratonovich methods. Micromixing using $T_{eddy} = 5$s and $T_{eddy} = 100$s.

2.2.6 Chemical Reaction

The Stochastic Fields method can in theory be applied with mechanisms of any level of complexity. However, detailed chemical mechanisms have been developed

for atmospheric chemistry which can contain very large numbers of species and reactions between them. The Master Chemical Mechanism for instance contains over 2400 chemical species and over 7100 reactions [70]. The computational cost of using a mechanism of this size with PDF methods for problems of practical interest is prohibitively high with current computing technology. Computer memory and time requirements will place a limit on the product of grid size, number of fields and the number of scalars per field. This means that reduced chemical mechanisms must be employed. Mechanism reduction can be performed on an ad-hoc basis using the experience of the researcher to identify the key reaction steps that must be retained. It can also be performed using a more formal mathematical method, such as Computational Singular Perturbation (CSP) [19], to identify fast species which can be assumed to be in steady state.

The mechanism used will depend on the situation being modelled as well as the computational requirements. In Chapter 3 a simple irreversible $NO + O_3 \rightarrow NO_2 + O_2$ chemistry is used to model reaction in a laboratory plume with no uv light source. In Chapter 4 a simple reversible NO_x/O_3 chemistry is used to describe the transformation of the main pollutants in a street canyon. The same street canyon is also modelled using the more complex 28 species, CBM-IV mechanism [71]. In the simulations of an aircraft jet plume in Chapter 4 a mechanism developed by Kärcher [72] for the early part of the jet exhaust is used which consists of 24 species.

When mechanisms with several species and reactions are used there may be a range of characteristic chemical timescales present which leads to numerical stiffness. Whereby if an explicit integration scheme is to be used the timestep must be smaller than the smallest timescale in the mechanism, if this is much smaller than the overall timescale of the problem then this method would take a prohibitively long time. Instead other integration techniques must be used [73]. Depending on the complexity and stiffness of the mechanism these techniques, whilst considerably faster than attempting to use explicit methods, can themselves be time consuming.

Chemistry has been implemented in the Ito Stochastic Fields code in two ways.

Firstly the chemistry term has been added to Eq. (2.10) and implemented simultaneously with the deterministic transport processes using the VODPK solver; this was the original motivation behind using the VODPK solver for this step. VODPK can be used in either stiff or non-stiff mode, in stiff mode it employs a fully implicit backward differencing scheme. The second method used is to implement the chemistry as a separate, final fractional step. This was done when using FLUENT to calculate the transport terms. In this method the species and temperature in each field at each grid node are passed in turn to the chemistry solver which returns the new values after the timestep Δt. Two different solvers were used for the chemistry here; VODPK, as discussed above, and also the CHEMEQ2 stiff ODE solver [74]. This is a predictor-corrector algorithm [73] which is described as an α-quasi-steady-state method. CHEMEQ2 is a single point method requiring only information from the current time level, this makes it particularly suited to solving the chemistry across a grid in this manner. VODPK is capable of greater accuracy, but the need to build up historical data for each calculation leads to a start-up penalty at each node. The two solvers were tested using a 0D calculation using the Kärcher chemistry, whereby only chemistry was considered for random initial conditions, and in an advection-diffusion-reaction calculation. With adjustment of its solution parameters it was possible to get acceptable accuracy from CHEMEQ2 compared to VODPK for both these cases. CHEMEQ2 was found to be significantly faster. The VODPK solver was chosen for its greater accuracy for the street canyon calculations, whereas for the aircraft jet simulation which requires greater computational effort CHEMEQ2 was chosen because of its higher speed.

When using the Stratonovich formulation chemistry cannot be included in the Runge-Kutta scheme (Eq. (2.13)) if it is stiff, as again it would require very small timesteps to avoid instability. This means that the Stratonovich method will require operator splitting to be employed as a stiff solver must be used to implement the chemistry fractional-step. As the chemistry is often the most computationally expensive part of the calculation this negates most of the speed advantage of using the

Stratonovich Runge-Kutta method over the Ito method described in Section 2.2.1.

2.3 Conclusions

In this chapter the Stochastic Fields method and its implementation has been discussed. There are two derivations of the method which result in apparently different governing stochastic pde's. However, providing the two methods are each integrated according to the correct stochastic calculus, the two spde's are equivalent. Methods of implementing the two formulations, Ito and Stratonovich, have been presented. It has been shown in this chapter by the use of a test case modelling the turbulent diffusion of an inert scalar that the spde's do produce the same solution. Furthermore it has been shown that both methods produce stable solutions with the correct mean distribution in the absence of chemistry.

The problem of stiff chemical mechanisms has been addressed; stable integration of the chemistry requires the use of stiff solvers such as VODPK or CHEMEQ2 in either of the two methods. These solvers are costly in terms of computational time and, as they will take a large proportion of the CPU time in either the Ito or the Stratonovich method, neither method will have a significant speed advantage over the other.

The magnitude of T_{eddy}, the turbulent mixing timescale, used in the IEM model for micromixing will affect the predicted variance and also the statistical accuracy of the solution. Lower values of T_{eddy} imply fast micromixing and hence lower variance. This will lead to higher statistical accuracy for the same number of fields. At higher values of T_{eddy} the means and variances are seen to be less smooth. However the solutions produced using the Ito method were seen to be smoother. Because of this and the greater ease with which the Ito method can be coupled with commercial CFD codes (see Chapter 4), most of the calculations presented in this work have been performed using the Ito formulation of the Stochastic Fields method. However some results have been produced with the Stratonovich formulation for comparison.

Chapter 3

Simulation of a Reacting Plume In Grid Turbulence

In this chapter numerical simulations, carried out using the Stochastic Fields method, of a laboratory reacting plume are presented. This has been done in order to develop a practical Stochastic Fields code for use with more realistic atmospheric reacting flow problems, which are presented in later chapters. By attempting to simulate an experiment for which detailed data is available, not only for means but also for fluctuating quantities, the accuracy of the method can be evaluated.

3.1 Model Problem

In order to test the usefulness of the Stochastic Fields model the experiment of Brown and Bilger [5] is modelled. Greater details of the experimental set-up are given in their earlier paper [75]. This consists of a plume of NO being released from a point source into an O_3 doped flow in a cylindrical duct, this is shown schematically in Fig. 3.1. A turbulence generating grid of pitch $M = 0.32$ m is placed $3M$ upstream of the NO source and hence the reaction takes place in a homogeneous decaying turbulence field. The mean velocity is virtually one-dimensional with zero values in

the cross stream direction for our domain of interest. As there is no UV light present, only the reaction $NO + O_3 \rightarrow NO_2 + O_2$ is expected to take place. Measurements of reactant and product volume fraction were performed using fast response probes. The volume fraction of species i is represented from here onwards as Γ_i with mean values as $\langle \Gamma_i \rangle$, fluctuating values γ_i and rms values γ_i'. The mean velocity was approximately $U = 0.5$ m s^{-1} and Brown and Bilger [75] give an empirical expression for variation of stream-wise and cross stream velocity fluctuations. A reaction rate constant $k = 0.37$ ppm^{-1} s^{-1} at 25° C and 1 atm has been used. Brown and Bilger define an overall Damköhler number for the experiment as

$$Da \equiv \frac{kM\Gamma_{O3,2}}{\overline{U}} \tag{3.1}$$

this ranges in this experiment from 0.1 to 0.6, hence assumptions based on slow chemistry should not be made.

For simulating this experiment, turbulent dispersion in the stream-wise direction can be neglected. Using the empirical expressions for velocity fluctuations contained in [75], it is possible to derive an expression for the turbulent kinetic energy, k, in terms of axial distance, mean velocity and grid pitch M:

$$k(x_0) = \frac{\overline{U}^2}{2}\left[0.173\left(\frac{x_0}{M}\right)^{-1.37} + 0.082\left(\frac{x_0}{M}\right)^{-1.27}\right] \tag{3.2}$$

where x_0 is measured from the grid, hence $x_0 = x + 3M$ if x is the distance downstream of the NO source. Differentiating Eq. (3.2) w.r.t. axial distance and multiplying by U gives the dissipation, ϵ.

$$\epsilon(x_0) = \frac{\overline{U}^3}{2}\left[\frac{0.237}{x_0}\left(\frac{x_0}{M}\right)^{-1.37} + \frac{0.104}{x_0}\left(\frac{x_0}{M}\right)^{-1.27}\right] \tag{3.3}$$

Using these, a value for $T_{eddy} = k/\epsilon$ can be found at a position, x_0, and related to a time in the unsteady calculation. The turbulent timescale so found is of the order of $4s$. A similar method could be employed for finding the turbulent diffusivity, $K = C_\mu k^2/\epsilon$, however this requires finding an appropriate value for C_μ. Instead [75]

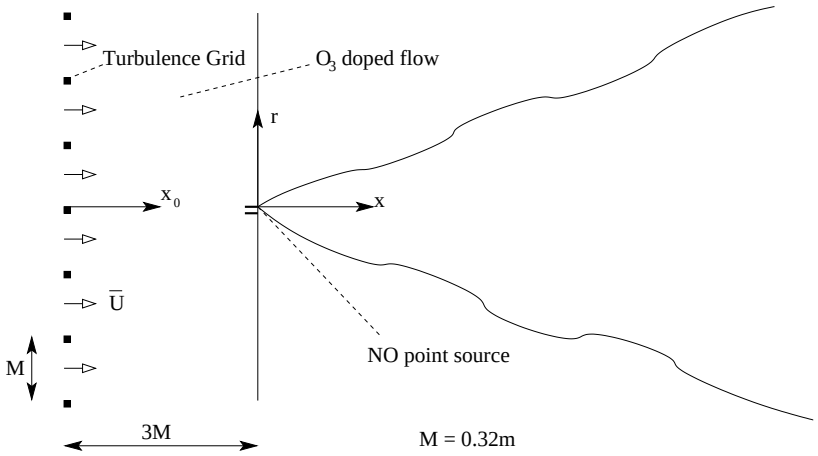

Figure 3.1: Schematic diagram of the NO_x/O_3 plume experiment of Brown and Bilger [5].

suggests that a value of $K = 0.0128UM$ is valid over the whole region of interest. Using a mean velocity of 0.5 m s^{-1} this gives $K = 2.048 \times 10^{-3}$ m^2 s^{-1}.

3.2 Numerical Methods

The 3D turbulent reacting plume was transformed into a 2D numerical problem by using a 2D domain, perpendicular to the plume axis, which is time-marched downstream. A 2-D grid was used rather than a 1-D axisymmetric for the reasons concerning boundary conditions described in section Section 2.2.4. In doing this, the assumption is made that axial fluctuations are negligible compared to those in the cross-stream direction. The Stochastic Fields method, using the Ito formulation (Eq. (2.6)), was implemented as described in Section 2.2.1. Hence a fractional-step method was used where the first step, comprising chemistry, micromixing and the 'diffusion' term, was solved using VODPK:

$$\overline{U}\frac{\partial \tau_i^n}{\partial x} = K\left(\frac{\partial^2 \tau_i^n}{\partial y^2} + \frac{\partial^2 \tau_i^n}{\partial z^2}\right) + \dot{w}\left(\tau_1^n, \tau_2^n, \ldots, \tau_I^n\right) - \frac{\tau_i^n - \overline{\phi}_i}{T_{eddy}} \tag{3.4}$$

where y and z are the two normal cross-stream directions. The second fractional-step was the explicit-Euler Wiener term shown in Eq. (2.12) where again the k-directions are y and z.

This method was solved over a 65×65 grid, covering a square domain of size 1.5 m. Zero gradient (i.e. no flux) boundary conditions were enforced at the edges of the grid. The spatial domain was chosen to be large enough that the plume was not affected by the boundaries during the time period of interest. Five hundred fields have been used in these calculations. This number is probably excessive but ensures that there is a high level of statistical accuracy in order to obtain a clear view of the performance of the SF method for this application. Using a desktop PC this code took approximately 20 hours to run to a point corresponding to a flow time of 10 s. The timestep used was $\Delta t = 10^{-2}$ s. See Section 3.3.1 for further discussion of timestep, grid spacing and number of fields used.

The initial inlet profiles were calculated by assuming Gaussian plume distribution from a point source with $K = 2.048 \times 10^{-3}\text{m}^2\ \text{s}^{-1}$. For the NO, this point source was of strength equal to $\Gamma_{NO,1}AU$, where A is the true area of the nozzle, equal to $7.79 \times 10^{-4}\text{m}^2$. For the O_3 the inlet profile was found by subtracting a plume from a source of strength $\Gamma_{O3,2}A\bar{U}$ from a uniform field of $\Gamma_{O3,2}$. The time used in these Gaussian plume calculations was 0.025 s, chosen as the minimum time at which all O_3 concentrations were positive.

Some results were also found using the Stratonovich formulation, Eq. (2.8). These simulations were obtained by using the two implementations shown in Section 2.2.2. Firstly using the operator-splitting method, whereby micromixing and chemistry are time-marched downstream using VODPK as a first step and then the Wiener term is implemented using the two-step method of Eq. (2.14). Secondly the third-order Runge-Kutta scheme, Eq. (2.13), with chemistry and micromixing added to the deterministic part. In fact, due to the absence of cross-stream velocities or gradients of turbulent diffusivity, there are no transport terms in the deterministic part of the Stratonovich implementation. The transport is due only to the action

of the Wiener term. These results were obtained using the same 65×65 grid and initial profiles and also using smoother initial profiles.

3.3 Results

3.3.1 Inert Flow

In order to characterise the inert mixing of the flow field, we follow Brown and Bilger [5] and use the conserved scalar $NO_x = NO + NO_2$. Figs. 3.2 and 3.3 show the effect, when using the Ito formulation, of varying the number of fields, Δt, and grid spacing on radial mean and rms NO_x profiles at $x/M = 15$. Using 100 fields rather than 500 gives only a small change in mean results and some distortion of the rms profile, so we can assume that using 500 fields has minimised statistical errors. Reducing Δt by an order of magnitude to 0.001 s has very little effect on the mean profile and has been omitted from Fig. 3.2 for clarity. It does, perhaps, lead to greater resolution of the rms around the centre-line, however the change is so small that we can safely choose 0.01 s as our time step. Increasing the grid spacing again has virtually no effect on mean results and very little on rms so, when using Gaussian inlet profiles, we can assume grid independence.

Fig. 3.4 shows the NO_x values calculated by the Ito Stochastic Fields model compared to experimental measurements at three downstream locations. It can be seen that using a constant value of K is a reasonable assumption, certainly over the region where experimental data is available, and that the actual value used is appropriate. The passive scalar rms (Fig. 3.5) is also predicted very accurately. This shows the accuracy of the IEM model for micromixing of a non-reacting scalar, which is not surprising given that this model has been widely validated against similar experimental data [63, 76]. More importantly, it shows that the Stochastic Fields model, which introduces a randomness in the whole of the spatial distribution of the scalar and then uses these random distributions to get first and second moments at

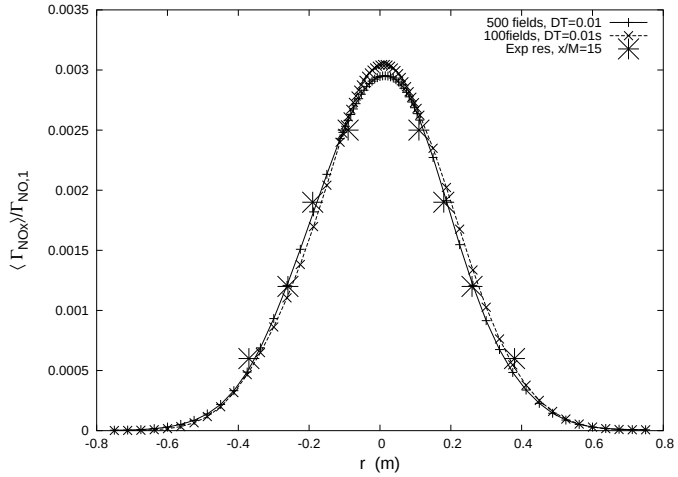

Figure 3.2: Mean NO_x predicted profiles, using Ito formulation, at x/M = 15 with $\Delta t = 0.01s$ using 100 and 500 fields. $\Delta t = 0.001$s and 4/3× grid spacing are close to 500 field, $\Delta t = 0.01$s case and are omitted for clarity. Experimental data from [5].

a point, has the correct behaviour. The good agreement shown in Figs. 3.4 and 3.5 also provides validation of the numerical method used here.

3.3.2 Development of Reacting Plume

Calculations of radial profiles at various axial locations are compared with experimental data from [5], using those cases where experimental data was obtained at various axial locations for the same inlet conditions. The conditions used in the Stochastic Fields model were $U = 0.519$ m s^{-1}, $\Gamma_{NO,1} = 515$ ppm and $\Gamma_{O3,2} = 1.02$ ppm. This data was normalised according to the method of [5]: the volume fraction was normalised by the O_3 inlet volume fraction and the radial distance is normalised by a characteristic plume width, σ, based on a Gaussian function. Brown & Bilger found this value by measurement of NO_x, while here $\sigma = \sqrt{2tK}$, where $t = x/U$. As would be expected, given the results shown in Section 3.3.1, there was good agreement for the values of σ so calculated.

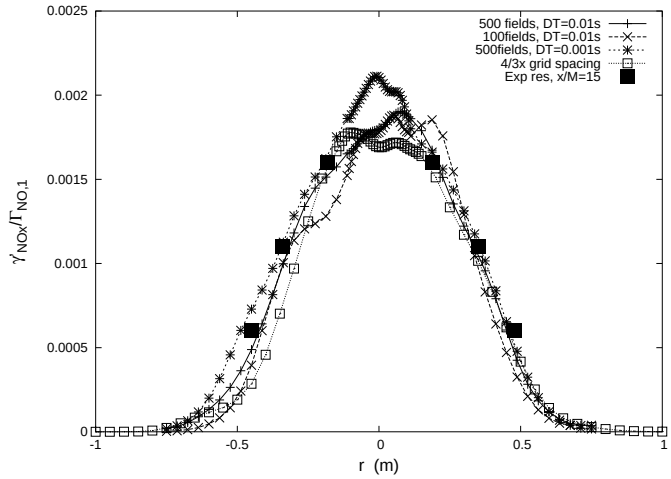

Figure 3.3: Rms of NO_x predicted profiles, using Ito formulation, at x/M = 15 with varying numbers of fields, time step size and grid spacing. Experimental data from [5].

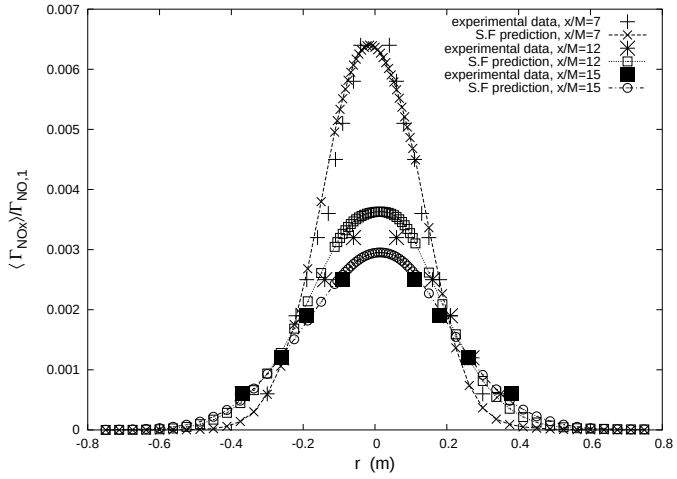

Figure 3.4: Radial profiles of mean NO_x at x/M = 7, 12 & 15. Predictions using the Ito Stochastic Fields method. Experimental data from [5].

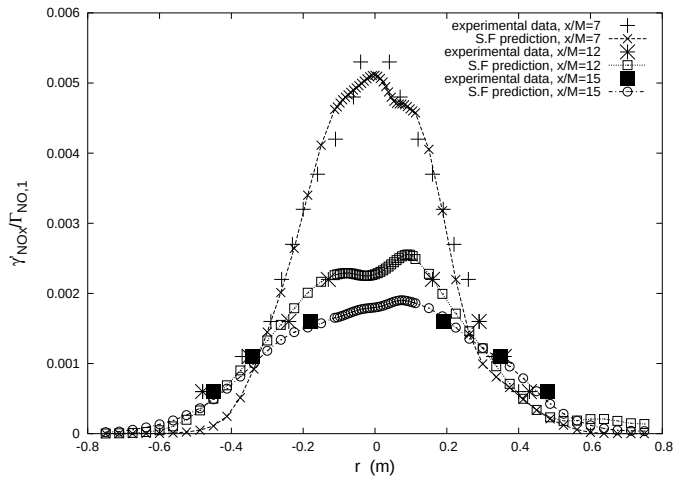

Figure 3.5: Radial profiles of rms NO_x at $x/M = 7$, 12 & 15. Predictions using the Ito Stochastic Field method. Experimental data from [5].

Results for the mean and rms values of NO_2, as predicted by the Ito Stochastic Fields method, are shown in Figs. 3.6 and 3.7. For both mean and rms, the data collapses well when normalised by σ, showing that NO_2 profiles develop at the same rate as the plume. For these inlet conditions, in the region where measurements were taken, the centre-line measurements of NO_2 mean and rms change very little. Only results at $x/M = 9$ and 15 are shown for clarity, but results at all other measuring locations also collapse to the same curves. It can be seen that the Stochastic Fields method predicts these trends well, with a $\langle \Gamma_{NO2} \rangle$ over-prediction of $\sim 5\%$. For γ'_{NO2} the shape of the curve is predicted accurately, but with an under-prediction of around 20%. As the rms values for the passive scalar were correctly predicted (Fig. 3.5), it may be conjectured that different turbulent timescales are needed for conserved and reactive scalars. Cha and Trouillet [45] discuss this in more detail and provide a model for T_{eddy} which may offer an improvement over our current modelling. However, the method of bounding the Wiener term numerically may also contribute to predicting a smaller variance than the measurement.

Also included in Fig. 3.6 are results obtained by using a non-stochastic advection-

diffusion-reaction method, i.e. applying Eq. (2.7). The same inlet conditions and value of K were used. As mentioned previously, this is equivalent to ignoring the effects of segregation and using only mean quantities in the calculation of the mean reaction rate. This method over-predicts NO_2 production by about 30%. Hence neglecting the effects of segregation appears to give a reaction rate that is too high. If we consider Eq. (1.3), we can infer that the correlation coefficient $\overline{\phi'_{NO}\phi'_{O_3}}$ is not negligible and takes a negative value. This is fully consistent with experimental data [5], as will be discussed later.

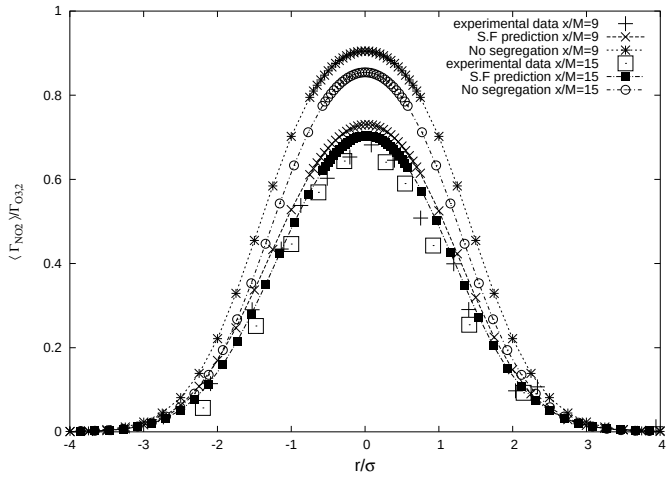

Figure 3.6: Radial profiles of mean NO_2 at $x/M = 9$ & 15. Predictions with the Ito Stochastic Fields method and also by ignoring segregation effects. Experimental data from [5].

3.3.3 Effect of Varying Inlet Concentrations

Brown and Bilger [5] also present measurements of reactive scalars taken at a fixed location, but with a range of inlet concentrations. This fixed point is the centre-line at $x/M = 15$. Our Stochastic Field code was also used to predict these results. $\Gamma_{O3,2}$ was varied, which has the effect of varying the overall Damköhler number, defined in Eq. (3.1). From here on 'low Da' refers to $Da \approx 0.1$, 'intermediate Da'

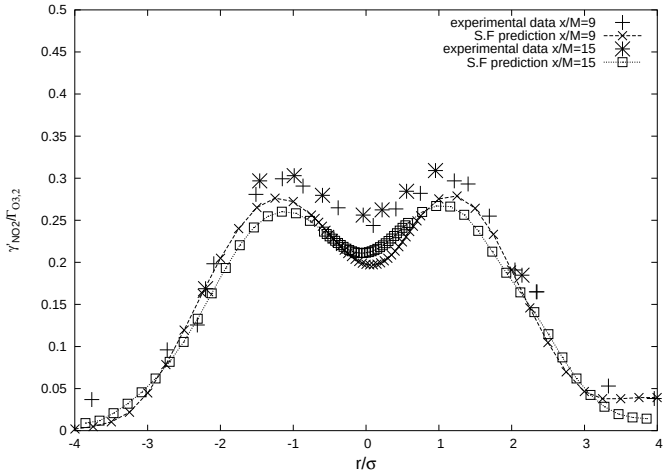

Figure 3.7: Radial profiles of rms of NO_2 at $x/M = 9$ & 15. Predictions with the Ito Stochastic Fields method. Experimental data from [5].

to $Da \approx 0.2$ and 'high Da' to $Da \approx 0.6$. The O_3 inlet concentration was also used to normalise mean and rms results for all reactive scalars. The NO inlet concentration was also varied and $\psi = \Gamma_{O3,2}/\Gamma_{NO,1}$ is the parameter used to characterise this. $\overline{U}$ only varied by small amounts and this was taken into account in the input used for each calculation.

Results for the mean values of NO and NO_2 are shown in Figs. 3.8 and 3.9. Calculations obtained by neglecting segregation are also shown for comparison. It can be seen that, for all Da, the experimental NO mean data collapse onto a single curve. The results produced by the Stochastic Fields model fit well on to this line. Results produced by neglecting segregation fit well at lower ψ, but the NO is under-predicted by almost an order of magnitude (Fig. 3.8) at higher ψ. Fig. 3.9 shows that the predicted trend for NO_2 with Da and ψ agrees well with experiment. Increasing Da increases the reaction rate and hence NO_2 concentration increases at a fixed point, while decreasing $\Gamma_{NO,1}$ (increasing ψ) decreases the amount of NO_2 produced at a point. These trends are predicted very well by the model. For high Da, the S.F. prediction agrees very closely with the experimental data, while

for intermediate and low Da, the NO_2 is over-predicted by about 10%. Without segregation effects, the NO_2 concentration happens to be correctly predicted only at the highest ψ, but is over-predicted by 20–30% at all other values measured. This is further evidence that segregation is important and should not be neglected in this experiment.

The observation that the smallest segregation effect for NO_2 is found with high Da but low $\Gamma_{NO,1}$ can be explained using Fig. 3.10. Case 1 is the case used in Section 3.3.2, i.e. $\Gamma_{NO,1} = 515$ ppm and $\Gamma_{O3,2} = 1.02$. Case 2 has $\Gamma_{NO,1} = 232$ ppm and $\Gamma_{O3,2} = 2.47$ ppm. As described above, Case 1 gives centre-line values of $\langle\Gamma_{NO2}\rangle$ that change very little, indicating that the production of NO_2 by the reaction balances the loss from the centre-line due to turbulent diffusion. In Case 2, on the other hand, the higher O_3 concentration leads to a higher initial reaction rate as shown by the high $\langle\Gamma_{NO2}\rangle$ near the nozzle. This higher reaction rate and hence higher Da also leads to a greater segregation effect than in Case 1 for this early part of the plume. However for Case 2 the high reaction rate, coupled with a smaller initial quantity of NO, leads to NO being used up so that reaction no longer balances the turbulent diffusion and the centre-line value of NO_2 declines. With the SF solution the decline is more gradual as the early plume reaction rate is less so the NO is not used up as rapidly. Hence both solutions converge towards an NO_2 level which is ultimately limited by the supply of NO.

Finally, shown in Figs. 3.11 and 3.12 are results for γ'_{NO} and γ'_{NO2}. Again, the results for the reactant NO collapse well on to a single curve and the model predicts this quite well. For NO_2, the trends with $\Gamma_{O3,2}$ and $\Gamma_{NO,1}$ are correctly reproduced, but the actual values are around 20-25% below experimental data at low ψ with the predictions becoming more accurate at higher ψ. The results seen for the rms of O_3 are almost identical to those for NO_2. We may conclude that the S.F. method predicts the mean concentrations of reactant and product species very accurately, while the variances are predicted with less, but still quite acceptable accuracy.

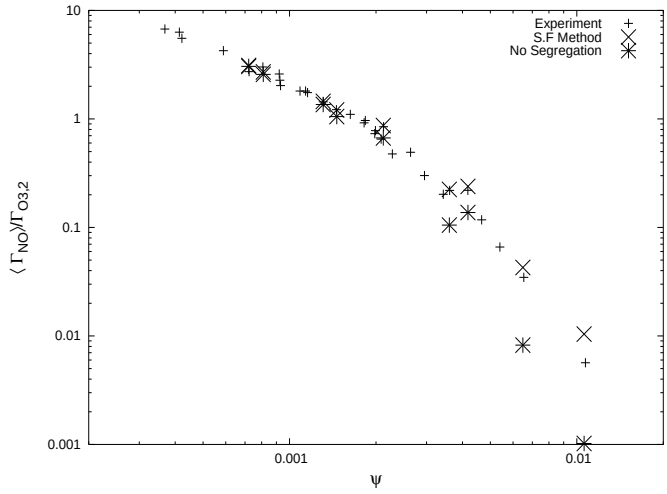

Figure 3.8: Experimental and predicted mean NO at $x/M = 15$, with varied initial reactant concentration ratio and Da. Predictions by the S.F. method and by ignoring segregation. Experimental data from [5].

3.3.4 Segregation Coefficient

The segregation coefficient, α, is defined as the covariance of the reactants divided by the product of the mean quantities of the reactants, i.e.

$$\alpha = \frac{\overline{\phi'_A \phi'_B}}{\overline{\phi}_A \overline{\phi}_B} \tag{3.5}$$

Therefore in this case,

$$\alpha = \frac{\overline{\gamma_{NO}\gamma_{O3}}}{\langle \Gamma_{NO} \rangle \langle \Gamma_{O3} \rangle} \tag{3.6}$$

Fig. 3.13 gives the clearest indication that segregation cannot be ignored since significant negative values for α were obtained in experiment. This means that the reaction rate will be markedly less than that calculated using only mean values, and this has indeed been found throughout the work presented in this chapter. The segregation coefficient decreases with increasing ψ, consistent with the decay of the reactant fluctuations (Fig. 3.11). The ability of the Stochastic Fields model

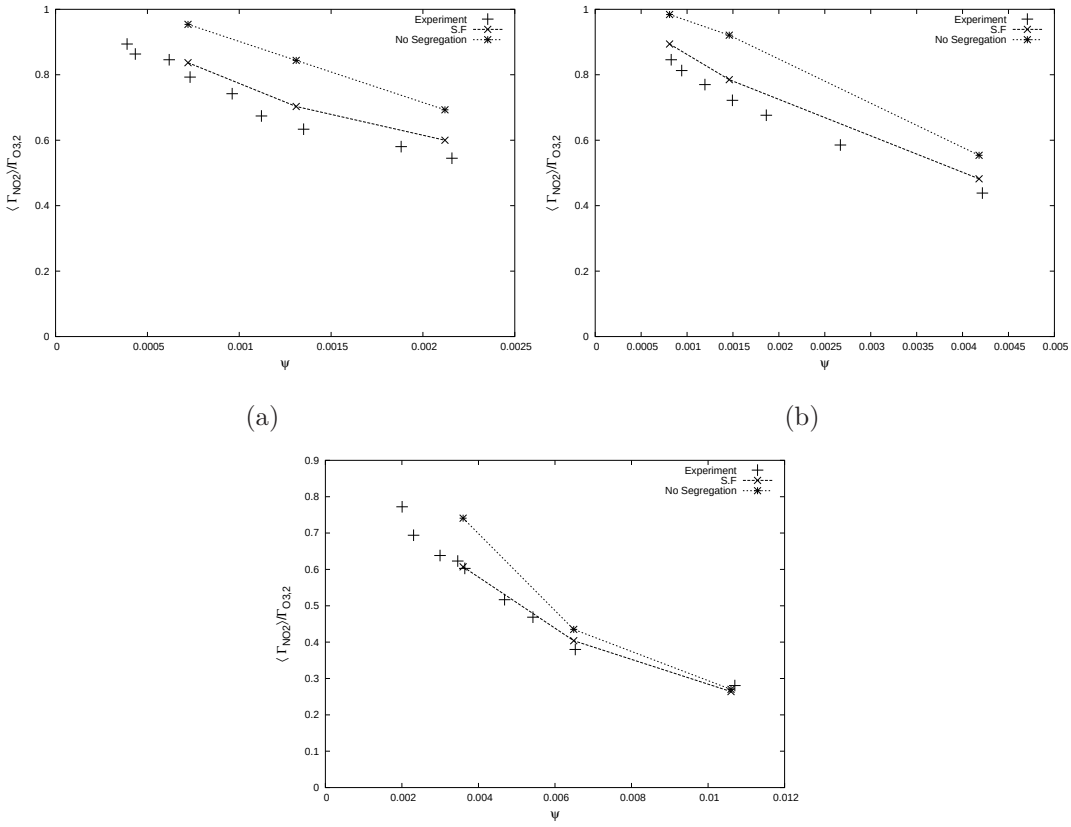

Figure 3.9: Experimental and predicted mean NO_2 at $x/M = 15$, with varied initial reactant concentration ratio. (a) Low Da; (b) intermediate Da; (c) high Da. Predictions by the S.F. method and by ignoring segregation. Experimental data from [5].

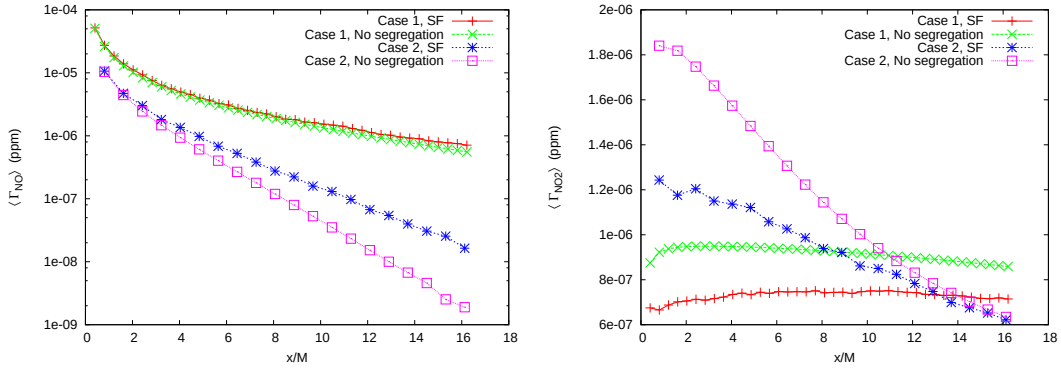

(a) (b)

Figure 3.10: Axial development along centre-line of (a) NO and (b) NO_2 concentration. Case 1: $\Gamma_{NO,1} = 515$ ppm, $\Gamma_{O3,2} = 1.02$ ppm. Case 2: $\Gamma_{NO,1} = 232$ ppm, $\Gamma_{O3,2} = 2.47$ ppm.

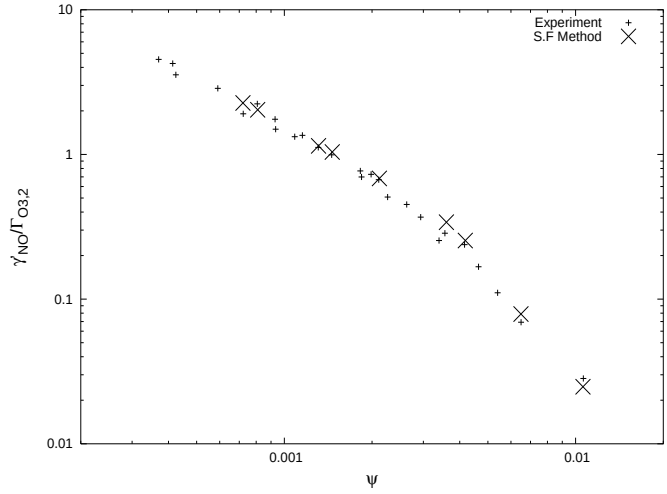

Figure 3.11: Experimental and predicted rms of NO at $x/M = 15$, with varied initial reactant concentration ratio and Da. Experimental data from [5].

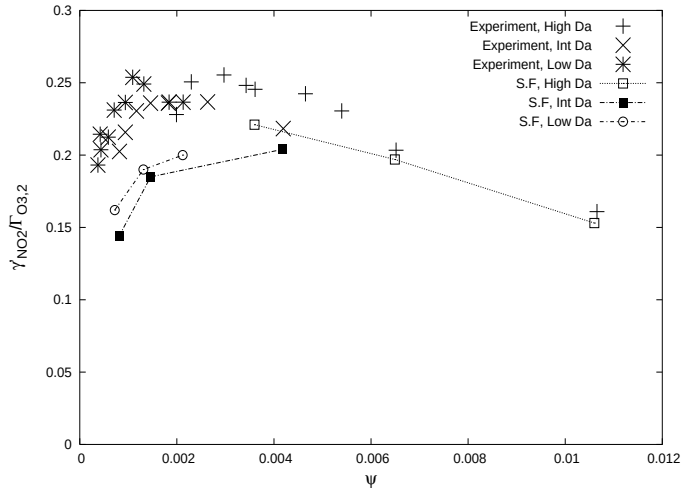

Figure 3.12: Experimental and predicted rms of NO_2 at $x/M = 15$, with varied initial reactant concentration ratio and Da. Experimental data from [5].

to take account of segregation is shown very clearly in Fig. 3.13, in which the calculated α agrees very well with experimental data. The close agreement in Fig. 3.13 also explains the accurate predictions of the mean values of reactant and product concentrations presented earlier.

3.3.5 Conditional Statistics

Brown and Bilger [6] also present conditional concentration statistics for their experiment. These are reacting scalar concentration statistics conditional on the value of the conserved scalar (NO_x) concentration. Fig. 3.14 shows a scatter plot of normalised O_3 (a reacting scalar) concentration against normalised NO_x concentration taken on the centre-line at $x/M = 15$ for $\psi = 0.00146$. Experimentally, the data was obtained by taking simultaneous measurements of two scalars. Numerically, the data was easily obtained from our Stochastic Fields code by plotting the O_3 and $NO_x = NO + NO_2$ values from each field for one spatial node and timestep. It can be seen that the conditional means from experiment and prediction are close to each other which further demonstrates our code's ability to predict the correct sin-

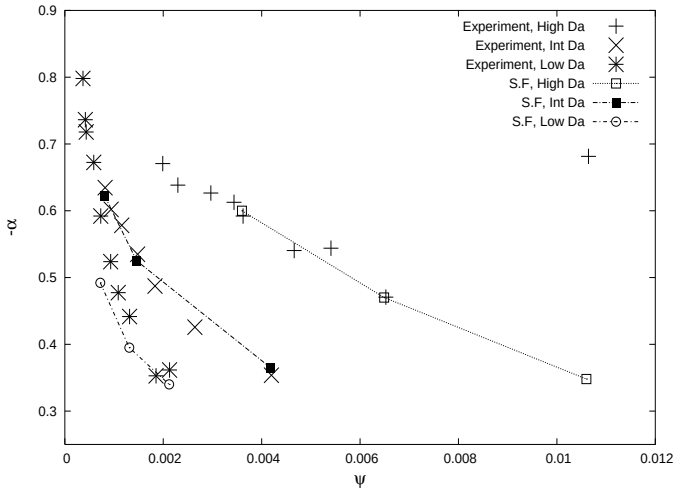

Figure 3.13: Experimental and predicted values of segregation coefficient, α, with varied initial reactant concentration and Da. Experimental data from [5].

gle point scalar statistics. It can also be seen that the conditional variance of O_3 is predicted to be too small. This is consistent with the observations made above that while conserved scalar variances are correctly predicted those for reacting scalars are under-predicted.

3.3.6 Reactive Flow Using Stratonovich Method

Simulations have also been attempted using the Stratonovich formulation, as described in Section 3.2. Initially the same inlet profiles as were used for the Ito simulations, i.e. a Gaussian plume with $K = 2.048 \times 10^{-3}\text{m}^2\ \text{s}^{-1}$ allowed to develop for 0.025s. When this was used with the two-step scheme of Eq. (2.14) it was found to be unstable even with a timestep reduced to $\Delta t = 0.001$s. The results were rapidly dominated by saw-toothed perturbations.

With the third-order Runge-Kutta scheme, Eq. (2.13), and $\Delta t = 0.01$s it was possible to obtain a solution. However as can be seen in Figs. 3.15 & 3.16 this solution is not accurate. The mean radial profile at $x/M = 7$ shows saw-toothed 'wiggles.' A solution produced using Eq. (2.7) for an inert scalar is also shown for

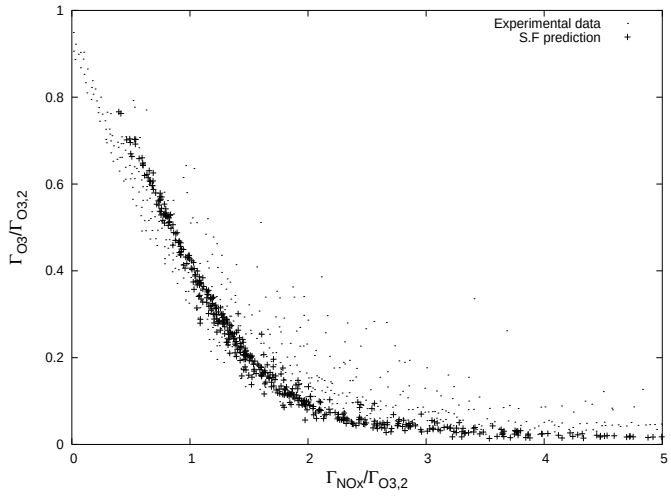

Figure 3.14: Experimental and predicted scatter plots of O_3 concentration versus conserved scalar NO_x concentration at $x/M = 15$. Experimental data from [6].

comparison. This diffusion-only solution agrees, as expected, with the experimental data and it can be seen that the Stratonovich solution gives values greater than this. Although not shown in Fig. 3.15, this is the case across the whole 2D profile. The SF method should leave inert scalar means unchanged and hence we can deduce that this Stratonovich solution has not conserved mass in this case. The error in the rms is even more apparent, whereas the Ito solution shows very good agreement with experimental data, the maximum for the Stratonovich solution is more than double the experimental value. Very little improvement was observed when a timestep of $\Delta t = 0.001$s was used.

It may have been possible with a refinement of the grid or still smaller timesteps to produce a stable, accurate solution but this would have caused the Stratonovich solution to take longer than the Ito solution. The presence of the VODPK solver in the Ito solution causes it to be more expensive for the same number of timesteps but, while 100 fields for 500 0.01s timesteps took the Ito code $\sim$ 141 minutes, 100 fields for 5000 0.001s timesteps took $\sim$ 420 minutes. As the Ito code has been shown here to produce results in very good agreement with the experimental data for the

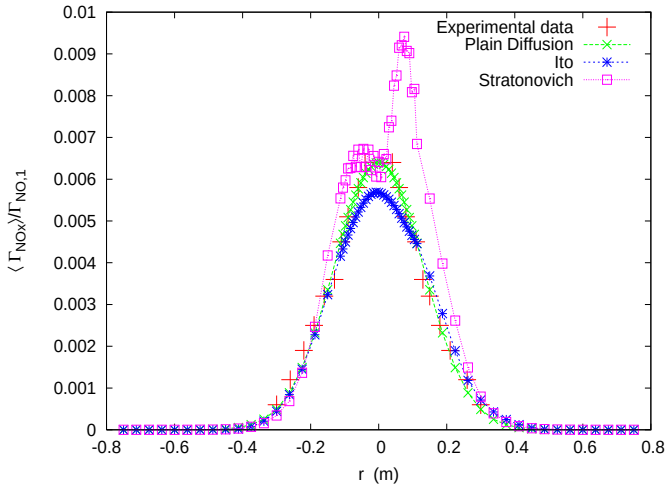

Figure 3.15: Radial profiles of mean NO_x at $x/M = 7$. Predictions using both Ito and Stratonovich Stochastic Fields method, $\Delta t = 0.01$s using 100 fields. Experimental data from [5].

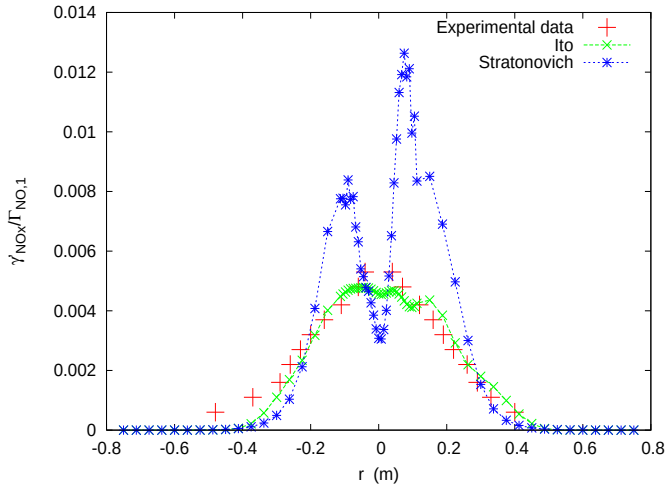

Figure 3.16: Radial profiles of NO_x rms at $x/M = 7$. Predictions using both Ito and Stratonovich Stochastic Fields method, $\Delta t = 0.01$s using 100 fields. Experimental data from [5].

larger timestep it was decided to pursue the Ito method. It may be the case that the increased numerical diffusion for the Ito method seen in Section 2.2.5 leads to increased stability for sharp initial gradients.

In order to show the equivalence of the two methods for reactive scalars the simulations were performed using smoothed initial profiles. The inlet profiles were changed to those given by a Gaussian plume with $K = 2.048 \times 10^{-3}\text{m}^2\ \text{s}^{-1}$ after 3s, equivalent to an approximate distance of $5M$ downstream of the nozzle. This was done for both Ito and Stratonovich cases. Mean NO_x profiles after 4.25s of simulated time, or $7M$, are shown in Fig. 3.17. This is equivalent to $12M$ downstream if the initial $5M$ is equivalent. It can be seen that the two methods agree well with each other and with the experimental data. However in Fig. 3.18 we see that, while the two methods agree well, they both under-predict the rms. This is because the initial part of the plume, where strong gradients lead to the production of variance, has been neglected. This shows the importance of using correct initial conditions.

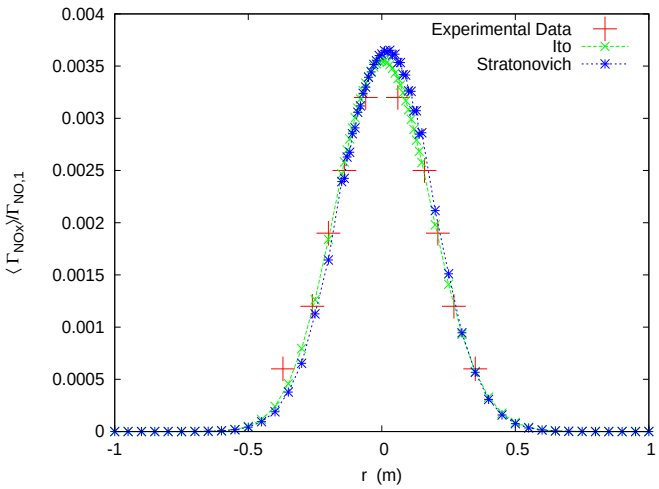

Figure 3.17: Radial profiles of mean NO_x at $x/M = 12$. Predictions made using Gaussian plume after 3s as initial profiles with both Ito and Stratonovich Stochastic Fields method, $\Delta t = 0.01$s using 100 fields. Experimental data from [5].

Figs. 3.19 & 3.20 show the normalised mean and rms of a reactive scalar, NO_2,

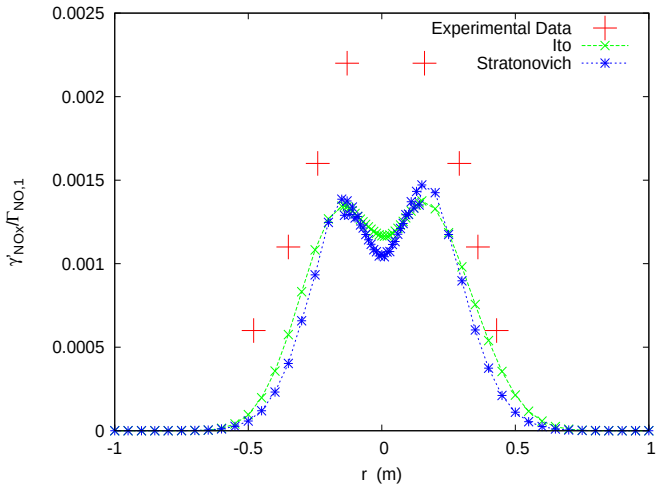

Figure 3.18: Radial profiles of NO_x rms at $x/M = 12$. Predictions made using Gaussian plume after 3s as initial profiles with both Ito and Stratonovich Stochastic Fields method, $\Delta t = 0.01$s using 100 fields. Experimental data from [5].

at an effective downstream position of $x/M = 12$. Here we can see that the two methods give almost identical results for both mean and rms for this species. All other species mean and rms values are also in agreement, so we can conclude that the two methods are equivalent for reactive scalars provided that the initial conditions are such that stable solutions can be generated.

3.4 Discussion

The Ito Stochastic Fields method predicts mean scalar concentrations with high accuracy when compared to experimental measurements in a reacting plume. The accuracy of the predictions is more impressive when compared to those neglecting the effects of segregation. The axial and radial development of the conserved scalar plume is predicted with high accuracy for both mean and rms values as shown in Section 3.3.1. The same is also true for the mean reactive scalar concentration, as seen in Section 3.3.2, although with peak values over-predicted by around 5%. The

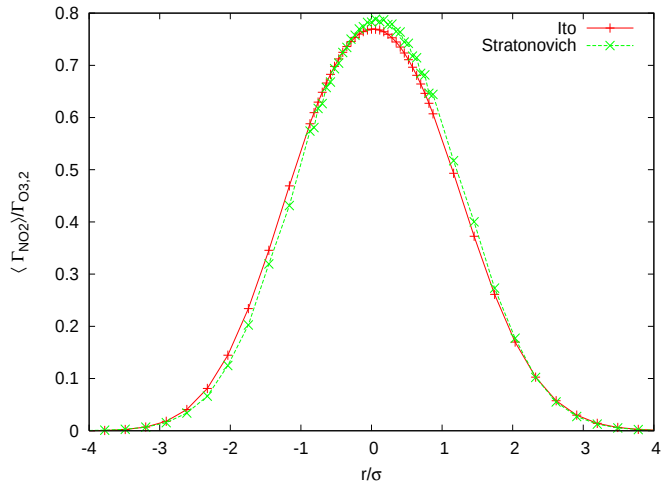

Figure 3.19: Radial profiles of mean NO_2 at $x/M = 12$. Predictions made using Gaussian plume after 3s as initial profiles with both Ito and Stratonovich Stochastic Fields method, $\Delta t = 0.01$s using 100 fields.

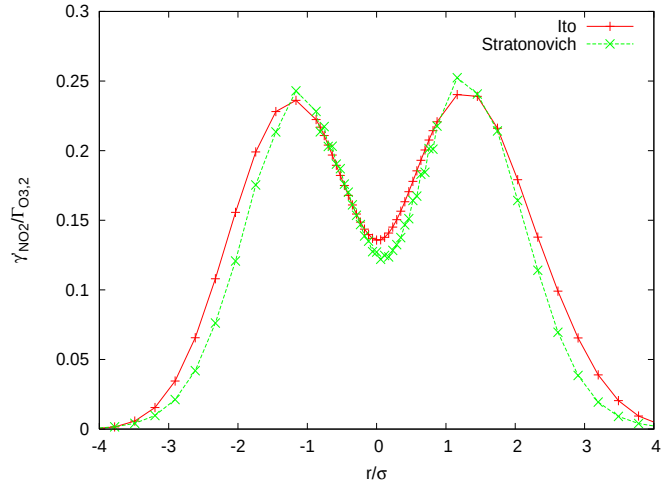

Figure 3.20: Radial profiles of NO_2 rms at $x/M = 12$. Predictions made using Gaussian plume after 3s as initial profiles with both Ito and Stratonovich Stochastic Fields method, $\Delta t = 0.01$s using 100 fields.

trends observed when inlet reactant concentrations are altered are also predicted well (Section 3.3.3).

The rms values for the concentrations of NO_2 and O_3 (i.e. reactive scalars) were consistently under-predicted by around 20%. As the inert scalar rms was predicted accurately, the smaller accuracy in the predictions of the reactive scalar rms may suggest that the micromixing model could be improved. One such improvement would be the use of different timescales [45], while another improvement could be the use of different models altogether (e.g. modified IEM [32, 38], IEM with stochastic frequency [77]). It may also be necessary to improve the numerical solution of the stochastic differential equation by use of a more complex scheme than the Euler approximation used here [67]. This would be at the expense of greater computational effort as any such scheme would involve a more complicated expression to be calculated.

In the present case, where only two species take part in a single reaction, it has been feasible to use 500 fields, which gave smooth results for the means, the rms, and the correlations. However, when more detailed chemistry is to be used, then it is not possible to use such a large number of fields as the computational requirements are too high. Although a direct comparison cannot be made, a crude assessment of the cost of the present Stochastic Fields method that used one-step chemistry, relative to the CMC method that has been used previously for a similar problem [17] with detailed chemistry, suggests that the CMC method may be cheaper. On the other hand, the Stochastic Fields method offers direct access to the whole PDF of the reacting scalar, which may have an implication for Air Quality studies.

3.5 Conclusions

In this chapter the results of applying the Stochastic Fields method to a laboratory reacting plume have been presented. This has been done using both the Ito and Stratonovich formulations. It has been found that the Ito method used here was

the more robust method when using sharp initial profiles. While giving identical results when used with a smooth inlet profile, the Stratonovich methods used here proved to be unstable when using the more realistic sharp inlet profiles. While the Stratonovich method could doubtless be improved, it was decided to concentrate on producing results with the Ito method, with which good results could be obtained with relative ease.

The experiment modelled [5, 6] was chosen because of its detailed measurements of not only mean quantities but also variances and co-variances. Results for the mean and rms of an inert scalar, NO_x, were found to be in very good agreement with the experimental data thus validating the values of K and T_{eddy} used. Predictions for mean values of reactive scalars were found to be within 5-10% of the experimental values. Predictions obtained by assuming perfect micromixing, on the other hand, were found to over-predict the production of NO_2 by upwards of 30%. The rms values for NO_2 using the SF method were found to be around 20% smaller than experimental values. Given that the inert scalar variance was correct this could be because different mixing timescales should be used for inert and reactive scalars. The SF code was also found to predict segregation coefficient (Eq. (3.5)) very accurately. Given that these values were of the order of -0.5, it can clearly be seen why neglecting reactant segregation can lead to large errors when attempting to simulate this experiment.

The success with which the Ito Stochastic Fields code modelled this experimental set-up can be taken as validation of both the Stochastic Fields method and the numerical implementation of it used here. In the next chapter the method is applied to more practical examples of turbulent reacting flows in a local 'street canyon' and also in the exhaust jet of an aircraft engine.

Chapter 4

Application of the Stochastic Fields Method to Practical Situations

In Chapter 3 the ability of the Stochastic Fields method to accurately predict the evolution of a simple turbulent reacting plume was demonstrated. In this chapter the method is applied to situations more closely resembling those found in the 'real world.' As was stated in Section 2.1.2, Eq. (2.6) requires information about the velocity and turbulence fields. In Chapter 3 this was provided by experimental data, however when attempting to simulate a reacting flow for which no such data is available, it can instead be provided by a CFD calculation. As transport terms for the scalars on an Eulerian grid must be calculated in the SF method, it makes sense to use the same grid for the CFD and Stochastic Fields and couple the two parts of the calculation. The ease with which this can be done represents one of the major advantages of using the Stochastic Fields method to perform transported PDF simulations. In the next section details of the method used to couple the CFD and SF solvers are described, while later sections present results of simulations of an aircraft jet exhaust plume and a polluted street canyon.

4.1 Numerical Methods

The results presented in this chapter have been obtained using a Stochastic Fields code coupled with the 'FLUENT' CFD package [10]. This has been done, as outlined in Section 2.2.1, by using a fractional step method where advection-diffusion terms are solved first, then the Wiener or random term and finally the chemistry and micromixing terms. We make use of the User Defined Scalars (UDS) available in FLUENT, these are up to 50 arbitrary scalars, ϕ_i, for which FLUENT solves a transport equation:

$$\frac{\partial \rho \phi_i}{\partial t} + \frac{\partial}{\partial x_k}(\rho u_k \phi_i - \Gamma_i \frac{\partial \phi_i}{\partial x_k}) = S_{\phi_i} \quad i = 1, ..., N \tag{4.1}$$

This equation is solved by an iterative, implicit method, which should ensure the stability of the advection-diffusion scheme. If we set the source term S_{ϕ_i} to zero and set $\Gamma_i = \rho K$ then FLUENT will solve the first advection-diffusion fractional step for each scalar in each field as required. We assume a turbulent Schmidt number of unity and thereby set ρK equal to the effective dynamic viscosity, which is calculated by FLUENT in the CFD solution. In order to have full control over the timestep, the simulation is run as an unsteady case, so advection-diffusion is solved for all scalars for one timestep before a user defined subroutine is used to perform the remaining fractional steps and update the scalar values before the next timestep. Full use of the UDS function in FLUENT can only be made by using the Ito implementation of the SF method. If the Stratonovich interpretation is used then the second-order 'diffusion' term is not required and the deterministic diffusivity gradient term of Eq. (2.8) would need to be calculated as part of the user defined subroutine. This would remove some of the advantage of coupling with the CFD solver.

The second fractional step is the random forcing term. The increment of a Wiener process is once again given by $dW_k^n = \xi_k^n dt^{1/2}$ where ξ_k^n is a Gaussian random number with zero mean and unity variance. An independent value of ξ is required for each spatial component in each field. Within the same field scalars will have the same

value for a given component. FLUENT provides the three Cartesian components of gradient for each scalar and hence the second fractional step can be calculated as

$$\begin{aligned}\tau_i^n(t+\Delta t) &= \tau_i^n(t^*) \\ &\quad +(2K)^{1/2}\left[\frac{\partial \tau_i^n(t^*)}{\partial x}\xi_x^n\right. \\ &\quad \left.+\frac{\partial \tau_i^n(t^*)}{\partial y}\xi_y^n+\frac{\partial \tau_i^n(t^*)}{\partial z}\xi_z^n\right](\Delta t)^{1/2} \end{aligned} \tag{4.2}$$

at each grid cell for each scalar i in every field n. K is found by dividing the effective dynamic viscosity from the CFD by the density. As in Chapter 3, the maximum size of the Wiener step is limited to the difference between the current scalar value and it's upper or lower physical limit. One scalar in each field represents temperature and by applying Eq. (4.2) to this scalar the effect of fluctuations of temperature on the reaction rate is considered. The temperature is unaffected by the reaction of other scalars in this flow as the heat released by them is small and as such the mean temperature is unaffected, as is the flow field. This means that, for this flow, the CFD solution does not require information from the Stochastic Fields code and hence a steady-state CFD solution can be used, i.e. one-way coupling.

The final fractional step involves the chemistry and micromixing terms. This is performed separately for each grid cell in turn. The mean for each scalar is calculated first before the scalars, together with $T_{eddy} = k/\epsilon$ (taken from the CFD solution), are used in Eq. (4.3) to evaluate the effect of chemistry and micromixing for each field at a time:

$$\frac{d\tau_i^n}{dt} = \dot{w}\left(\tau_1^n, \tau_2^n, \ldots, \tau_N^n\right) - \frac{\tau_i^n - \overline{\phi}_i}{T_{eddy}} \tag{4.3}$$

In both the jet exhaust and street canyon solutions stiff chemistries are used and hence stiff solvers are required to solve Eq. (4.3). The solvers used were VODPK and CHEMEQ2, which is faster but at the expense of some accuracy when compared to VODPK. Further details about the two solvers can be found in Section 2.2.6. In

order to place a check on the errors due to calculating the mean concentration $\overline{\phi}_i$ before Eq. (4.3) is solved we also calculated the micromixing term separately after the chemistry using the analytical solution to the IEM model shown in Eq. (2.16).

As the chemical mechanisms used in this chapter have several species (24 species for the jet problem and 28 for the street canyon) and FLUENT only allows for 50 UDS, it can be seen that this does not leave much scope for using many fields. However, the only term in which the fields influence one another is the micromixing term. Therefore, the first two fractional steps can be performed in batches of one or two fields, while the other fields are stored in memory. After the first FLUENT timestep the user subroutine performs the second fractional step on the UDS before writing these scalars to memory and writing a new batch of scalars to the UDS. This is repeated until all scalars have undergone the first two steps. The chemistry and micromixing step is then performed on all scalars before the process starts again. It has been found that this swapping process takes very little time compared to the rest of the calculation and, as the flow solver can be switched off, this method is not significantly slower than calculating all fields simultaneously. Means and rms values for each scalar can be calculated and stored in memory throughout the grid. These can then be processed using FLUENT's post-processing tools.

There are several advantages to using an existing CFD package. A CFD solution has to be produced anyway to provide $\overline{u}$, K and T_{eddy} so it is clearly useful to use this same solution for the Stochastic Fields simulation, there is no need to produce a new grid and export flow field data from the CFD to the new grid. The treatment of advection and diffusion as well as boundary conditions is well developed in commercial CFD and hence there is no need for this to be repeated. It is also straightforward to switch between the different modelling options in the CFD, provided that $\overline{u}$, K and T_{eddy} can be found. The existing meshing and post-processing tools can be used making it simple to set up new problems and extract required data. Furthermore, parallelisation with splitting the mesh between CPU's is then easily done. This is particularly efficient with this Stochastic Fields code

as the expensive chemistry and micromixing terms require only local data, so that during this fractional step each CPU can run without incurring penalties due to the need to communicate with others.

4.2 Simulation of the Evolution of An Aircraft Exhaust Plume

4.2.1 Introduction

Given the rise in commercial air travel in recent times, the levels of pollution that people living or working near airports are actually exposed to has become increasingly important [78]. This is currently even more important as future designs of jet engines will have to compromise between higher efficiencies and reduced NO_x emissions [79]. In order to calculate correctly the levels of pollution the chemistry of individual plumes needs to be considered rather than just long term average concentrations. The large amounts of pollutants such as NO_x in the jet exhaust mean that even a considerable distance away from the aircraft the concentration in the plume will be much greater than an averaged background value. Some practical studies have been conducted to measure these levels such as by [80] who measured NO, NO_2 and CO_2 downwind of a runway at JFK airport and matched peaks with individual aircraft. Predicting computationally these levels is complicated by the turbulent nature of the flow and the reactions taking place destroying the primary pollutants and producing other, secondary, species.

Studies have been performed on the chemical evolution of jet plumes at altitude, some of these [81] concern the region where the plume interacts with the wake vortices. However, much of the production of these secondary pollutants will take place close to the jet exhaust. The extent of this production will be controlled by the conditions in the jet itself and as such an insight into the effect of the jet on the chemistry will be of use. Whereas the wake vortex region at altitude will have

a different composition and temperature from sea level, conditions in the early jet are set by the engine and so may be compared. Kärcher et al [72] have performed calculations of this early jet regime (1-2km) for an aircraft cruising at altitude using a reaction mechanism with 23 species and 65 reactions. They calculate the flow field on an axisymmetric grid and use the velocity and temperature field from this at each step to calculate the transport of the scalars. The chemical kinetics are calculated in a separate operator-splitting stage at each step. The key chemical processes they studied were the transformation of NO to NO_2 and primary NO_x and SO_2 pollutants into nitrous, nitric and sulphuric acid, along with the evolution of radicals within the plume. The transformation of NO to NO_2 is of particular importance because, while it is primarily NO that is emitted in the exhaust, it is NO_2 levels that are controlled by regulation [82]. They found that much of the chemistry takes place very early in the jet before turbulent mixing has a significant effect. Sulphuric acid and its precursor SO_3 play an important part in the generation of aerosols in the jet plume both directly and through interaction with carbon particles. This is discussed by Brown et al [83], who also found that condensation occurs closer to the exhaust nozzle when there is a bypass duct compared to a single jet for a High Speed Civil Transport (HSCT) aircraft on account of the mixing due to the bypass being more rapid compared to the axial velocity.

The work discussed above does not include the full effect of the interaction of turbulence and chemistry. It does not include segregation or micromixing. Some attempts to take reactant correlation, or segregation effects, into account in the jet plume problem have been made. Wang and Chen [84] made comparisons for a HSCT at Mach 2.4 between a box model technique assuming perfectly mixed reactants, a box model assuming imperfect micromixing (but perfect macromixing across the plume), a PDF simulation assuming perfect micromixing within a cell and a PDF simulation using the modified Curl's mixing model. Their conclusion was that using the PDF method without micromixing lead to about a 1% reduction in NO_x consumed by reaction compared to the box model approaches and that

inclusion of Curl's model leads to a further 0.2% reduction.

Another simulation of a HSCT plume has been made by Menon and Wu [85] who use a linear-eddy model (LEM) to account for micromixing effects. This method uses a 1D grid with high enough resolution to resolve all length scales in the flow. This grid is marched downstream and expanded to account for large scale entrainment by assuming that the jet can be approximated by a round free jet. The turbulent mixing is represented by random mixing events whose position, timescale and length scale are chosen from appropriate distributions. Reaction-diffusion equations are then solved on the 1D grid. Using this method Menon and Wu show that NO_x consumption is reduced by a further 1% compared to [84]. It is evident from these simulations that segregation has a small impact on ozone and NO_x far downstream from the exhaust, but the extent to which this conclusion can be carried over to the region close to the source and to other species is not fully explored yet.

In this section the Stochastic Fields method has been applied to a hot jet with a bypass flow using the chemistry of [72]. The conditions in our jet were chosen to give a thrust approximately equal to that of a 100kN rated engine at idle thrust on the ground. The size and complexity of the chemical mechanism that can be used with the Stochastic Fields method is limited only by the time and computing resources available. There must be a compromise between having enough fields for statistical accuracy, high enough spatial grid resolution and using a realistic mechanism. We have used 12 and 18 fields and the mechanism used here is taken from [72]. It was developed to model the evolution of the first 2-3km (or around 10s) of a jet engine plume. It has 24 scalars (including temperature) and 65 reactions. It does not include any hydrocarbon chemistry as their reactions take place on a timescale of minutes, too long to affect conditions in our period of interest. This was confirmed in preliminary work undertaken with an alternative mechanism taken from Treviño and Méndez [86]. This 13 species ozone chemistry includes NO_x and CH_2O. The latter affects the chemistry through photolysis reactions which have timescales longer than our period of interest.

It is not the purpose of this work to produce an accurate simulation of a particular jet plume. Rather, the objectives are: (i) to develop a Field Monte Carlo code coupled with a CFD solver that can readily be applied to practical problems. (ii) To investigate the effects of segregation on the chemical evolution of a jet in its very early stages using a realistic chemistry.

4.2.2 Model Problem

4.2.2.1 Jet Plume Flow Field

In this section we discuss the CFD simulation of the jet plume and the conditions in the jet and its surroundings. A simplified geometry is used to represent the rear of a jet engine, it consists of a 0.48m diameter core surrounded by an annular bypass of outer diameter 1.0m. This geometry was incorporated into two grids. The first, known as Mesh 1, has the jet centrally positioned in a 10m diameter circular inlet plane. The mesh extends 50m downstream with the diameter increasing to 60m. There are 72 triangular faces on the core, 206 on the bypass and 1538 on the surrounding ambient air inlet where the meshing has the same spacing as the bypass close at the centre becoming coarser towards the edge. The meshing is projected downstream with the cell sizes growing at the same rate as the overall diameter. The spacing in the downstream direction is initially 0.2m growing with a ratio of 1.112. The total number of grid cells is 50,848.

Mesh 2 is a 5x5x10m box with the jet centre central in the horizontal direction and 2m up in the vertical direction. It has 48 triangular faces on the core, 154 on the bypass and 956 on the surrounding ambient air inlet. The downstream spacing is 0.1m initially growing to a maximum of 0.4m with a ratio of 1.05, giving a total number of grid cells of 45,162. This mesh has greater resolution in the jet axis direction to allow rapid chemical evolution close to the jet to be better observed.

The flow field was computed prior to the reacting flow modelling as a steady-state compressible flow by solving equations for continuity, energy and turbulence using

the $k-\epsilon$ model [10]. Solution parameters used in the CFD solution of the jet are shown in Table 4.1. The jet is assumed to be air. For inlets to the domain static pressure, p; total pressure, P_0 and total temperature, T_0 are specified along with turbulent kinetic energy k and turbulent dissipation rate, ϵ. For outlets from the domain p, T_0, k and ϵ are specified.

Table 4.1: Solution parameters used in FLUENT CFD solution of jet exhaust plume [10].

Solver	3D, segregated, implicit
$k-\epsilon$ model constants	$C_\mu = 0.09$, $C_{1\epsilon} = 1.44$, $C_{2\epsilon} = 1.92$
Pressure-velocity coupling	SIMPLE
Density	Ideal Gas Equation
Discretisation - pressure	PRessure STaggering Option
Discretisation - momentum	1^{st}-order upwind
Discretisation - k	1^{st}-order upwind
Discretisation - ϵ	1^{st}-order upwind

The boundary conditions for the core and bypass have been chosen to give a total thrust of 7kN. The conditions used were atmospheric pressure (101.325kPa) for both core and bypass with gauge total pressures (above atmospheric) of 1.12kPa for the bypass and 15.81kPa for the core. Total temperatures were $T_{0b} = 290$K and $T_{0c} = 422$K, these conditions correspond to Mach numbers of $M_c = 0.46$ and $M_b = 0.13$. Hence the velocities at the engine exit plane were 186ms^{-1} at the core and 43ms^{-1} at the bypass. Static temperatures were 405K in the core and 289K in the bypass.

The total pressure on the conical side boundary was set to be equal to ambient pressure while that on boundary surrounding the bypass was set to be 10Pa above ambient. The latter was done in order to aid convergence of the CFD solution. The ambient turbulence was set to be very low, with values of $k = 1.0 \times 10^{-3}\text{m}^2\text{s}^{-2}$ and

$\epsilon = 1.0 \times 10^{-4}\mathrm{m}^2\mathrm{s}^{-3}$. The turbulence in the jet at inlet was also set to relatively low values of $k = 1.0\mathrm{m}^2\mathrm{s}^{-2}$ and $\epsilon = 1.0\mathrm{m}^2\mathrm{s}^{-3}$, however the results were found to be very insensitive to these parameters. It was found that the turbulence field observed in the plume is that produced by the shear layers between core and bypass and also bypass and ambient.

Fig. 4.1(a) shows a contour plot of mean velocity magnitude on a plane containing the jet axis for Mesh 1. Fig. 4.1(b) depicts contours of radial velocity on a plane 10m downstream of the exhaust, which shows the entrainment of ambient air into the jet. The key turbulence parameters for the Stochastic Fields method are K and T_{eddy}. Contours of ρK are shown in Fig. 4.2(a) and T_{eddy} in Fig. 4.2(b). The very small turbulent timescale in the jet indicates rapid micromixing in this region. A CFD calculation was also performed using the same boundary conditions with the Reynolds Stress model, which gave very similar results. We will use the values of T_{eddy} later for calculating species Damköhler numbers.

To ascertain whether Mesh 2 gives acceptable results, it was used with the same conditions as described above in this section. It was found that there was good agreement for the velocity and turbulence field, indicating that the shorter distance to the side boundaries in Mesh 2 is acceptable. The finer spacing in Mesh 2 should also lead to better resolution for the jet in still air, particularly for the fast chemistry in the early plume.

4.2.2.2 Initial Compositions

The background air chemical composition used in this work is shown in Table 4.2, together with volume fractions of the primary species at the exit plane of the engine core. Conditions in the bypass stream are assumed to be the same as the background. Background O_3, NO and NO_2 values were chosen to be representative of values at sea level in the United Kingdom, 1.0×10^{-13}ppm was chosen for O as this was close to the equilibrium level. Other radical volume fractions have been set to the same

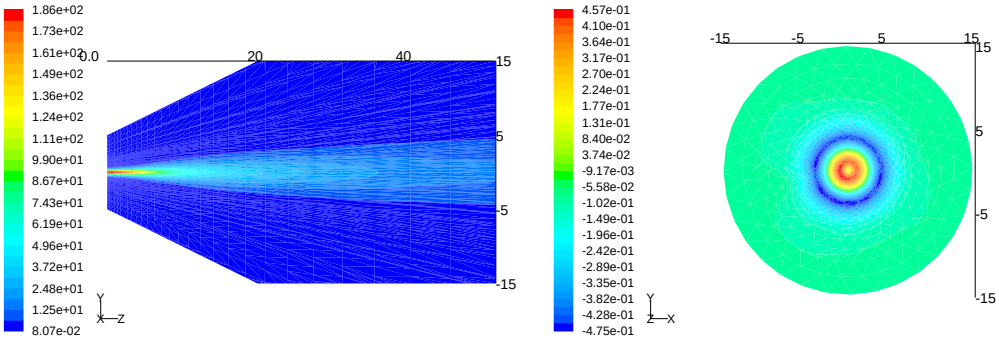

(a) (b)

Figure 4.1: Contours of (a) Mean Velocity Magnitude [m s^{-1}] for Mesh 1 on plane containing the jet axis, (b) Mean Radial Velocity [m s^{-1}] on a plane perpendicular to jet axis 20m downstream.

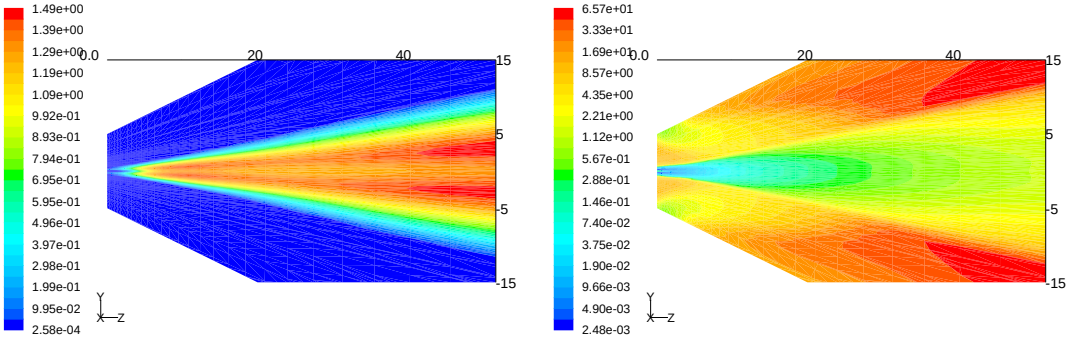

(a) (b)

Figure 4.2: Contours of (a) turbulent viscosity, ρK, [kg m^{-1} s^{-1}] and (b) turbulence timescale, T_{eddy}, [s] for Mesh 1 on plane containing the jet axis.

values as those given in Kärcher et al [72], who suggest that these values are not crucial.

For the conditions at the jet exit plane we again take the values from [72], which should still be representative of a jet at ground level for all species other than NO, NO_2 and OH. The CO_2 level may be higher than in a real jet exhaust, but as an inert scalar in this mechanism it will not affect the chemistry. To estimate the NO_x volume fraction we have used data from the ICAO Emissions Data Bank for the IAE V2525-D5 engine [87] (which has a thrust of 7kN at idle). This gives a fuel flow rate and Emission Index (EI) in g per kg for NO_x at idle thrust at sea level, from which a NO_x mass flow rate can be found. By using perfect gas relations for a compressible flow the total mass flow rate for the core can be found from the conditions at the core (Section 4.2.2.1). This is found to be 29.3kg s^{-1}. Volume fraction can then be found:

$$X_i = \frac{\overline{MW}_{air}}{MW_i} \frac{\dot{m}_i}{\dot{m}_{tot}} \tag{4.4}$$

We chose to follow [72] and make the NO_x at the exit plane 95% NO and 5% NO_2. The SO_2 level corresponds to an EI of 2.9g kg^{-1}, which is not far above the range expected from kerosene [72]. For OH the emission index is uncertain so we chose to use a value that maintained the same proportion between NO_x and OH as found in [72].

4.2.3 Results

For Mesh 1 both the plain advection-diffusion-reaction code and the Stochastic Fields code were used with a timestep of $\Delta t = 5.0 \times 10^{-4}$s. For the Stochastic Fields code a total of 18 fields were used. The solution was found to be steady on average after about 6.0s of simulated time. Results were taken after 8.0s and 10.0s of simulated time. The turbulent time scale in the plume is of the order of 10^{-2}s so taking further results at 2.0s intervals is equivalent to using different random

Table 4.2: Jet core exhaust and background volume fractions.

Species	Core, ppm	Background, ppm
O	0	1.0×10^{-13}
O_2	1.35×10^{5}	2.1×10^{5}
O_3	0	3.86×10^{-2}
H	0	0
H_2	0	9.0×10^{-1}
OH	9.5×10^{-1}	2.8×10^{-7}
HO_2	0	3.6×10^{-6}
H_2O	3.6×10^{4}	8.8×10^{1}
H_2O_2	0	2.4×10^{-5}
NO	1.89×10^{1}	1.86×10^{-2}
NO_2	9.9×10^{-1}	3.14×10^{-2}
NO_3	0	8.9×10^{-9}
N_2O_5	0	1.0×10^{-5}
HNO_2	0	3.4×10^{-7}
HNO_3	0	2.0×10^{-3}
HNO_4	0	1.1×10^{-4}
CO	9.4×10^{1}	4.0×10^{-2}
CO_2	3.8×10^{4}	3.3×10^{2}
SO	0	0
SO_2	5.8	9.1×10^{-6}
SO_3	0	0
HSO_3	0	0
H_2SO_4	0	0

number sequences for results in the plume. Mesh 2 has a finer axial grid resolution and so both the Stochastic Fields code and the plain advection-diffusion-reaction code were used with a timestep of $\Delta t = 10^{-4}$s. For Mesh 2 (Section 4.2.2.1) it was found that the solution was steady on average by 0.5s of simulated time. Mean results were taken at this point for the plain code and Stochastic Fields code. This was done for several runs with different random number sequences, 12 stochastic fields were used with Mesh 2. To run to a simulated time of 0.5s using Mesh 2 the Stochastic Fields code took approximately 100 hours when running in parallel on two Pentium 4, 3.0GHz HT CPU's with 2GB dual channel memory.

4.2.3.1 Inert Mixing

CO_2 is unaffected by chemical reaction in this mechanism, and hence its chemical reaction rate is explicitly set to zero in the solver. Because of this it can be used to characterise the inert mixing of species in the plume. The evolution of CO_2 along a line extending from the centre of the jet is shown in Fig. 4.3. Shown here is the mean volume fraction as calculated by both a simple advection-diffusion method, Eq. (4.1) (labelled "plain"), and by the Stochastic Fields method with 12 fields. There is an almost constant value in the potential core (about 4 core diameters) before rapid dilution when the turbulent mixing reaches the centre of the jet. We also see that the RMS is zero before increasing sharply at this point, this is as expected as the scalar variance is caused by the gradients of the mean.

In the absence of chemistry, terms 4 and 5 of Eq. (2.6) should not affect the first moment of the scalars. Therefore any difference between results for inert mixing by the S.F. method and by Eq. (4.1) must be due to statistical error. The agreement between the two lines on Fig. 4.3 indicate an acceptable level of statistical accuracy in this calculation. This is also supported by the magnitude of the RMS values, which have a peak of 25% of the mean before falling to around 15% downstream, using Eq. (2.19) this corresponds to statistical errors with a peak value of 6% of

the mean, falling to 3.5% downstream, when 18 fields are used. If 12 fields were used the peak statistical error would increase only to 7.2%. It is worth noting that to reduce the peak error to 1% it would be necessary to use 625 fields, which is a prohibitively high number.

As CO_2 is an inert species here and its volume fraction in the background is negligible compared to its value in the jet we can use it to give a mixture fraction by normalising using the jet core inlet value. Richards and Pitts [7] give expressions for mean and rms of mixture fraction ($\overline{\xi}$ and ξ') for the axisymmetric free jet. Along the axis of the jet these become:

$$\overline{\xi} = \left(\frac{\rho_{jet}}{\rho_{air}}\right)^{1/2} \frac{9.52 r_0}{z - z_{0Y}} \tag{4.5}$$

$$\xi' = \left(\frac{\rho_{jet}}{\rho_{air}}\right)^{1/2} \frac{2.19 r_0}{z - z_{0Y}} \tag{4.6}$$

where r_0 is the jet nozzle radius and z_{0Y} is the virtual origin taken at $7.2r_0$. The presence of a co-flowing bypass jet means that this expression is not fully valid here but it may be used to give an approximation. Fig. 4.4 shows the above expressions compared to our simulations. Eqs. (4.5) & (4.6) have been evaluated both by considering only the jet core, which has a radius of 0.24m, and by assuming the jet radius to include the bypass (0.5m) as well. We see that our data initially agrees with the data for $r_0 = 0.24$m, but further downstream the bypass jet has an effect and the gradient of our data with downstream distance becomes closer to that of the larger jet radius case. We also see reasonable agreement between results using the 10m and 50m meshes.

4.2.3.2 Concentrations in the Reacting Plume

First we will consider the progress of the primary pollutants in this mechanism, namely NO and NO_2, using Mesh 1. We can see in Fig. 4.5(a) that in the first few metres NO_2 is produced within the plume. Fig. 4.5(b) shows a corresponding reduction in NO, however due to the much greater concentration of this species in

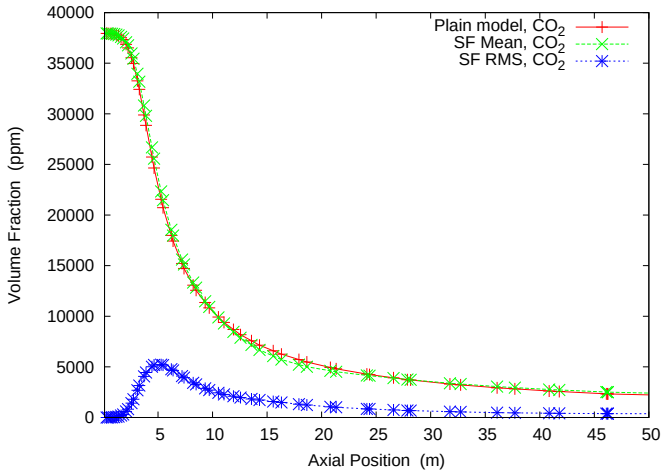

Figure 4.3: Evolution of CO_2 volume fraction in Mesh 1 along the jet axis downstream from jet exit plane. Results for the mean values using the full SF method and simple advection-diffusion are shown together with RMS values from SF.

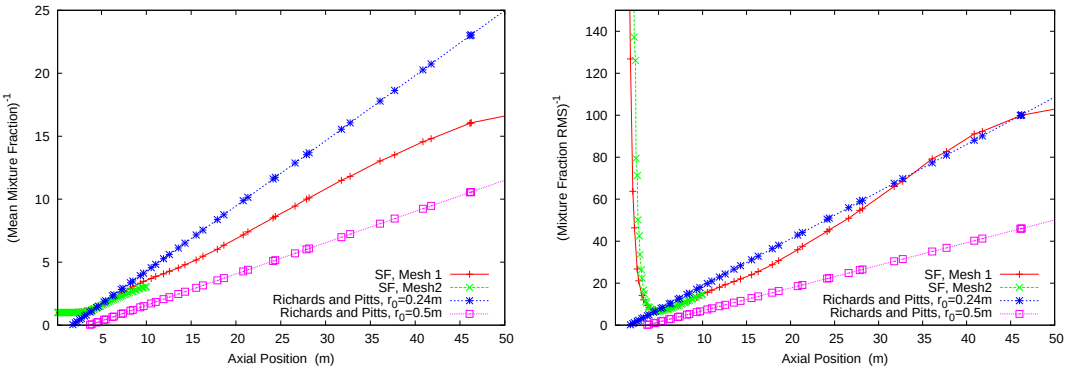

(a) (b)

Figure 4.4: Mean (a) and RMS (b) of mixture fraction, ξ, along jet axis compared with the expression for mixture fraction from [7].

the plume the effect is less pronounced. Once the end of the jet core is reached these species are mixed out into the background. For NO in particular it can be seen that the profile in the reacting jet is very similar to that in an inert simulation. This is due to the high initial concentration in the jet, which means that the chemical effects caused by other more dilute species is small compared to turbulent mixing.

In the jet core ozone, which was set to zero at the exit plane, is initially produced by the reaction $O+O_2 \rightarrow O_3$. The level produced is much lower than ambient levels, and a sharp increase is seen caused by the jet mixing out, Fig. 4.5(c). Further downstream into the mixing regime, the O_3 levels do not approach those in the background and in fact decrease. This is due to the very high level of NO in the plume which reacts with the O_3 by the reaction $NO + O_3 \rightarrow NO_2 + O_2$. The effect on NO and NO_2 is less obvious due to their high concentrations at this stage. In the presence of VOC's, NO_x will act to increase ozone levels overall, but this happens on a timescale considerably longer than the one we are considering. We see in Fig. 4.5 that neglecting micromixing effects does not have a significant effect on predicted levels of these three pollutants. We have seen that the chemistry has little effect on NO_x compared to turbulent mixing, so we would not expect the effect of micromixing on chemistry to have a noticeable influence.

We also see that for NO (and NO_2), see Fig. 4.6(a), the peak variance is located around the end of the jet core and that this peak is relatively distinct. If we compare it with O_3, Fig. 4.6(b), we see that there is also an area of high variance close to the end of the jet core, where large gradients are encountered due to mixing. However, unlike NO, we also observe another region of high variance further downstream, around 40-50m from the jet. This is likely to be because the $NO + O_3 \rightarrow NO_2 + O_2$ reaction is reducing the O_3 concentration significantly compared to its effect on NO and NO_2. In this case the chemistry leads to larger gradients and hence variance downstream for O_3 than NO and NO_2.

We now turn to look at some of the secondary pollutants produced. To do this we use Mesh 2, which has a greater resolution particularly in the downstream direction.

We follow Kärcher [72] by specifying a high initial level of OH and allowing the concentration of other 'fast' species to be determined by the chemical mechanism. These other 'fast' species, O, H, HO_2, NO_3, SO_3 and HSO_3 are produced very rapidly (within the first grid spacing, indicating that they would be formed within the engine). They then decay quickly within the first few metres of the jet. Further downstream they decay to levels lower than those in the background. Fig. 4.7 shows the evolution in the first 10m of three radicals (O, OH and SO_3), O shows the most rapid decay with OH slightly slower. SO_3 actually increases in the first part of the jet, although all three have been substantially consumed well before the end of the jet core at around 3m. When the Stochastic Fields method is used we see a difference in the predicted evolution of these radicals from when segregation is ignored, this can be seen in Fig. 4.8. There is some statistical noise here due to the use of relative few fields (twelve) and higher variance (c.f. Eq. (2.19)). This could be improved by the use of more fields. However, the underlying trend here is clear and the integrated flow rates for the species shown in Section 4.2.3.3, below, show good agreement between simulations using different random number sequences, also even if 18 fields were used instead of 12 the statistical error would only be reduced by less than 20%. After 2.5m the Stochastic Fields and plain chemistry profiles for O and OH are very similar whereas for SO_3 the profile where segregation effects are included shows a reduced concentration. After 7.5m O and OH levels with the plume have fallen to values lower than those in the background, the presence of segregation, however, appears to retard their decay within the plume. The SO_3 level has fallen in the centre of the plume by 7.5m leaving a region of increased concentration at the edge of the plume. Again, when we take into account segregation we see that this peak is reduced in height and moves towards the plume centre and the concentration within the plume is increased. These differences are seen because the reactions involving these radicals at the edge of the plume are fast enough for the segregation to affect the reaction rate.

Brown et al [83] discuss the role of H_2SO_4 in aerosol production. This is formed

from SO_2 in the exhaust via the intermediate species SO_3 and HSO_3. Fig. 4.9 shows the evolution of H_2SO_4 along the centre-line of the jet. We see that it is produced very rapidly; i.e. within the jet core before being mixed out by turbulent diffusion. Taking segregation into account has no discernable effect on the mean concentration, however the RMS fluctuations are of the order of 10% of the mean from the point where the turbulence reaches the centre-line (3-4m) onwards. Given the highly non-linear nature of the binary nucleation process [88] these fluctuations in acid vapour concentration could have a significant effect on aerosol production. For further discussion on the effects of turbulence on aerosol formation see Chapter 5.

HNO_2 and HNO_3 are produced in the jet until a constant equilibrium level is reached which lasts until the end of the jet core. H_2O_2 is produced very rapidly, and would in fact be produced in the engine itself. Its concentration is reduced slightly by chemistry in the core before it is mixed out. Again we find that considering micromixing effects does not have a significant bearing on the predicted concentrations of these species. Fig. 4.10 shows this along the centre-line of the jet. The two predictions also agree in the radial direction as well, although this is not shown. This lack of segregation is most likely to be because most of the chemistry takes place early on within the plume rather than between species mixing from inside and outside of the plume [72]. The exception to this is the $NO - O_3$ reaction discussed above. We have specified the inlet concentrations to be uniform across the jet. Due to this there are no gradients to cause segregation in the region where most of the reaction takes place. By the time the turbulence mixes into the jet the reaction has been nearly completed. If the concentration were not uniform in the jet, perhaps due to effects in the nozzle, then the effect of segregation may not be insignificant.

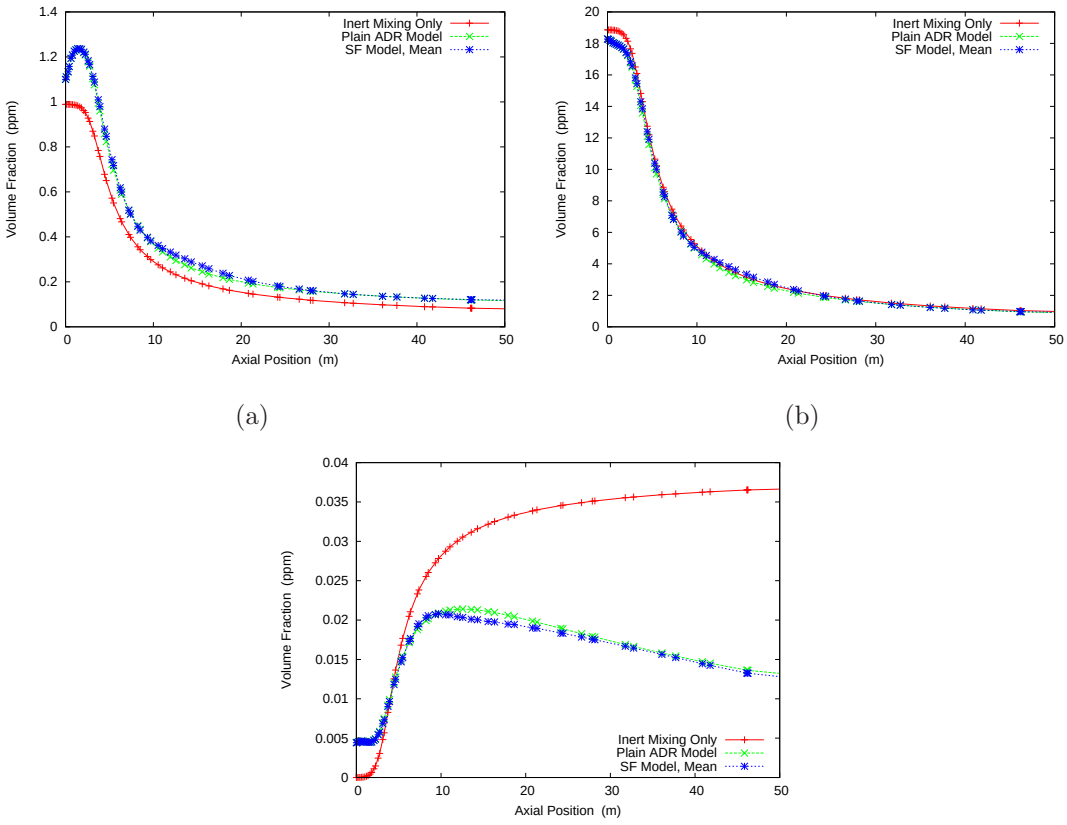

Figure 4.5: Axial evolution of the means of (a) $NO2$, (b) NO and (c) O_3 along the centre-line of jet into still air using Mesh 1. Calculations using inert mixing only, plain advection-diffusion-reaction model and Stochastic Fields model.

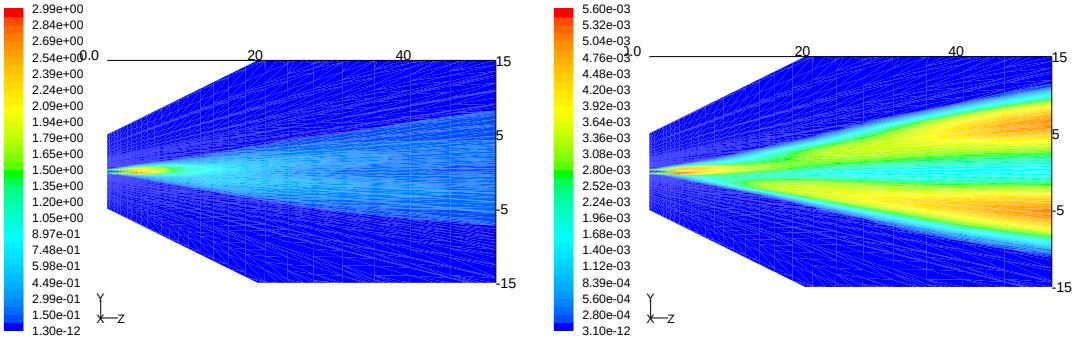

(a) (b)

Figure 4.6: Contours of (a) NO and (b) O_3 RMS [ppm] on plane parallel with jet axis. Results from Stochastic Fields method for jet in still air.

4.2.3.3 Damköhler Number

As discussed in Chapter 1 the parameter that characterises the effect of segregation on reaction rate is the Damköhler number, Da. This is the ratio of a physical mixing timescale to a chemical timescale. A physical timescale has already been calculated in the CFD solution and is assumed to be the same for each species, this is shown in Fig. 4.2(b). An approximate method of obtaining a chemical timescale for each species is to find the rate at which it relaxes back to a local equilibrium value [19]. We can split the reaction rate for species i into production and loss terms:

$$\frac{d\phi_i}{dt} = P_i - L_i\phi_i \tag{4.7}$$

P_i and L_i are determined by the concentration of other species and the rate constants. If they are assumed to be constant and ϕ_i is perturbed, $\Delta\phi_i$, then it will relax back to its equilibrium level according to:

$$\Delta\phi_i \propto exp(-L_i t) \tag{4.8}$$

The timescale for species i is, therefore, $T_{chem} = 1/L_i$. The loss rates can easily

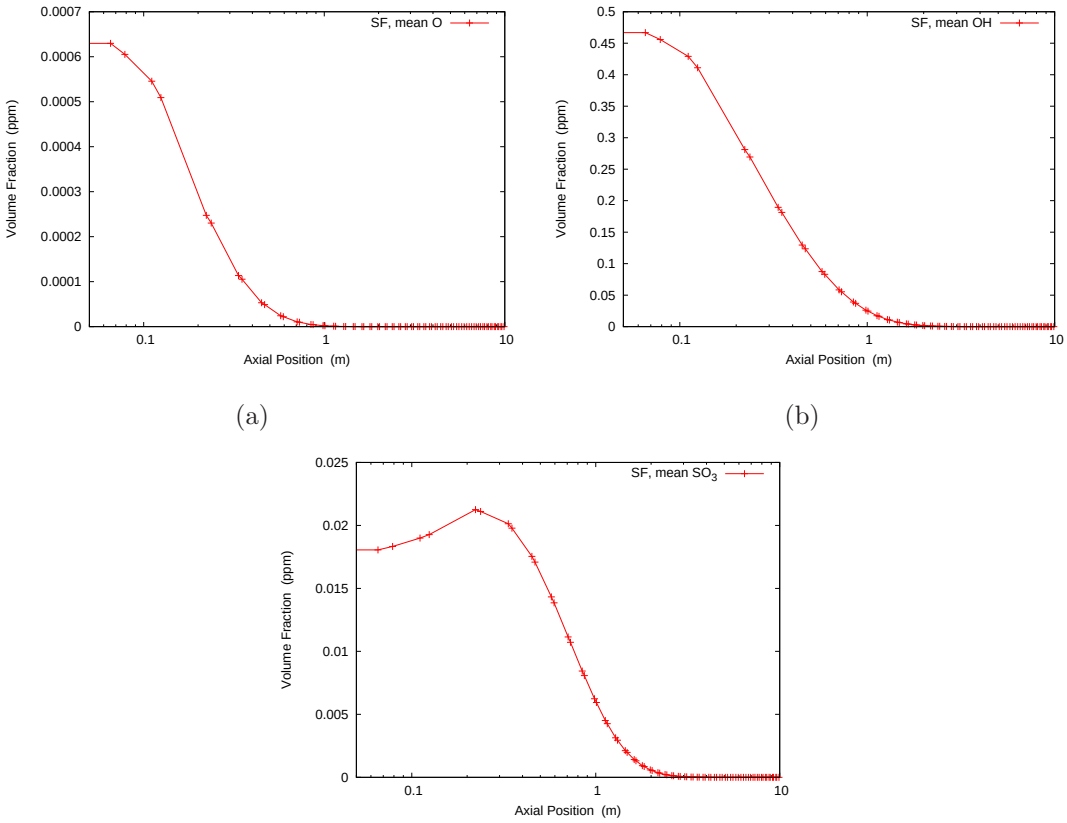

Figure 4.7: Axial evolution of (a) O, (b) OH and (c) SO_3 along centre-line of jet into still air using Mesh 2. Calculations Stochastic Fields model.

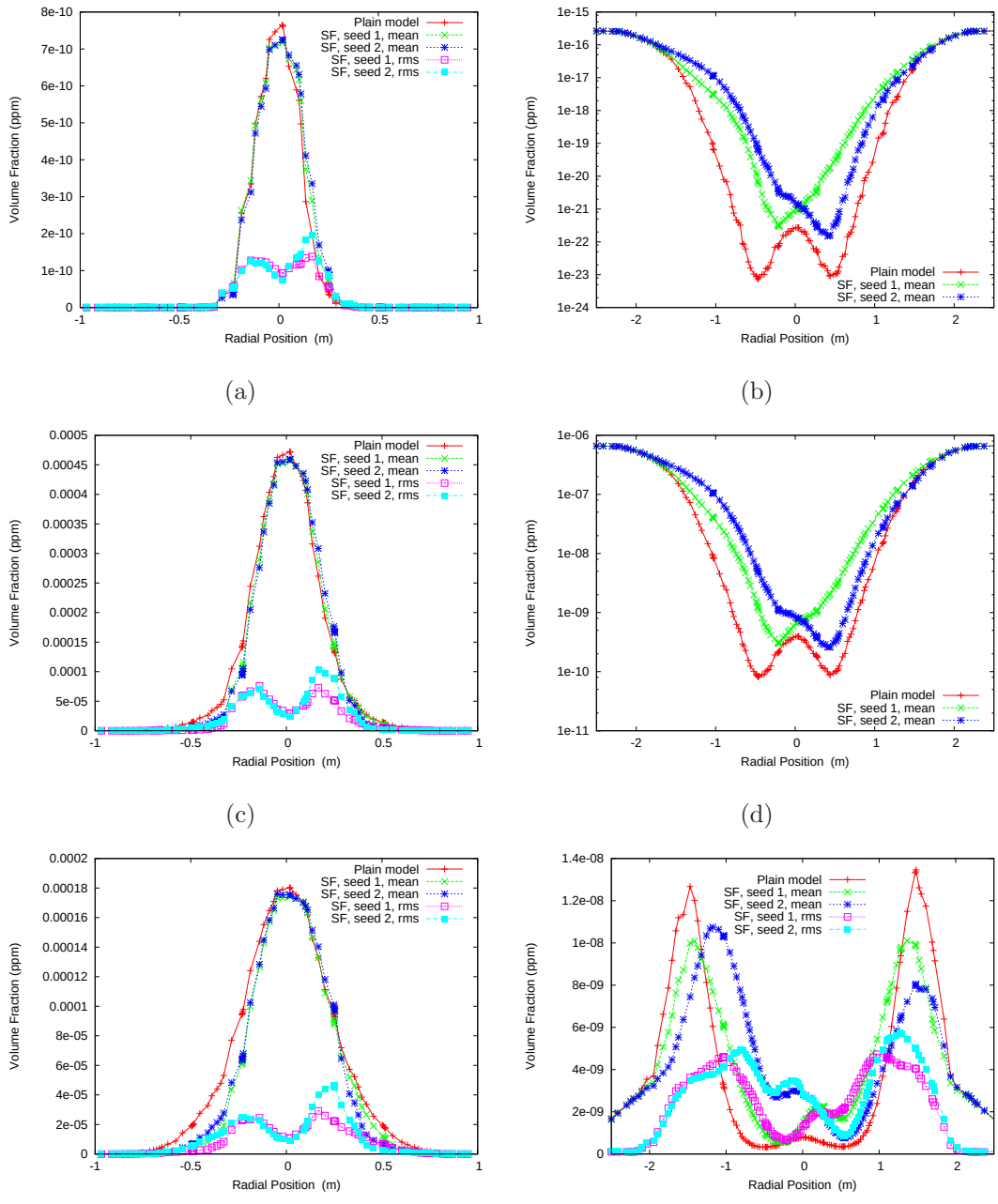

Figure 4.8: Radial profiles of O, OH and SO_3 volume fraction mean and rms by Stochastic Fields Method and simple advection-diffusion-reaction code. O, 2.5m downstream (a); O, 7.5m downstream (b); OH, 2.5m downstream (c) and OH, 7.5m downstream (d); SO_3, 2.5m downstream (e) and SO_3, 7.5m downstream (f). Results from Mesh 2, seed 1 and seed 2 refer to different random number sequences.

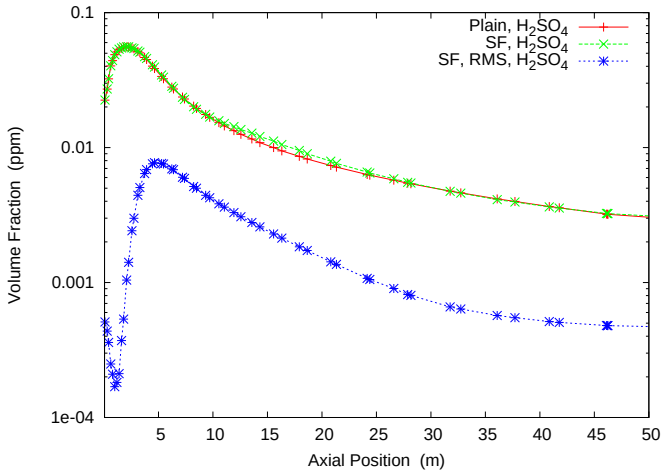

Figure 4.9: H_2SO_4 volume fraction along centre-line of Mesh 1. Mean results from plain advection-diffusion-reaction code. Mean and RMS from Stochastic Fields.

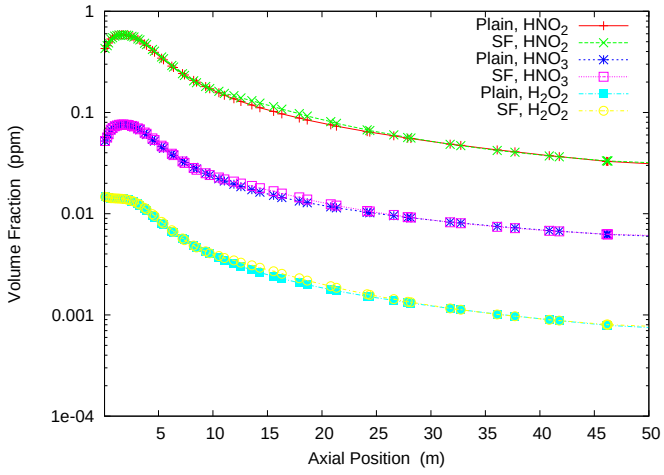

Figure 4.10: Evolution of HNO_2, HNO_3 and H_2O_2 along centre-line of jet in Mesh 2 by both Stochastic Fields method and plain advection-diffusion-reaction method.

be extracted from the CHEMEQ2 solver at each cell to give the distribution of timescale and hence $Da = T_{eddy}/T_{chem}$ can be calculated across the domain for each species. This is done for each field and the mean taken. Contour plots of mean Da for NO_2, O_3, SO_3, OH and O are shown in Fig. 4.11.

To investigate the influence of Da a quantitative measure of the effect of segregation on the different species is required. We use the total species flow rate through a plane perpendicular to the flow, $\dot{X}_i$, which is found by integration using FLUENT.

$$\dot{X}_i = \int X_i \rho \boldsymbol{v} \cdot d\boldsymbol{A} \tag{4.9}$$

This was evaluated on planes perpendicular to the jet at 0.5m, 2.5m, 5.0m and 7.5m downstream of the jet using Mesh 2. This was done for the plain solution and three Stochastic Fields solutions using different random number sequences. The normalised difference between the plain and Stochastic fields solution was then found as $(\dot{X}_{SF} - \dot{X}_P)/\dot{X}_{SF}$. These results are shown in Table 4.3 for a selection of species.

As noted earlier, CO_2 is an inert species in the mechanism employed here and as such should be unaffected by the Stochastic fields method. Therefore we can use the normalised difference in flow rates for CO_2 as an approximate measure of the statistical uncertainty at that point. If we look at NO_2 and O_3 we see that at all four downstream positions the magnitude of the difference caused by considering segregation is of the same order as for CO_2, i.e. less than 2% for z=7.5m. This indicates that the difference is likely to be largely due to statistical error rather than micromixing effects. This supports the results seen in Fig. 4.5. We might expect the reaction $NO + O_3 \rightarrow NO_2 + O_2$ to be affected by segregation, in this situation a plume of one reactant spreads into the other so that their gradients have the opposite sign and hence turbulence would be expected to lead to $\overline{\phi'_A \phi'_B}$ taking a significant negative value, reducing the reaction rate as was observed in Chapter 3. However, Figs. 4.11(a) & 4.11(b) show that Da is relatively low for these species (< 1) other than in the core of the jet where it takes a value of around

20. Within the core there are no gradients and hence no segregation effects. For NO_2, Da rapidly drops to values of the order of 10^{-6} indicating that the chemistry is much slower than the mixing for this species and hence reactant segregation does not have time to have an effect. For O_3, Da in the plume falls to a level of $O(10^{-1})$, while the chemistry is faster for O_3 than for NO_2, the chemistry is still not fast enough compared to the mixing for segregation to have an effect noticeable within the accuracy of this simulation.

The result of ignoring segregation on the predicted levels of SO_3, OH and O are seen in Table 4.3. O has the largest Da, taking a minimum value of 60 (Fig. 4.11(e)). This means that throughout the flow the chemistry will always be fast compared to the mixing and hence segregation will have an effect. This agrees with the results seen in Table 4.3 where the differences increase with downstream distance. These differences are significantly and consistently bigger than those for CO_2 hence we can be confident that this is due to segregation rather than statistical accuracy. The large increase between the difference at 2.5m and 5.0m is consistent with the turbulence reaching the centre of the jet within this region. Figs 4.11(c) & (d) show that Da for OH and SO_3 are similar, taking values of the order of 10 in the early part of the plume. Again we see that for these species segregation has an effect. At 2.5m the SO_3 flow rate is reduced by $\sim$20% by segregation, but by 7.5m it has been increased by $\sim$40%. This is consistent with the results seen in Fig. 4.8. SO_3 initially increases in the jet core before decaying (Fig. 4.7(c)). This suggests that segregation may lead to slower radical chemistry when either producing or destroying radicals. The differences for SO_3, OH and O at 7.5m do not show any trend with Da, this may be because of some other coupled effects in the mechanism or to the simplistic method we have used to calculate chemical timescales.

Table 4.3: Normalised difference between integrated species flow-rate (see Eq. (4.9)) with and without segregation effects at axial locations, z, downstream of jet.

z (m)	Species	Normalised integrated difference (%)			
		Seed 1	Seed 2	Seed 3	Mean
0.5	CO_2	-0.7	0.0	0.1	-0.2
	NO_2	-0.7	0.0	0.4	-0.1
	O_3	0.0	0.0	0.0	0.0
	SO_3	-1.0	-0.4	-3.2	-1.5
	OH	0.5	1.2	-3.7	-0.1
	O	7.1	7.9	-1.0	4.7
2.5	CO_2	1.6	1.5	-2.4	0.2
	NO_2	1.6	1.5	-2.0	0.3
	O_3	-0.2	-0.1	0.5	0.1
	SO_3	-22.4	-21.6	-20.0	-21.3
	OH	-8.0	-7.0	-8.6	-7.9
	O	9.6	10.0	5.9	8.5
5.0	CO_2	2.8	-1.6	-1.0	0.1
	NO_2	2.7	-1.3	-0.9	0.2
	O_3	-0.3	0.5	0.7	0.3
	SO_3	5.1	15.6	12.7	11.1
	OH	5.7	13.4	9.7	9.6
	O	23.0	34.3	20.4	25.9
7.5	CO_2	0.9	-5.6	-0.2	-1.6
	NO_2	0.9	-4.9	-0.2	-1.4
	O_3	0.1	1.9	1.1	1.0
	SO_3	30.2	47.7	35.8	37.9
	OH	25.6	36.6	28.8	30.4
	O	25.6	36.6	27.8	30.0

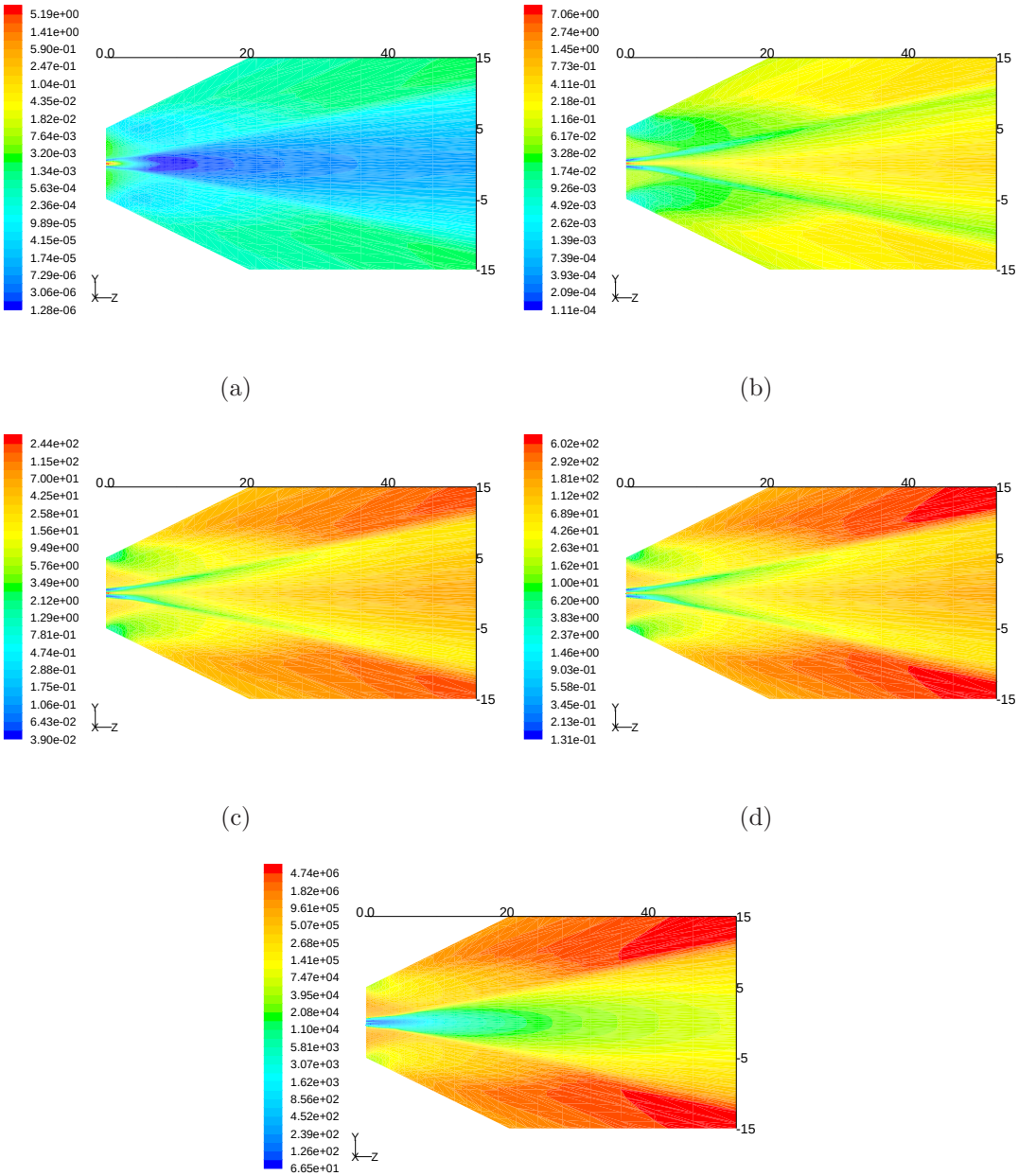

Figure 4.11: Contours of Damköhler number for (a) NO_2, (b) O_3, (c) SO_3, (d) OH and (e) O on a plane containing the jet axis using Mesh 1.

4.2.4 Discussion

The Stochastic Fields method has been found to predict changed concentrations of fast decaying species around the edge of the jet core. This is the result of imperfect mixing at the microscale. For primary pollutants, such as NO_x, and secondary pollutants, such as HNO_2, the effects of micromixing are less significant. Dilution of the early plume by macromixing has a much greater effect on the dispersion and chemistry of the plume than the effect of imperfect mixing at the microscale. Work by Wang and Chen [84] and Menon and Wu [85] suggest that micromixing can effect NO_x and O_3 depletion by 1-2% over longer distances from the jet than studied here (up to 1000 jet diameters).

Not included in the simulations here are aerosol effects. Brown et al [83] discuss the important role of H_2SO_4 and its precursor SO_3 in the production of aerosols in an engine jet plume. In this work we have found that micromixing could have a significant effect on SO_3 levels in the plume. On the other hand it was found that the concentration of H_2SO_4 was unaffected. However the fluctuations of acid vapour concentration, which were of the order of 10% of the mean, may have a significant effect on the highly non-linear nucleation process - particularly when coupled with temperature fluctuations. Such phenomena are explained in Chapter 5.

There are several advantages to coupling with a commercial CFD package. Setting up new cases and altering conditions is made easier by using the existing mesh building tools and user interfaces. Problems of exporting necessary data about the flow to the reacting flow code are avoided and the treatment of advection and diffusion is well established in the commercial code and does not need to be repeated. Finally, exporting and displaying data after the calculation is made easier. A disadvantage is that a fractional step method has to be used, there is no option to calculate all terms together. Here we have used the IEM model for micromixing, however future work could make use of alternative models [32, 38, 77] that may be more difficult to implement in this coupled arrangement. A limit on the number

of scalars that can be solved and the number of memory location at each cell in FLUENT would also provide difficulties if using more complex micromixing models as well as limiting the size of mechanism or number of fields.

We have included some calculations of Damköhler number, which were calculated using the loss rate (see Eq. (4.7)) as the chemical timescale for each species. These rates appear as the diagonal elements of the Jacobian. A better method of finding chemical timescales is to find the eigenvalues of the Jacobian and associate each one with a particular species [19]. The advantage of this is that it takes account of the effect of off-diagonal elements on the timescale and will also provide a timescale for each species unlike the present method which gives no timescale for those species (e.g. H_2SO_4) that do not have loss terms in the mechanism.

4.3 Simulation of a Polluted Street Canyon

The street canyon has for many years been an active area of study in air quality modelling, both in terms of predicting actual roadside exposure to pollution and as a more theoretical test-case for using different numerical models. Experimental data has been obtained both from field studies [89] and from wind-tunnel and water tank models [90]. Computational modelling has been carried out in order to investigate the fluid mechanics and the dispersion of pollutants in and around the canyon [91, 92]. Work has also been carried out which attempts to quantify the exchange of mass and momentum at roof-top level using an exchange velocity in order to provide a model that can be applied to a real-world situations [93].

Recent studies have focused on the turbulent dispersion of reactive pollutants in the street canyon setting. Baker et al [94] have carried out a LES study of a street canyon using a simple, reversible NO, NO_2 and O_3 chemistry using a constant temperature in the canyon. They found that spatial variation of species within the canyon was significant. Baik et al [95], on the other hand, have used RANS modelling to predict the flow field in the canyon while using a similar chemistry

to [94]. They performed a budget analysis of the terms in the advection-diffusion-reaction equation, which showed that the chemical reaction term is comparable to the advection and diffusion terms for O_3. Both these studies found that the air composition is close to chemical equilibrium within the canyon but is far from equilibrium where polluted air from the canyon is mixed with clean air at the top of the canyon.

Most reactive pollutant studies of street canyons so far have not included the effect of turbulence on the mean reaction rate. In this section results are presented of applying the Stochastic Fields method to a simple street canyon problem. This allows the effects of segregation to be studied and also provides details of higher moments of the PDF of the pollutants throughout the canyon. Simulations have been performed using the simple chemistry of [95] and also using the more complex, 28 species, CBM-IV mechanism [71].

4.3.1 Model Problem

The production of the CFD solution for the street canyon was carried out by Dr Ik Soo Kim, formerly of the Hopkinson Laboratory, and details are produced here to provide necessary background to the discussion of the Stochastic Fields solution for this problem which was carried out by the author. The velocity and turbulence fields were calculated using a RANS method with the $k-\epsilon$ model in FLUENT. Solution parameters are the same as those shown in Table 4.1 except the 2D solver is used instead of the 3D and density is assumed to remain constant in this calculation. The two-dimensional CFD domain consisted of seven identical evenly spaced street canyons of width 20m and height 24m. The total height of the domain was 100m and it extended 50m upstream of the first 'building.' This grid contained a total of 79,680 grid cells and is shown in Fig. 4.12. An inlet boundary layer profile for velocity was used at the upstream boundary, which obeys a $(1/7)^{th}$ power-law:

$$u(y) = \frac{8}{7} U_{bulk} \left(\frac{y}{d} \right)^{1/7} \tag{4.10}$$

The bulk velocity, U_{bulk}, was specified as 5m s^{-1}, and d = 50m. A turbulence intensity of 10% and a length scale of 100m are used as the turbulence boundary conditions. The downstream boundary was set to be an outflow. The top of the domain was set as a symmetry boundary condition, but this was sufficiently far above the canyons that its effect is negligible.

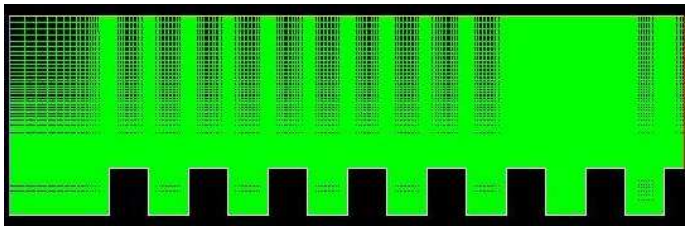

Figure 4.12: Street Canyon CFD grid as used to generate velocity and turbulence data for reacting flow calculations.

Seven adjacent canyons were used in the CFD solution so that within the sixth canyon a typical, fully-developed single vortex is produced. The Stochastic Fields calculations were performed using using a domain that includes only this sixth canyon and extends 20m along the neighbouring rooftops. The height of this grid was 70m in total and a grid resolution half of that for the CFD solution was used, giving a total of 14,700 cells in this grid. This grid is shown in Fig. 4.13, together with a schematic diagram of the canyon, including some salient features of the problem, in Fig. 4.14. The velocity and turbulence fields were fixed as those produced in the larger CFD calculation by turning off the flow and turbulence solvers in FLUENT for the duration of the SF calculation. This is possible as the reactions involved do not produce sufficient heat to effect the density of the flow. The velocity, turbulent viscosity and turbulent mixing timescale (again found by using $T_{eddy} = k/\epsilon$ and assuming unity turbulent Schmidt number) used in these calculations is shown in Fig.

4.15. A background concentration for each species was set at the inlet (left hand edge, above the building level) and initially at all points in the grid. The emission source was defined by setting a fixed value for each species in a 0.6 x 0.3m region consisting of 4 grid cells centred on a point on the centre-line of the canyon 0.45m above the ground. The time-step used was 0.1s and it was found that the solution did not change appreciably after 100s. 60 fields were used with the simple Baik et al chemistry but only 14 for the CBM mechanism due to constraints of user defined memory in FLUENT.

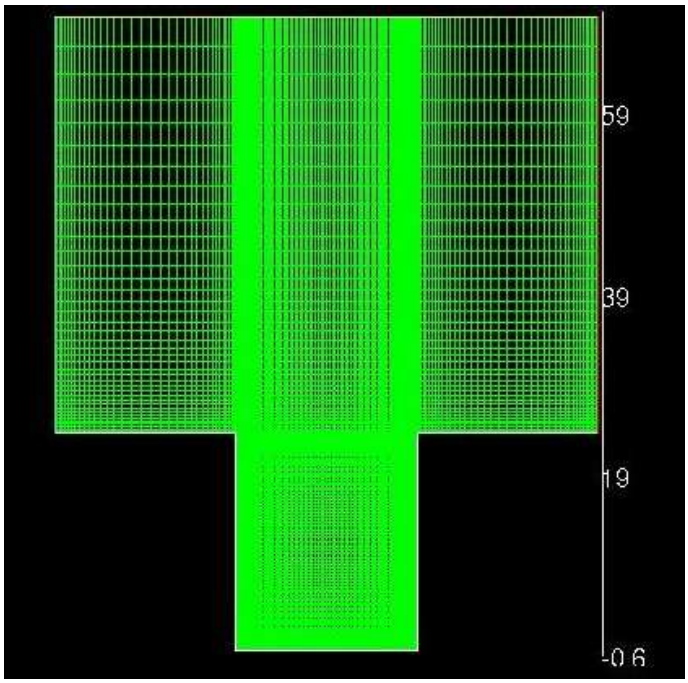

Figure 4.13: Mesh used for Stochastic Fields calculations of street canyon. Corresponds to sixth canyon of CFD grid with halved resolution.

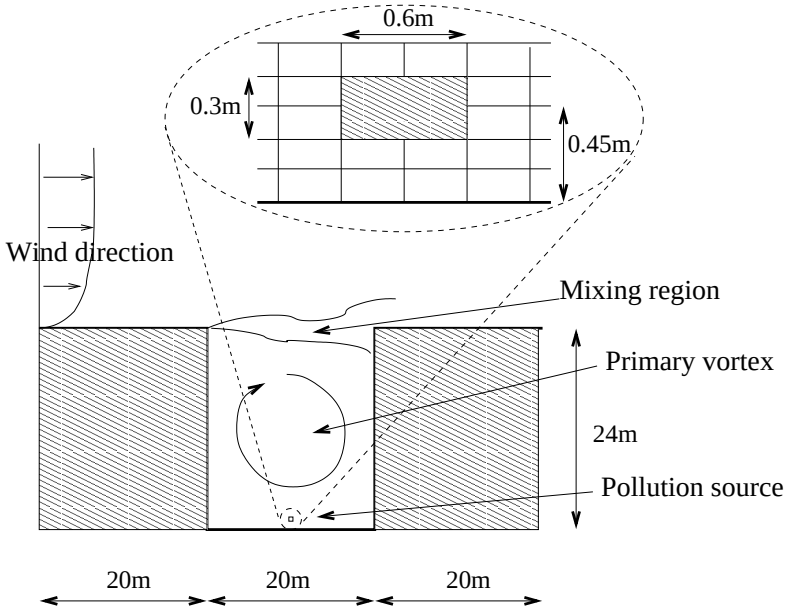

Figure 4.14: Schematic diagram of 2D street canyon.

4.3.2 Results

4.3.2.1 Simple Chemistry

For the simple chemistry taken from [95] background and pollutant source concentrations as shown in Table 4.4. The NO_2 level at the source is rather low, levels equal to 10% of the NO level are more common in other work [94, 95]. However the value used here allows the production of NO_2 by chemical reaction in the canyon to be observed more clearly.

Table 4.4: Street canyon source and background volume fractions.

Species	Background (ppb)	Source (ppb)
NO	0.05	1000
NO_2	0.2	10
O_3	30	0

Figs. 4.16(a) & (b) show the mean and rms values for NO_2 in and above the

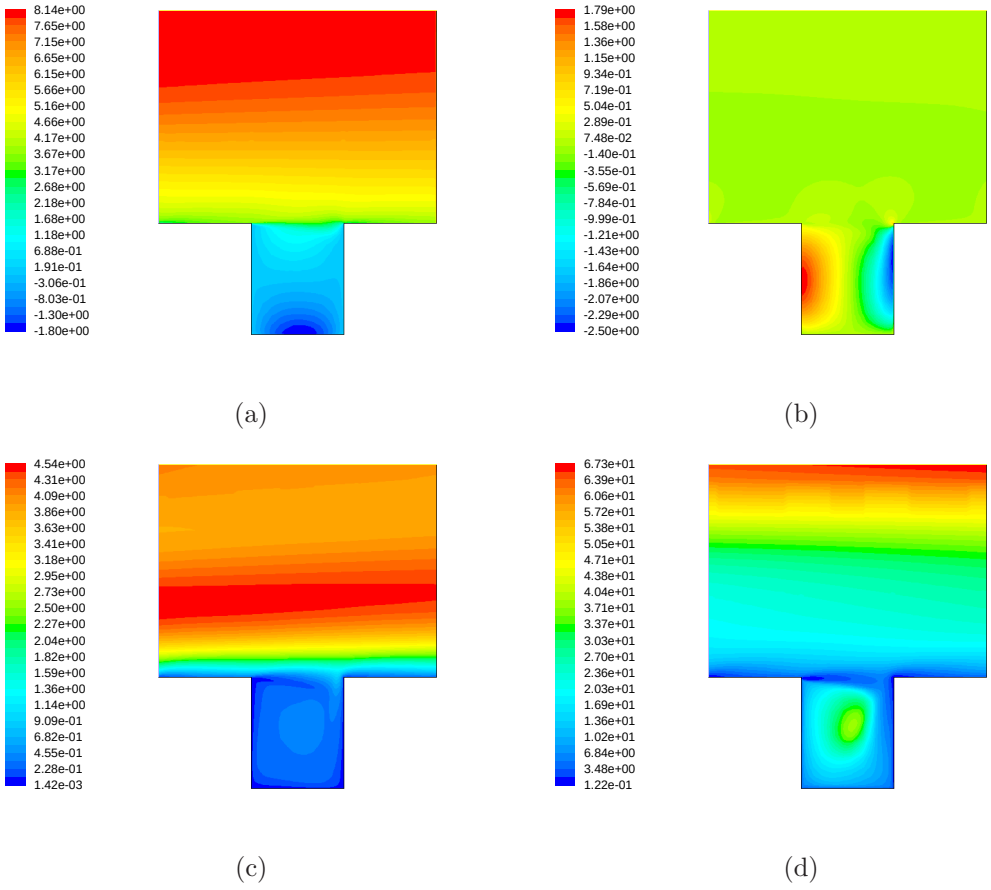

Figure 4.15: Velocity and turbulence fields used in SF street canyon simulations. (a) horizontal velocity [m s^{-1}] with positive to the right; (b) vertical velocity [m s^{-1}] positive upwards; (c) turbulent viscosity, ρK, [kg m^{-1} s^{-1}] and (d) turbulence timescale, T_{eddy}, [s].

canyon as calculated by the SF method. The relatively long residence time allows the reaction of NO and O_3 to build up the NO_2 in the centre of the canyon to a level of approximately 23ppb, which is more than double the level in our source. The mixing layer at the building height introduces relatively clean air into the canyon along the windward (right hand) wall, while polluted air is transported out of the domain in the downwind direction. As expected, the highest variance is observed where the scalar gradient is largest hence the variance is particularly large around the source, where the chemistry produces strong gradients, and in the mixing layer.

In the mixing layer the rms is of the order of the mean concentration in this region. One of the advantages of using a PDF method is that the statistical distribution of the scalars can be investigated in greater detail. Figs. 4.16(c) & (d) show contours of the skewness and kurtosis excess of NO_2 in and above the canyon. It can be seen that there is a region of positive skewness above the mixing layer, which indicates that the NO_2 concentration will usually be low with occasionally much higher concentration. There is a corresponding region of negative skewness just below the mixing layer which extends round the canyon vortex, surrounding the region of high NO_2. In these areas the concentration will generally be high with occasional lower values. Fig. 4.16(d) shows contours of kurtosis excess with only negative parts shown to increase clarity. A strongly negative region is observed at the level of the roof-tops indicating that the PDF here is not clustered around the mean. For reference, a two delta-function distribution would have a kurtosis excess of -2. These results are consistent with the idea that the chemical composition found in and either side of the mixing layer will, at a given instant, be more likely to be either 'in canyon' or 'out of canyon' compositions rather than a mixture of the two. This homogenised composition would be obtained if a simple gradient diffusion based model were to be used.

Fig. 4.17 shows mean and rms concentrations for an inert scalar (mixture fraction) and for O_3 along vertical lines extending through the canyon, one 2.5m from the left-hand wall and the other 2.5m from the right-hand wall. These results were

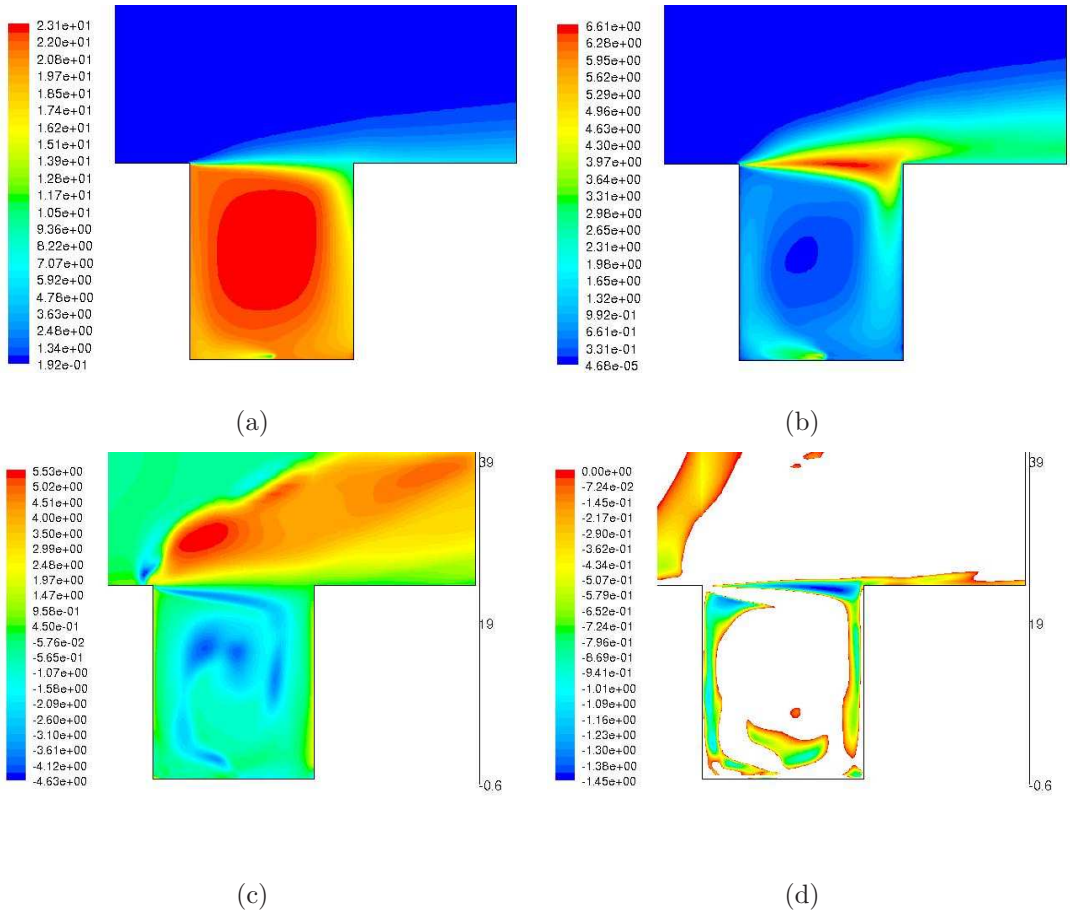

Figure 4.16: Contours (in ppb) of NO_2 distribution in and above canyon. (a) Mean values; (b) rms; (c) skewness and (d) kurtosis excess with positive values omitted.

produced using the SF method, Eq. (2.6), and also a plain advection-diffusion-reaction method, Eq. (2.7). Once again the very high variance at roof-top level is seen. It can also be seen that the two solutions for O_3 do not differ by more than the statistical noise seen in the inert scalar results. Similar results are seen for NO and NO_2, indicating that segregation does not play a significant role in this situation. This conclusion is supported by consideration of the Damköhler number. If Da is obtained according to the same method used in Section 4.2.3.3 it is found that the highest Da is found for O_3, which takes a maximum value of approximately three. This maximum value occurs in the centre of the canyon where the gradients are small and hence variance is low. In Section 4.2 segregation effects were seen when $Da \geq\sim 5$ in regions where scalar gradients were found. As such segregation effects should not be expected in this situation.

Photostationary State Defect

The photostationary state defect, δ_{ph}, is defined in [95] as:

$$\delta_{ph} = \left(\frac{k_1 X_{NO} X_{O_3}}{J_{NO_2} X_{NO_2}} - 1 \right) \times 100 \tag{4.11}$$

where k_1 is the reaction rate of the forward $NO + O_3 \rightarrow NO_2 + O_2$ reaction and J_{NO_2} is the photolysis rate of $NO_2 \rightarrow NO + O$. As the subsequent combination of the oxygen radical with an oxygen molecule to form ozone happens very quickly, a dynamic equilibrium, or photostationary state, will be achieved between NO, NO_2 and O_3 if they are left unperturbed. When this occurs the above expression takes a value of zero. A departure from zero indicates how far the NO_x/O_3 system has moved from equilibrium with positive values indicating an excess of NO and O_3. The idea of the photostationary state defect is also used in air quality measurement as a means of detecting other pollutants [96]; departures from the photostationary state value in unperturbed air will reveal the presence of other pollutants. However in our simple chemistry modelling case, where there are no other species used, values

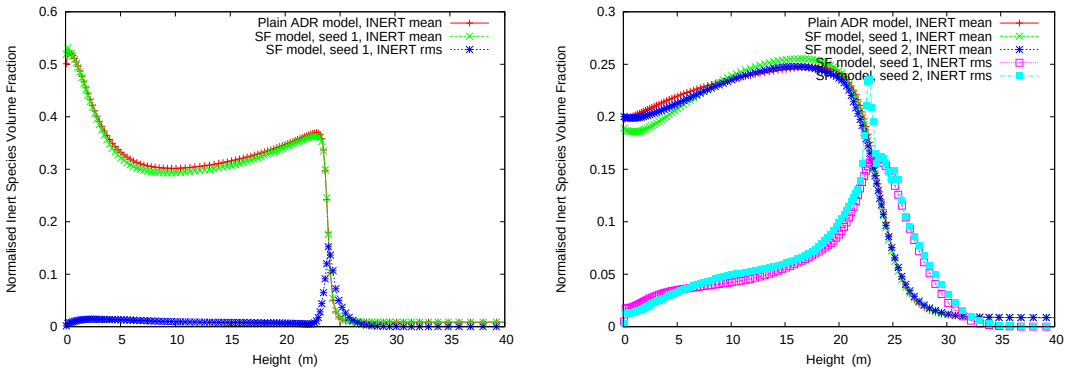

(a)

(b)

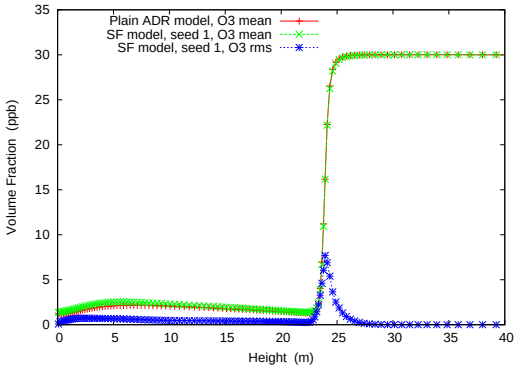

(c)

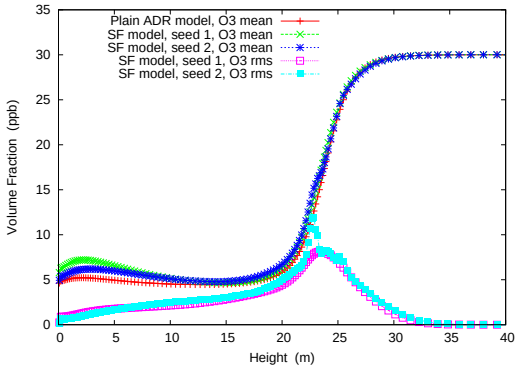

(d)

Figure 4.17: Profiles of mean and rms concentrations, using both SF and plain advection-diffusion-reaction model, taken along vertical lines extending through and above canyon. (a) inert scalar 2.5m from left wall; (b) inert scalar 2.5m from right wall; (c) O_3 2.5m from left wall and O_3 2.5m from right wall.

of δ_{ph} away from zero indicate only that the reversible system is not in steady-state.

Values of δ_{ph} throughout the grid can easily be extracted from the FLUENT/SF code. This was done in three ways: firstly it was calculated from the plain advection-diffusion-reaction solution. Secondly it was calculated using the mean species and temperature values from the SF solution at each point, known here as 'defect of means.' Finally δ_{ph} was calculated for each field at each grid node and the mean and rms of this taken, known as 'mean defect' and 'rms defect.' Contours found using the second and third methods are shown in Fig. 4.18. The results here agree with those seen in [94, 95] with low positive values found inside the canyon and a ridge of high values along the mixing layer at the top of the canyon. This indicates that the chemistry is close to equilibrium in the canyon but is far from equilibrium at roof-top level where polluted air from the canyon is mixed with fresh, O_3 rich, air from above. Our values are higher than those of [95] due to the lower concentration of NO_2 used at the source.

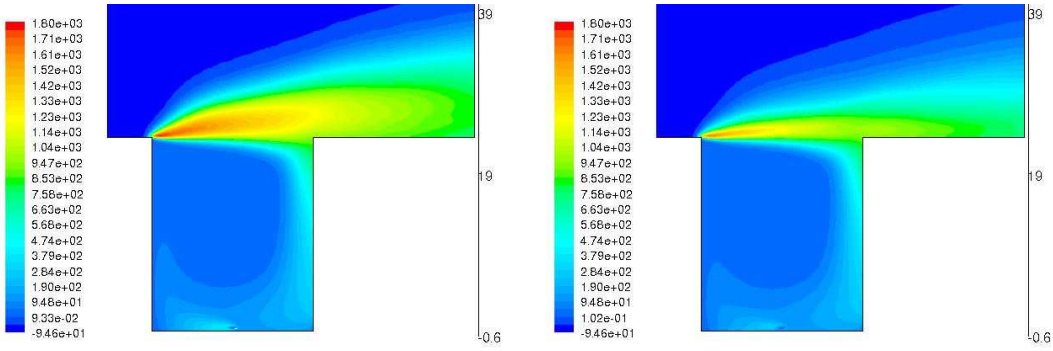

(a) (b)

Figure 4.18: Contours of photostationary state defect found using SF method. (a) Found from means of species and temperature and (b) mean of the value found in each field.

It can be seen that taking the mean defect of all fields leads to a lower and thinner peak that that found from mean values. This can be seen more clearly in

Fig. 4.19 which shows δ_{ph} along vertical lines through the canyon. Also shown here is the defect as calculated using the plain method. We see that the SF defect of mean values are slightly higher than when fluctuations are ignored, suggesting that there are small differences in calculated values of means that are not apparent when considered individually. The peak true mean defect is significantly smaller and narrower than those using mean quantities, indicating that the chemistry is closer to equilibrium. The co-variance of O_3 and NO caused by their opposite gradients in the mixing region will have an effect on mean δ_{ph} which, unlike reaction rate, will be unaffected by micromixing. This is further evidence to suggest that the composition found in the mixing layer at a given instant will retain some of it's 'in canyon' or 'out of canyon' equilibrium composition rather than being a fully mixed intermediate composition (which would be further from chemical equilibrium). This is illustrated by Fig. 4.20 which shows the PDF of NO_2, as calculated from three SF simulations, at a point at roof-top level in the centre of the canyon.

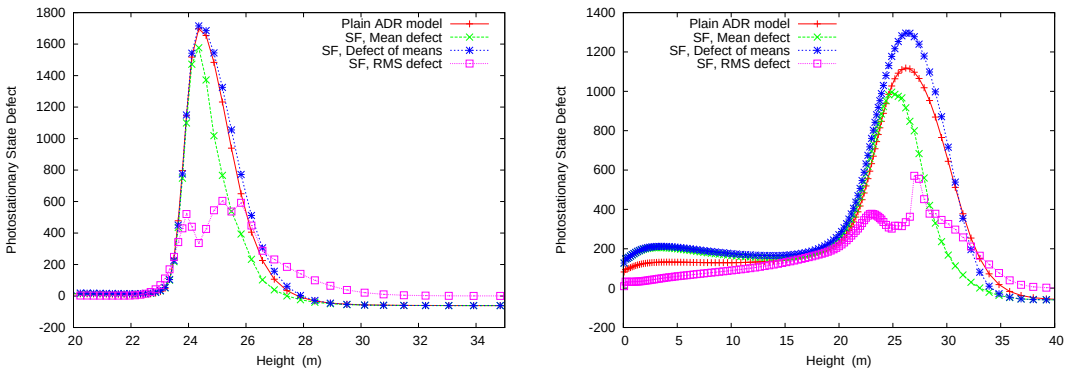

Figure 4.19: Vertical profiles of photostationary state defect (a) 2.5m from left-hand wall and (b) 2.5m from right-hand wall.

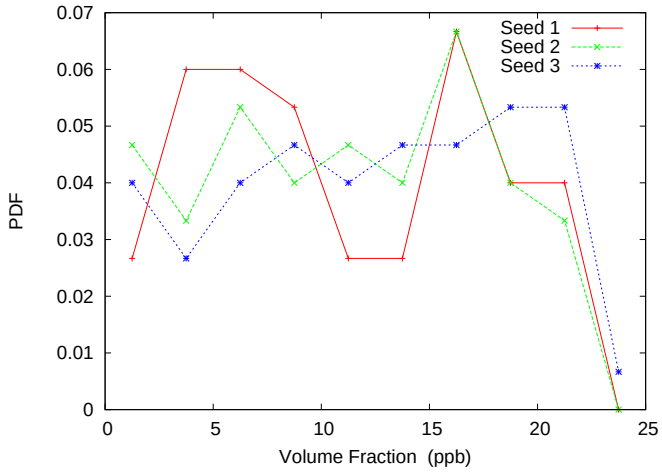

Figure 4.20: Probability Density Function of NO_2 volume fraction at roof-top height (24m) in the centre of the canyon.

4.3.2.2 CBM-IV Mechanism

For the simulations with the CBM-IV chemistry NO, NO_2 and O_3 levels for both background and source were kept the same as for the simple chemistry, see Table 4.4. A VOC/NO_x ratio of 35 was used for the background and a ratio of 1.0 for the source, the VOC's comprised 70% PAR and 5% each of ETH, OLE, ALD, $FORM$, XYL and TOL. CO was set to 1000ppb in the background and 40ppb at the source, OH and HO_2 were set to 4×10^{-6}ppb and 4×10^{-5}ppb respectively for both source and background. All other species were set to small values and allowed to achieve equilibrium levels during the calculation.

Contours for those species which appear in both chemistries used here were found to be same with the CBM-IV mechanism as with the simple chemistry within ~ 1 ppb. This suggests that the use of the simple chemistry in the street canyon situation is valid for finding $NO/NO_2/O_3$ levels. Again the levels of these species were found to be unaffected by segregation effects. There was also no significant difference observed for VOC's or secondary pollutants such as HNO_2 and HNO_3. Vertical profiles are shown in Fig. 4.21 for NO_2 and HNO_3. The variance is again seen to

be very high in the region at the top of the canyon. The reduction in the statistical accuracy caused by the reduced number of fields used here compared to the simple chemistry is shown by the decreased agreement between SF results using different random number sequence.

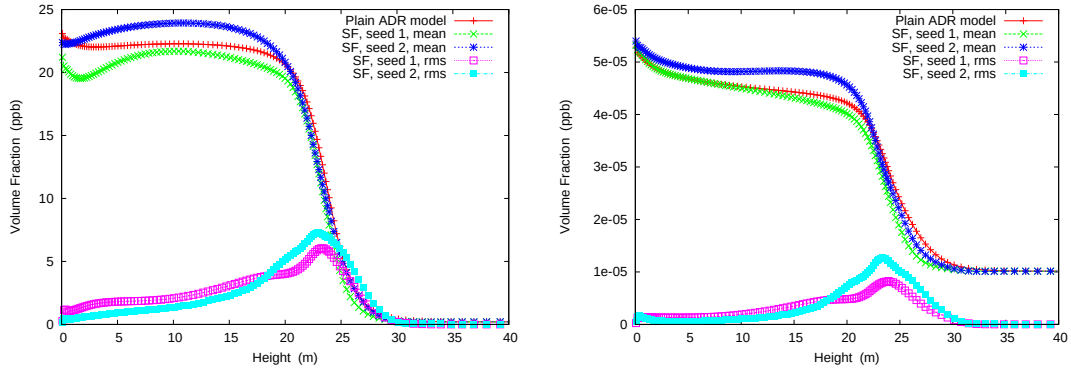

(a) (b)

Figure 4.21: Vertical profiles of (a) NO_2 and (b) HNO_3 2.5m from right-hand wall, using CBM-IV chemistry.

However significant differences were observed for some species between the plain advection-diffusion-reaction and Stochastic Fields results. These differences were observed in the mixing region above the top of the canyon where strong gradients and mixing occurs, as shown by the high variance in this region (see Fig. 4.16). The variation of mean and rms volume fraction with height along the line 2.5m from the right-hand wall for OH is shown in Fig. 4.22 to illustrate this. It can be seen that when segregation is ignored the peak OH level observed in the mixing layer is too large and its vertical position is too high.

We again calculated Da values for each species using the same method as in Section 4.2.3.3. As segregation effects were observed to have an effect in the mixing region the top of the canyon, a representative value of Da for each species was obtained by taking an area-weighted average in a region covering the width of the canyon and extending from a height of 20m to 35m, i.e. from 4m below roof level

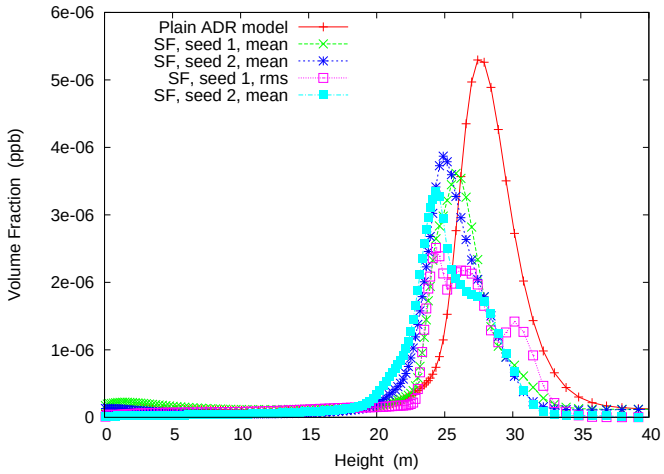

Figure 4.22: Vertical profiles of OH 2.5m from right-hand wall, using CBM-IV chemistry.

to 11m above. These values are given in Table 4.5 for the twelve 'fastest' species as calculated using this method. Vertical profiles of mean volume fraction though this region, along a line in the centre of the canyon, are shown in Fig. 4.23.

Again we see strong agreement between high Da and a significant segregation effect on calculated species concentration. Those species for which large differences were seen between the two methods were the seven fastest species, namely OH, NO_3, C_2O_3, HO_2, XO_2N, XO_2 and PHO. These species all had Da values greater than approximately ~ 1. Those with lower Da, including those not shown in Fig. 4.23, did not show a significant segregation effect. Furthermore the Computational Singular Perturbation (CSP) method has been used to calculate chemical timescales for the CBM-IV mechanism [19]. The seven fastest species found using the CSP method for their daytime, urban case were found to be the same seven species found here to show significant effects due to segregation. These results also agree with those for photostationary state defect which showed that the chemistry in the mixing layer is closer to equilibrium locally in the mixing layer than is suggested by use of only mean quantities. The peak in concentration of radicals such as OH is caused by the

Table 4.5: Area-weighted averages of Damköhler numbers in the mixing region for the twelve fastest species using the CBM-IV mechanism. Also shown is the key to the corresponding figure in Fig. 4.23.

Species	Da	Position in Fig. 4.23
OH	389	(a)
NO_3	387	(b)
C_2O_3	199	(c)
HO_2	120	(d)
XO_2N	111	(e)
XO_2	111	(f)
PHO	20.0	(g)
N_2O_5	0.469	(h)
NO	0.288	(i)
O_3	0.210	(j)
PAN	0.00265	(k)
$PHEN$	0.00158	(l)

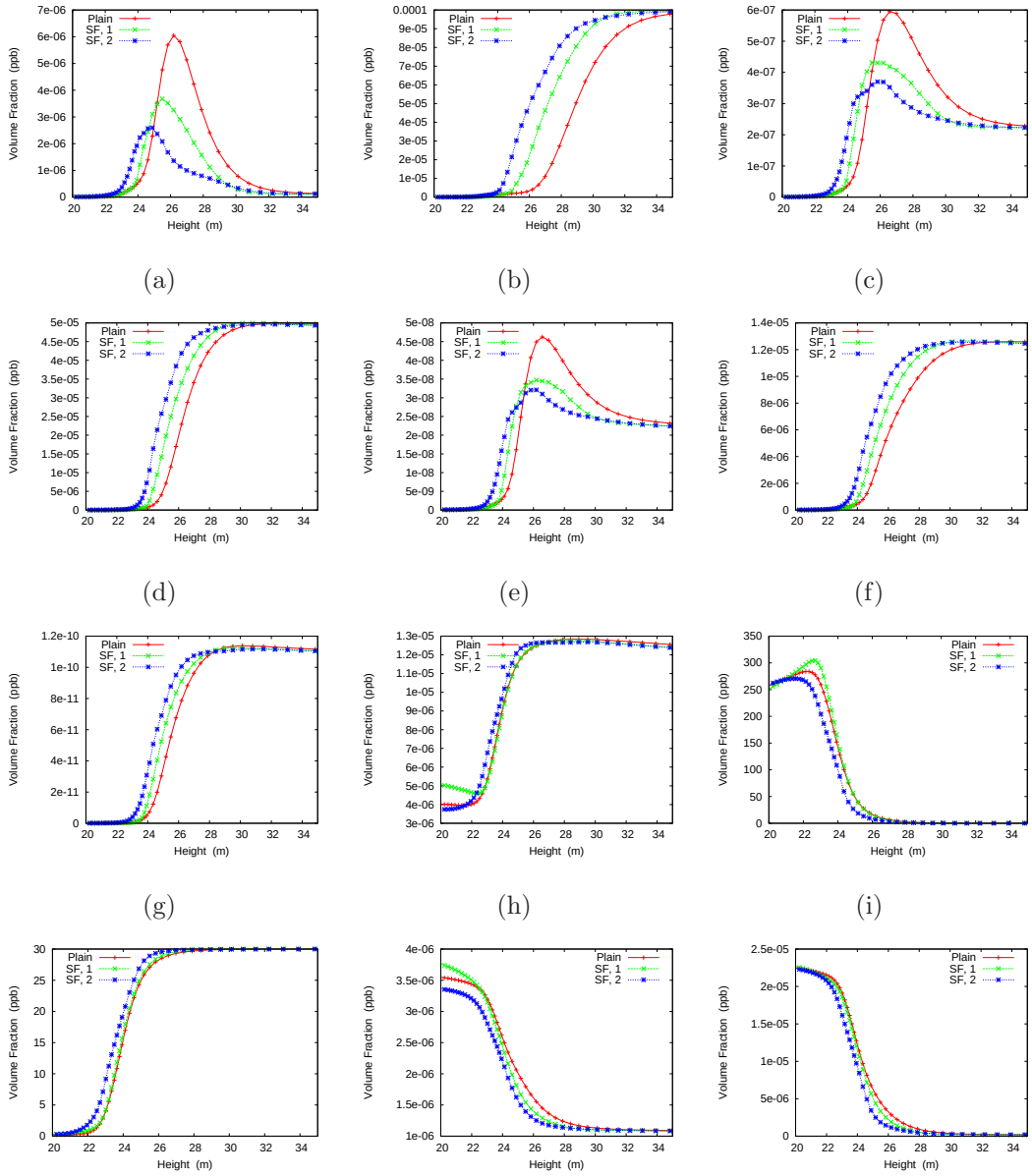

Figure 4.23: Vertical profiles, between 20m and 35m, of volume fraction for the twelve species with the highest Da at the centre of the canyon, using CBM-IV chemistry. Key to labels given in Table 4.5.

departure from equilibrium at that point, a reduction of this peak indicates that the chemistry is closer to equilibrium.

4.3.3 Discussion

The Stochastic Fields method has been used to investigate the effect of segregation on the chemistry in a street canyon. It has been found that, for most of the species, segregation does not have a significant effect using either the simple or more complex chemical mechanisms. However for seven species (NO_3, OH, HO_2, C_2O_3, XO_2, XO_2N and PHO) a difference was seen in the predicted concentration in the mixing region above the top of the canyon. These were the seven species with the fastest chemistry, as found by the method described in Section 4.2.3.3 and by a more sophisticated method [19]. All other species were found to have Damköhler numbers of less than five.

Values of Da for most of the major species would be increased if higher concentrations of the species they react with are used, as this would lead to higher reaction rates. In addition to this changes in the configuration of the street canyon or the flow inside it would cause the turbulent timescale to change; leading to a different timescale for molecular mixing. Hence while for the conditions modelled here there are no segregation effects for the major species, it cannot be said that this will be the case in all conditions. However, for most of the species the Da number and hence chemical or physical timescale would have to change by orders of magnitude in order to reach those at which segregation effects have been seen.

Calculations of the photostationary state defect using the simple chemistry have shown that air in the mixing layer above the canyon is closer to chemical equilibrium when the value in the individual fields are considered rather than only mean species concentrations. This is supported by the observation that the peak in OH concentration is also reduced when fluctuating values are considered. Together with the results seen for the higher moments of the PDF of the scalars seen in this re-

gion this seems to suggest that the composition of the air in this region if sampled instantaneously would tend to be largely either polluted air from inside the canyon or clean air from outside, rather than a well-mixed combination of the two. This would be consistent with mixing being performed by large eddies at the larger scale but with imperfect mixing at the molecular scale.

4.4 Conclusions

In this chapter the results of applying the Stochastic Fields method to the simulation of an aircraft jet exhaust plume and a polluted street canyon have been presented. These were carried out using an Ito SF code which has been coupled with the commercial CFD package FLUENT. This coupled code has been found to work well and incorporate many of the advantages of an existing CFD code. As the existing pre and post-processing tools are available it is relatively simple to set up new geometries and extract data from the solution.

For the 50m section of the jet plume studied, the primary pollutant, NO, was little affected by chemistry in the plume. The concentration is so high compared to other species that its evolution is dominated by turbulent mixing, which occurs at the end of the jet core. Those species (OH, HO_2, O, H, SO_3 and HSO_3) which decay rapidly away from the jet exit plane do show a difference when micromixing is taken into account. A changed concentration of these radicals is found at the edge of the plume when the Stochastic Fields method is used. Subsequently an increase in volume fraction is seen across the plume at 7.5m from the jet exit. These species are associated with relatively high Damköhler numbers. However, most of the chemistry with this mechanism takes place very early in the jet before the turbulence created in the shear layers diffuses into the jet [72]. The chemistry producing secondary pollutants, such as H_2SO_4 or HNO_2, takes place in a region of low turbulence and uniform concentrations. Consequently we see that using the Stochastic Fields method does not always give significantly different results from

a simple advection-diffusion-reaction model that does not take micromixing into account. Micromixing will only have an effect on reaction rates when there are temporal or spatial fluctuations in reactant concentration. The reaction between $NO + O_3 \rightarrow NO_2 + O_2$ is the only major reaction to take place between a species from inside the plume and one in the background and is, therefore, controlled by the mixing out of the plume. However Da was found to be relatively low for these species in the region where the reaction takes place, meaning that micromixing destroys segregation before it can alter the reaction rate.

In the street canyon it was found that both mechanisms used give very similar predictions for NO_2 and O_3 concentrations. The rms of concentration was found to be very high in the mixing layer at roof top level. It was found that neglecting segregation does not lead to significant errors in the calculation of major species concentrations. However a difference is seen for the photostationary state defect using the simple chemistry and in the concentration of NO_3, OH, HO_2, C_2O_3, XO_2, XO_2N and PHO using CBM-IV. These seven species have large Da compared to others in the mechanism. For both situations studied it has been found that there is a good correlation between local Da and which species are affected by segregation. It was found that the species so affected were those for which Da took values greater than $\sim$5.

Chapter 5

Application of the Stochastic Fields Method to Aerosol Processes

5.1 Introduction

5.1.1 Background and Basic Phenomena

Aerosol is the general term given to suspensions of small particles, above the molecular size, in gases. This can refer to particles produced when solids break up and wear, and to particles formed from gas phase material converting to the solid or liquid phase [15, 23]. In this chapter aerosols formed by the transformation of vapour into liquid droplets is considered. This is done for particles of homogeneous composition. Growth on pre-existing particles (heterogeneous nucleation) is not addressed in this work.

Aerosols of the type studied in this chapter undergo four main physical processes [23]:

- Nucleation. Particle nuclei form from the parent vapour phase. This process

affects the number density of the aerosol population and also the total volume of condensed material.

- Growth/Evaporation. Vapour diffuses toward existing nuclei and condenses causing the nuclei to grow. Alternatively, depending on the ambient conditions, aerosol material can evaporate from the aerosol and diffuse away. This process will change the total volume of condensed material but leave the number density untouched.

- Coagulation. Particles can collide and stick together, forming fewer but larger particles. This will affect number density, but leave total aerosol volume unchanged.

- Transport. The aerosols will be transported by their surrounding gas flow field. If the particles are small they can be assumed to move with the same velocity as the gas, while larger particles will have a slip velocity due to particle inertia.

If the aerosols are assumed to be spherical droplets of homogeneous composition then the population can be entirely characterised by the number of particles of a given size per unit volume of carrier gas. The size can be defined by diameter, surface area, volume or mass. In this chapter particle volume is chosen as the measure of aerosol size. A continuous distribution function can be employed, where dN is the number density of particles in the size range v to $v + dv$, so that [23]

$$dN = n(v, \boldsymbol{x}, t)dv \tag{5.1}$$

Eq. (5.1) defines the size distribution function, $n(v, \boldsymbol{x}, t)$, where $\boldsymbol{x}$ and t denote the dependence of the distribution on space and time. If a sample of particles is considered then we can think of $n(v)dv/N_T$, where N_T is the total number density, as giving the probability of a particle having a particular volume. Further discussion of the representation of aerosol size distributions follows in Section 5.1.2.

The instantaneous evolution of n can be described by the general dynamic equation for the continuous distribution function [23, 97], which is a partial differential equation that models the simultaneous nucleation, growth, coagulation and transport of the aerosol population. It is expressed as:

$$\frac{\partial n}{\partial t} + \nabla \cdot n\boldsymbol{u} + \frac{\partial (Gn)}{\partial v} = \nabla \cdot D\nabla n + J(v^*)\delta(v - v^*) + \frac{1}{2}\int_0^\infty \beta(v - v', v')n(v - v', t)n(v', t)dv' - n(v, t)\int_0^\infty \beta(v, v')n(v', t)dv' \tag{5.2}$$

The second term on the LHS of Eq. (5.2) represents advection by the carrier gas assuming low Stokes number, i.e. that the particles are sufficiently small to follow the flow with no slip. The first term on the RHS describes diffusion of the particles (not to be confused with diffusion of gas molecules to and from the aerosols). This diffusion will be due to Brownian motion. As motion of the particles due to a turbulent velocity field will be much greater than due to Brownian motion, the diffusion term is sometimes dropped altogether [98]. Another approach is to follow the procedure seen for scalars such as volume fraction and replace the instantaneous velocity with the mean velocity and model the turbulent advection by using a turbulent eddy diffusivity. This can be added to the Brownian diffusivity, which will be much smaller than the turbulent diffusivity [23]. In either case turbulent transport of small aerosols (i.e. with no slip velocity) can be treated in the same way as for scalars such as volume fraction as seen in previous chapters.

The third term on the LHS represents movement through the size distribution due to the growth of the particles, where $G(v)$ is the volume growth rate of particles of volume v. The second term on the RHS is the nucleation rate, J. This shows the rate of creation of new particles of a certain critical volume, v^*, hence the delta function. The final two terms on the RHS describe respectively production and loss of particles of size v due to coagulation. $\beta(v_1, v_2)$ is a collision kernel or collision frequency function which models the probability of particles of volume v_1 and v_2 colliding and successfully coalescing to form a new particle of volume $v_1 + v_2$. The

first integral term represents the production of particles of volume v by integrating over all combinations of volume that combine to give this volume. The factor of 1/2 is to prevent double counting. The second integral term represents the loss of particles of volume v by integrating over all sizes of particle that those of v can combine with. Nucleation, growth and coagulation are discussed in the following sections, together with the mathematical models used simulate them.

Nucleation

Nucleation is the process of new aerosols forming from vapour in the gas phase. This can occur when gas molecules cluster onto the preexisting surface of a third party, this is known as heterogeneous nucleation. If the gas molecules cluster together without the aid of a surface the nucleation is said to be homogeneous. These clusters will form spontaneously within the gas but will only form a stable nucleus if the cluster reaches a certain critical size. According to classical nucleation theory [15] this critical size or radius will depend on the change in Gibbs free energy (ΔG) when a cluster forms. When molecules cluster together the surface of the cluster will have a surface tension, and energy must be consumed to create this. When molecules join the cluster they release latent heat (energy) as they condense. This will depend mainly on the saturation ratio, S, which is the ratio of the partial pressure of the vapour to the saturation vapour pressure above the surface of the cluster. For small clusters the energy required to form new surface when new molecules join the cluster is smaller than that released by the condensation and hence the cluster is unstable. However for clusters above the critical size adding more molecules to the cluster will release more latent heat than is required to form the new surface. Hence for stable new particles to be produced clusters must form greater than this critical size. Using classical theory [15, 23] the critical radius is

$$r_c = \frac{2\sigma m}{\rho_p R^* T \ln S} \tag{5.3}$$

where σ is the surface tension of the droplet, m is the mass of one molecule, ρ_p is the density of the condensed liquid and R^* is the universal gas constant. In this theory aerosols are assumed to be created at the critical radius before attaining greater volume due to subsequent growth. There are several versions of the expression found for the rate of formation of nuclei of this critical size [9, 15, 23], but the one used here is that given by Lesniewski and Friedlander [99] whose experiment is simulated in this chapter:

$$J = \frac{P_v X_v}{kT}\left(\frac{2\sigma}{\pi m}\right)^{1/2} \exp\left[-\frac{16\pi\sigma^3 m^2}{3(kT)^3\rho_p^2(\ln S)^2}\right] \tag{5.4}$$

where P_v is the vapour partial pressure, X_v is the vapour mole fraction and k is the Boltzmann constant. Surface tension, condensed density and particularly saturation ratio are all functions of temperature. Classical theory has been criticised for not accurately predicting the nucleation rate in some circumstances and the theory relies on the assumption that macroscopic material properties can be applied to nuclei which may consist of only a handful of molecules. The situation becomes more complicated when the nucleation of aerosols containing two types of molecules, binary nucleation, is considered. Kusaka et al [100] used Monte Carlo simulations at the molecular level to investigate nucleation of sulphuric acid/water aerosols and found that nuclei so formed are far from the spherical shape assumed in classical theory. However, other theories are often too computationally intense to use in practical models [15] and the classical theory is widely used.

Growth

Once particles have been nucleated they can then increase in size due to more gas molecules diffusing to and condensing on the surface. Or, conversely they can shrink if molecules evaporate from the surface. The direction of this mass transfer will depend on the saturation ratio, i.e. the ratio of partial pressure of the vapour to the saturation vapour pressure over the surface. If the ratio is greater than one then

vapour will condense on the surface and the particle will grow. It should be noted that while values of S only slightly greater than one will lead to growth it may not lead to the nucleation of new particles as the critical radius will be too large to give significant nucleation rates. The speed of the transfer of mass to or from the particle will depend on departure from $S = 1$ and also on the speed at which gas molecules can diffuse to or from the particle. Pratsinis [97], using work from [23, 101] gives expression for the growth rate (G in Eq. (5.2)) both for the case where the nuclei is smaller than the mean free path of the gas (free molecule regime, G_{FM}) and also when the nuclei is large enough the gas to be treated as a continuum (continuum regime, G_C).

$$G_{FM} = (36\pi)^{1/3}\left(\frac{kT}{2\pi m}\right)^{1/2} v_m n_s v^{2/3}(S-1) \tag{5.5}$$

$$G_C = (48\pi^2)^{1/3}\left(\frac{8kT}{\pi m}\right)^{1/2} \frac{\lambda v_m n_s}{3} v^{1/3}(S-1) \tag{5.6}$$

In the above expressions v_m is the volume of a single molecule, v is the volume of the particle, λ is the mean free path of the gas and n_s is the saturation number density in molecules per unit volume related to the saturation vapour pressure as $n_s = p_s/kT$.

Coagulation

Coagulation is the term given to the process where droplets collide and coalesce to form a new droplet, both parent and daughter droplets are assumed to be spherical in this situation. This should not be confused with agglomeration, which is the joining of particles that do not coalesce in this manner. As is shown in Eq. (5.2) the rate of successful collisions between particles of size v_i and v_j to form a new particle of v_{i+j} is given by:

$$\dot{N}_{ij} = \beta(v_i, v_j) n_i n_j \tag{5.7}$$

The factor $\beta(v_i, v_j)$ is the collision frequency function, analogous to a reaction rate between two species. This are also known as collision kernels and [15] splits these further into the kernels due to various physical processes such as turbulent shear and turbulent inertial motions [102]. However [15] also shows that for small particles, such as those considered in this chapter, the collision frequency is dominated by Brownian motion. Pratsinis [97] gives expressions for the collision frequency $\beta(v_i, v_j)$ due to Brownian motion for particles in the free molecule regime

$$\beta_{FM}(v_i, v_j) = \left(\frac{3}{4\pi}\right)^{1/6} \left(\frac{6kT}{\rho_p}\right)^{1/2} \left(\frac{1}{v_i} + \frac{1}{v_j}\right)^{1/2} (v_i^{1/3} + v_j^{1/3})^2 \tag{5.8}$$

and in the continuum regime

$$\beta_C(v_i, v_j) = \left(\frac{2kT}{3\mu}\right) \left(\frac{C(v_i)}{v_i} + \frac{C(v_j)}{v_j}\right) (v_i^{1/3} + v_j^{1/3}) \tag{5.9}$$

where μ is the gas viscosity and $C(v) = 1 + 1.257\lambda/r$ if r is the particle radius.

The coagulation process in Eq. (5.7) is a local one, that is, it affects the number density at a point and is a function of the population at the same point, analogous to a reaction rate. However this assumes that there is a sufficiently large number of particles within the locality of point where the rate is being calculated for the particle number densities to be properly defined. So at low number concentrations Eq. (5.7) may not be accurate, although lower number concentrations lead to low coagulation rates and so this may not be important relative to other processes.

5.1.2 Representations of Aerosol Size Distributions

Eq. (5.2) can be solved computationally in two main ways [15, 23]. Firstly the size range can be discretised into a number of 'size-bins' [30]. If this is done then the simulation can be thought of as a system of N_T reacting scalars, where N_T is the number of size bins. The number density in each bin will then be transported by the flow field and will have production and loss terms due to growth and coagulation

which are functions of concentrations in other size bins and local vapour concentration and temperature. There will also be a production term due to the nucleation rate, which will only affect the bin which coincides with the critical volume.

An alternative method is to use an assumed shape for the size distribution that is characterised by a number of moments of the size distribution [97, 103]. These moments are defined as

$$M_k = \int_0^\infty v^k n(v) dv \tag{5.10}$$

Thus the first moment, M_0, is the total number density of particles of all sizes and the second moment, M_1, is the total volume, i.e. the volume of aerosol per unit volume of carrier gas. A governing equation for moment, M_k, can be obtained by multiplying both sides of Eq. (5.2) by v_k and integrating over all v. This leaves:

$$\frac{\partial M_k}{\partial t} + \boldsymbol{u} \cdot \nabla M_k = \int_0^\infty v^k s dv \tag{5.11}$$

where $\boldsymbol{u}$ is a turbulent velocity field and s contains the nucleation, growth and coagulation terms from Eq. (5.2). When the integral is performed (see Pratsinis [97] for details) an equation is obtained which is a function of other moments. Some of these moments may be tracked as well, but others will not. For these unknown moments a closure is required which must be provided by assuming a shape for the distribution. If coagulation is neglected this can be done most simply by using the first two moments and assuming that locally all particles have the same volume (monodisperse), which can be found by dividing the second moment (total volume) by the first (total number). Pratsinis [97] uses three moments and assumes a log-normal distribution from which any moment can be found from the first three. In order to fully close the three moment system an assumption also has to be made that the effect of particle curvature on the saturation vapour pressure (the Kelvin effect) can be neglected.

The advantage of the first method is that it accurately models the evolution

of the actual size distribution and will properly take account of the effects of a distribution away from a presumed one on aerosol processes. However, to accurately model the size distribution a large number of size bins must be used. Also the range of particle volumes expected must already be known before the calculation is attempted. Further, there are discretisation errors associated with the growth term. These are discussed in [15].

5.1.3 The Effect of Turbulence on Aerosol Processes

Rigopoulos [30] performs Reynolds averaging of the General Dynamic Equation Eq. (5.2) in order to examine the effects of turbulent fluctuations on these processes. It is shown that when this is done all three of nucleation, growth and coagulation have unclosed terms. If growth was only a function of the particle then the mean growth rate would be in closed form. However, as can be seen from Eqs. (5.5 & 5.6), the growth rate is a function of local vapour pressure and temperature and hence correlations between these must be taken into account.

While attempts have been made to model the effect of turbulence on coagulation via the collision frequency function [102], this does not account for the correlation of fluctuations in number densities of particles of different sizes. These correlations were first noted by Scott [104] and Warshaw [105]. The latter concluded that the correlations would have a greater effect in small volumes of air rather than in large volumes such as clouds. Friedlander [23] states that these correlations require further study.

As can clearly be appreciated from Eq. (5.4) the homogeneous nucleation rate is a highly non-linear function of local vapour concentration and temperature. For instance a 10K change in temperature can lead to changes in nucleation rate of several orders of magnitude. Because of this attempting to calculate a nucleation rate for the mean population using only mean vapour concentration and temperature will lead to large errors. This is shown by Lesniewski and Friedlander [99] who

show that for nucleation at the edge of a turbulent jet a sharp ring of nucleation is predicted, if only mean quantities are used, but when turbulence is considered the nucleation region is spread out and the peak significantly lowered.

5.2 Implementation of Stochastic Fields Method for Aerosol Processes

As was seen in the previous section, turbulence has an affect on aerosol processes that would not be captured if only mean quantities were used in calculations. The extreme non-linearity of many of the terms in Eq. (5.2) makes the use of PDF methods, which capture the effect of fluctuations from the mean directly, highly attractive. Rigopoulos [30] has obtained a transport equation for the joint particle number density - species PDF, i.e. $f(\phi_1, \ldots, \phi_\alpha, n_1, \ldots, n_N)$, where ϕ_1 to ϕ_α are the scalars and n_1 to n_N are the number densities of particles in size bins from 1 to N. The equation is found to be similar to the scalar PDF transport equation, Eq. (1.6), with nucleation, growth and coagulation appearing in closed form in the source term.

They appear in this form in the source term because they are modelled in Eqs. (5.4, 5.5, 5.6, 5.8 & 5.9) as production and loss terms that are functions purely of local conditions. Because of this they can be treated in the same way as other reacting scalars and appear in the source term as such. Terms are present in Rigopoulos's equation both for molecular diffusion of the ordinary scalar terms and also for diffusion of the particles. This particle diffusion will be due to Brownian motion and it is not at present clear how this should be modelled in the PDF approach. If this Brownian diffusion is dealt with in the same way as for the vapour phase and temperature scalars then the joint particle number density - species PDF can be treated in the same way as a standard joint scalar PDF equation, as is done in [30]. This includes following the procedure of either Valiño [49] or Sabel'nikov [50] to derive the

Stochastic Fields equation in either Ito or Stratonovich form for the aerosol system. If this is done then Eq. (2.6) or Eq. (2.8) will be solved for vapour concentration, temperature and the particle number concentration in each size bin for each field. A decision would need to be made as to the timescale used for 'micromixing' of the particles in the IEM model.

If a fine discretisation of the size distribution is required then a very large number of equations will need to be solved at a high computational cost, effectively multiplying the problem faced in using a full size distribution in a non-stochastic approach. There is, therefore, an advantage in using moment methods for the size distribution in Monte-Carlo solutions such as the Stochastic Fields method. If this is done then the object will be to find the joint scalar - size distribution moment PDF in the flow, i.e. $f(\phi_v, M_0, \ldots, M_X, T)$ for an assumed distribution using X moments. This approach is followed by Lindstedt and Louloudi [106] in their transported PDF simulation of a jet flame with soot formation. They use a transported particle PDF approach where each particle has a value for each scalar and also for each of a number of moments of the soot size distribution. For the remainder of this chapter a moment method is employed with the Stochastic Fields method. The three-moment log-normal distribution of Pratsinis [97] (as described in Section 5.1.2) is used for most calculations. A simple monodisperse distribution is also used for comparison.

It can be seen that Eq. (5.11) models a quantity, M_k which is dispersed by a turbulent velocity field and is produced and destroyed by source terms which are the integrated aerosol process term on the RHS. These are treated in the models used for the RHS of Eq. (5.11) as being essentially functions of local vapour concentration, temperature and the other moments at the same location. As this is the case the system of scalars and moments can be treated in the same way as a system of reactive scalars and a modelled PDF transport equation, Eq. (1.6), can be derived with the aerosol processes in closed form in the source term. From this the Stochastic Fields equation can be derived in the usual way. There is still an outstanding issue of the treatment of the micromixing term for the aerosols. Lindstedt and Louloudi [106]

apply Curl's mixing model to their notional particles. If the IEM model is used and the timescale is assumed to be the same for all sizes of particle then integrating the IEM term over all particle sizes would yield the IEM term for the moments.

When solving for the evolution of an aerosol population there are issues concerning the validity of assuming processes to be functions of 'local' conditions, although these are issues concerning the validly of the population balance equation, Eq. (5.2), rather than the solution method. Assuming the moment source terms to be functions of local vapour concentration and temperature is sound. Gas phase concentration and temperature are both scalars and can be thought of as having a defined value at any point in the same way as for gas phase chemical reactions. Hence there should be no error in calculating the nucleation rate which is a function of these scalars and not the particle distribution. There may be errors associated with assuming moment source terms to be functions of the local particle distribution if the 'local' population is small. The coagulation rate may not follow Eq. (5.7) if only a few particles are present. Total volume growth rates may also be in error as they are a function of the number of particles at differing sizes. Eqs. (5.5 & 5.6) for the growth rate of individual particles should still hold, but with small particle populations this growth rate may be multiplied by fractions of particles. The largest error associated with a small total number density will be that the assumed shape of the distribution may not be valid [107]. However any errors associated with this are inherent to the moment method as described by Pratsinis [97, 98] and will be present whether the moment source terms are employed in a PDF simulation or in a 'plain' calculation based which takes no account of turbulent fluctuations.

The SF method with a log-normal distribution should capture some of the effect of turbulence on particle size distribution and hence on aerosol processes. For example, if the first two moments are used, at a given point in a field a random combination of particle number and volume density will be found; thus the effect of correlations involving these two parameters is considered. However, in each field the distribution will conform to the same assumed overall shape, and the full ef-

fect of turbulent fluctuations on the shape of the distribution will therefore not be considered. Wu and Menon [108] employ the three moment system of [98] together with the multiscale random mixing technique employed in their earlier paper [85] to investigate production of binary water and acid aerosols in aircraft plumes. They found that inclusion of random mixing events, as opposed to large scale turbulent entrainment alone, led to particle number density being increased by around 40%. They attributed this increase to turbulent mixing bringing together SO_3 and H_2O to form H_2SO_4, which in turn leads to increased particle nucleation.

In this chapter the Stochastic Fields equation has been employed together with with Pratsinis's three moment method [97] to model the experiment of Lesniewski and Friedlander [9, 99]. This experiment consists of a heated nitrogen jet carrying Dibutyl Phthlalate vapour mixing out into a cooler background. Details of the experiment are given in Section 5.3 followed by the numerical procedure adopted here in Section 5.3.2.

5.3 Aerosol Production in a Turbulent Jet

5.3.1 Flow Considered

Lesniewski and Friedlander [9, 99] studied the homogeneous nucleation and growth of Dibutyl Phthalate (DBP) droplets. DBP was chosen as it will condense at room temperature but will remain as vapour at temperature not far above this. This means that there is no need for cooling the flow. The experiments were carried out in a 15cm diameter glass chamber, and the jet nozzle diameter was either 0.235cm or 0.375cm. The calculations presented in this chapter use the 0.235cm nozzle. The jet velocity was in the range 30 - 80m s^{-2} and a co-flow velocity of 0.18m s^{-2} was used to prevent recirculation. Measurements were restricted to the region where the jet could be considered a free jet, i.e. before the onset of plug-flow.

For all experiments the co-flow was air at a temperature of 299K. The jet was

at a temperature of 413K and consisted of nitrogen with DBP vapour. The vapour concentration and temperature were chosen such that no nucleation would take place in the delivery system or on the nozzle and also so that measured number concentrations downstream would be in all cases less that 10^4 cm^{-3}. At this low number concentration the effect of coagulation can be expected to be negligible [99].

5.3.2 Numerical Methods

In order to apply the Stochastic Fields method to this problem the approach used has been similar to that used in Chapter 3 for the NO_x/O_3 plume. The three-dimensional problem was transformed into a two-dimensional problem by taking a grid perpendicular to the jet axis and time marching Eq. (2.6) downstream from the nozzle exit. A fractional-step method was used in which the first step is to solve, for each field n in turn, the advection, 'diffusion,' micromixing and aerosol reaction terms employing the method of lines with VODPK.

$$U_1\frac{\partial \tau_i^n}{\partial x_1} = -U_k\frac{\partial \tau_i^n}{\partial x_k} + \frac{\partial}{\partial x_k}\Big(K\frac{\partial \tau_i^n}{\partial x_k}\Big) + \dot{w}\left(\tau_1^n, \tau_2^n, \ldots, \tau_5^n\right) - \frac{\tau_i^n - \overline{\phi}_i}{T_{eddy}} \tag{5.12}$$

Here τ_i^n represents the value of the i^{th} scalar in field n. The five scalars used for this problem are the concentration of DBP in the vapour phase (molec cm^{-3}), temperature (K) and the first three moments of the aerosol size distribution (particles per cm^3, cm^3 of aerosol per cm^3 gas and cm^6 of aerosol per cm^3 gas). $k = 2, 3$ and represents the two cross stream directions. x_1 is the axial distance from the nozzle exit and U_1 is the axial velocity. This is solved for five scalars; DBP vapour, temperature and three moments of the log-normal aerosol size distribution. The reaction term $\dot{w}\left(\tau_1^n, \tau_2^n, \ldots, \tau_5^n\right)$ refers to the aerosol processes and is discussed further below. In comparison to Eq. (3.4), Eq. (5.12) has an extra cross stream advection term, this is to take account of radial velocity in the jet without which the entrainment of the jet will not be captured correctly. The turbulent diffusivity, K, is inside the second spatial derivative as it is not constant across the jet in this case. In this chapter

Brownian diffusion of the particles has been neglected, by doing this the timescale T_{eddy} for M_0, M_1 and M_2 is made effectively infinite and the micromixing term is dropped for these three. For temperature and gas phase concentration the turbulent mixing timescale is again made equal to the turbulent velocity timescale.

The second and final step is to apply the random Wiener term to each scalar in each field using the Euler-Maruyama approximation as before. The local increment of the Wiener process in this case will be

$$\begin{aligned} \Delta W_k^n &= \xi_k^n (\Delta t)^{1/2} \\ &= \xi_k^n \left(\frac{\Delta x_1}{U_1} \right)^{1/2} \end{aligned} \tag{5.13}$$

this makes the final fractional-step

$$\tau_i^n(t + \Delta t) = \tau_i^n(t^*) + (2K)^{1/2} \frac{\partial \tau_i^n(t^*)}{\partial x_k} \xi_k^n \left(\frac{\Delta x_1}{U_1} \right)^{1/2} \tag{5.14}$$

where ξ_k^n is a random number with zero mean and unity variance, chosen independently for each direction in each field. Velocity and turbulence information in the form of U_k, K and T_{eddy} were taken from a CFD simulation of the jet. A limit is placed on the maximum size of the Wiener step to prevent unbounded scalars, as in Section 2.2.1.

The aerosol source terms for vapour concentration and distribution moments, $\dot{w}\left(\tau_1^n, \tau_2^n, \ldots, \tau_5^n\right)$, used are those derived assuming a log-normal distribution by Pratsinis [97] and used by Ford et al [98] and Wu and Menon [108]. These are

$$\dot{w}_{vap} = (Jv^* + C_1)/v_m \tag{5.15}$$

$$\dot{w}_{M_0} = J - B_1 \tag{5.16}$$

$$\dot{w}_{M_1} = Jv^* + C_1 \tag{5.17}$$

$$\dot{w}_{M_2} = Jv^{*2} + C_2 + B_2 \tag{5.18}$$

$$\dot{w}_T = 0 \tag{5.19}$$

where v_m is the volume of a single molecule. The critical volume v^* is found from the critical radius in Eq. (5.3) and the nucleation rate is calculated using Eq. (5.4). The B and C terms account for coagulation and growth respectively and are calculated as harmonic averages of the free molecule and continuum values. The coagulation terms are found from Eqs. (5.8 & 5.9) and result in:

$$\begin{aligned} B_1^{FM} &= b_0\beta_2(M_0^{151/72}M_1^{-13/36}M_2^{19/72} \\ &+ 2M_0^{131/72}M_1^{7/36}M_2^{-1/72} + M_0^{127/72}M_1^{11/36}M_2^{-5/72}) \qquad (5.20) \\ B_1^{C} &= \beta_4\Bigg(M_0^2 + M_0^{19/9}M_1^{-2/9}M_2^{1/9} \\ &+ \beta_5\lambda\Big(\frac{4\pi}{3}\Big)^{1/3}(M_0^{23/9}M_1^{-7/9}M_2^{2/9} + M_0^{25/9}M_1^{-11/9}M_2^{4/9})\Bigg) \qquad (5.21) \\ B_2^{FM} &= 2b_2\beta_2(M_0^{19/72}M_1^{47/36}M_2^{31/72} \\ &+ 2M_0^{-1/72}M_1^{67/36}M_2^{11/72} + M_0^{-5/72}M_1^{71/36}M_2^{7/72}) \qquad (5.22) \\ B_2^{C} &= 2\beta_4\Bigg(M_1^2 + M_0^{1/9}M_1^{16/9}M_2^{1/9} \\ &+ \beta_5\lambda\Big(\frac{4\pi}{3}\Big)^{1/3}(M_0^{2/9}M_1^{17/9}M_2^{-1/9} + M_0^{4/9}M_1^{13/9}M_2^{1/9})\Bigg) \qquad (5.23) \end{aligned}$$

where β_2, β_4 and β_5 taken from Eqs. (5.8 & 5.9) are given by:

$$\begin{aligned} \beta_2 &= \left(\frac{3}{4\pi}\right)^{1/6}\left(\frac{6kT}{\rho_p}\right)^{1/2} \qquad (5.24) \\ \beta_4 &= \left(\frac{2kT}{3\mu}\right) \qquad (5.25) \\ \beta_5 &= 1.257 \qquad (5.26) \end{aligned}$$

and b_0 and b_2 are used in order to approximate the integral over all particle sizes and are given by

$$b_0 = 0.633 + 0.092a^2 - 0.022a^3 \quad (5.27)$$

$$b_2 = 0.39 + 0.5a - 0.214a^2 + 0.029a^3 \quad (5.28)$$

$$a = \exp\left(\sqrt{\frac{1}{9}\ln\left(\frac{M_0 M_2}{M_1^2}\right)}\right) \quad (5.29)$$

The growth terms are calculated according to Eqs. (5.5 & 5.6) as

$$C_1^{FM} = (36\pi)^{1/3}\left(\frac{kT}{2\pi m}\right)^{1/2} v_m n_s (S-1) M_0^{2/9} M_1^{8/9} M_2^{-1/9} \quad (5.30)$$

$$C_1^{C} = (48\pi^2)^{1/3}\left(\frac{8kT}{\pi m}\right)^{1/2} \frac{\lambda v_m n_s}{3} (S-1) M_0^{5/9} M_1^{5/9} M_2^{-1/9} \quad (5.31)$$

$$C_2^{FM} = 2(36\pi)^{1/3}\left(\frac{kT}{2\pi m}\right)^{1/2} v_m n_s (S-1) M_0^{-1/9} M_1^{5/9} M_2^{5/9} \quad (5.32)$$

$$C_2^{C} = 2(48\pi^2)^{1/3}\left(\frac{8kT}{\pi m}\right)^{1/2} \frac{\lambda v_m n_s}{3} (S-1) M_0^{-1/9} M_1^{8/9} M_2^{2/9} \quad (5.33)$$

In order to investigate the effect of the assumed size distribution shape an alternative distribution will be used, where all aerosols are locally assumed to be of the same volume. This assumes that there will be no coagulation and M_2 can be discarded. This should not make a large difference for the DBP experiment. The volume is given by $v = M_1/M_0$ and the remaining growth terms will therefore be

$$C_1^{FM} = (36\pi)^{1/3}\left(\frac{kT}{2\pi m}\right)^{1/2} v_m n_s (S-1) M_0^{1/3} M_1^{2/3} \quad (5.34)$$

$$C_1^{C} = (48\pi^2)^{1/3}\left(\frac{8kT}{\pi m}\right)^{1/2} \frac{\lambda v_m n_s}{3} (S-1) M_0^{2/3} M_1^{1/3} \quad (5.35)$$

The constants and property values needed in the above expression are given in Table 5.1.

5.3.3 Jet CFD

A CFD solution of the jet was produced using the FLUENT software. A 2D axisymmetric grid was used which extends 3cm upstream of the end of the nozzle exit.

Table 5.1: Properties and constants used in Dibutyl Phthalate aerosol process calculations.

DBP molecular weight (g molecule^{-1}) [99]	$m = 278.4/N_A$
Saturation vapour pressure (mm Hg)[99]	$\log P_{sat} = 7.065 - 1666/T - 547700/T^2$
Surface tension (g s^{-2}) [99]	$\sigma = 35.3 - 0.0863(T - 273)$
Condensed density (g cm^{-3}) [99]	$\rho_p = 1.063 - 0.000826(T - 273)$
Molecular volume (cm^3)	$v_m = m/\rho_p$
Mean free path (cm) [23, 97]	$\lambda = 6.5 \times 10^{-6}$
Gas viscosity (g cm^{-1} s^{-1}) [97]	$\mu = 1.8 \times 10^{-4}$
Avagadro's number (mol^{-1})	$N_A = 6.022 \times 10^{23}$
Boltzmann constant (J K^{-1})	$k = 1.381 \times 10^{-23}$

This is equal to the length of tube used for the nozzle in the experiment and allows for the development of pipe flow in the simulation. The nozzle radius is 0.1175cm and the grid extends 20cm downstream of the nozzle and the maximum radius is 7.5cm. At the nozzle exit there are 19 cells across the pipe radius and the same resolution is initially used in the axial direction. Grid spacing in both radial and axial directions increases away from the nozzle as shown in Fig. 5.1. A total of 55,600 grid cells were used in the mesh.

The solution was produced using the Reynolds stress model with the solution parameters as shown in Table 5.2. The beginning of the nozzle tube and the co-flow were set to be mass-flow rate boundaries. With a temperature specified and the gauge pressure set to zero this is effectively the same as a velocity inlet. For the jet a mass flow rate of 1.378×10^{-4}kg s^{-1} of nitrogen and a temperature of 413K is specified, this corresponds to the 10 l min^{-1} used in [99]. Turbulence boundary conditions of $k = 0.001\text{m}^2\text{s}^{-2}$ and $\epsilon = 0.0001\text{m}^2\text{s}^{-3}$ are used in the jet. The co-flow mass inlet extends from a radius of 1.35cm to 7.5cm (taken from scale drawing in [9]) and a flow rate of 4.0833×10^{-3}kg s^{-1} of air at a temperature of 299K. A turbulence intensity of 10% is used as measured in the experiment and a length scale

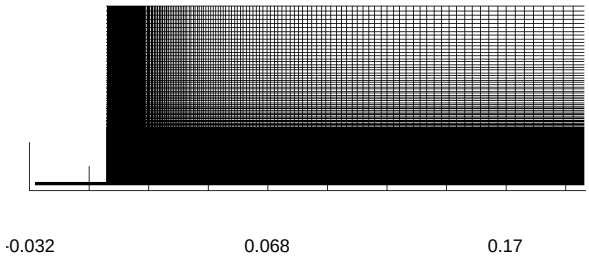

Figure 5.1: Aerosol nucleation jet CFD grid as used to generate velocity and turbulence data for reacting flow calculations.

of 1.5cm, equal to the diameter of the glass spheres placed upstream of the co-flow. Between the nozzle and the co-flow is a wall boundary condition representing the insulation around the nozzle. A wall boundary is used at the edge of the domain and the outlet is specified as an outflow. In order to examine the effect of velocity, a second solution was produced using a jet mass flow half that above, but with all other boundary conditions unchanged.

The SF equation was solved on a square 2cm by 2cm grid which was time-marched to 4.5cm downstream of the nozzle. This small domain is consistent with [99] which states that most of the nucleation takes place around the potential core of the jet, around 1cm downstream of the nozzle in this case. The flow field data for the SF equation was provided by using a 5cm by 5cm section of the axisymmetric CFD from adjacent to the nozzle. At each SF step flow data at each grid point is found by calculating the axial and radial position at that point and interpolating linearly from this CFD section. The axial velocity is always limited to a minimum value of 0.18m s^{-1}. The axial velocity, radial velocity, turbulent viscosity and turbulent timescale in the 5cm by 5cm section of the CFD solution used are shown in Fig.

Table 5.2: Solution parameters used in FLUENT CFD solution of aerosol nucleation jet [10].

Solver	2D axisymmetric, segregated, implicit
Reynolds stress model constants	$C_\mu = 0.09$, $C_{1\epsilon} = 1.44$, $C_{2\epsilon} = 1.92$, $C_{1PS} = 1.8$
Reynolds stress model options	Wall BC from k equation, wall reflection effects
Pressure-velocity coupling	SIMPLE
Density	Incompressible ideal gas
c_p	Mixing law using Nitrogen and air
Discretisation - pressure	Standard
Discretisation - momentum	1^{st}-order upwind
Discretisation - k	1^{st}-order upwind
Discretisation - ϵ	1^{st}-order upwind
Discretisation - Reynolds stresses	1^{st}-order upwind
Discretisation - Energy	1^{st}-order upwind

5.2. The calculated axial velocity along the axis of the jet is shown in Fig. 5.3. Also shown is the velocity predicted by using an empirical expression from Tieszen et al [8] for axial velocity of a free jet with different density to the background:

$$\frac{\overline{W}}{W_0} = 11.8\left(\frac{\rho_{jet}}{\rho_{back}}\right)\left(\frac{r_{noz}}{x_1}\right)\exp\left[-93.7\left(\frac{r}{x_1}\right)^2\right] \tag{5.36}$$

$\overline{W}$ is the axial velocity, W_0 is the mean nozzle velocity. There is very good agreement between the two solutions.

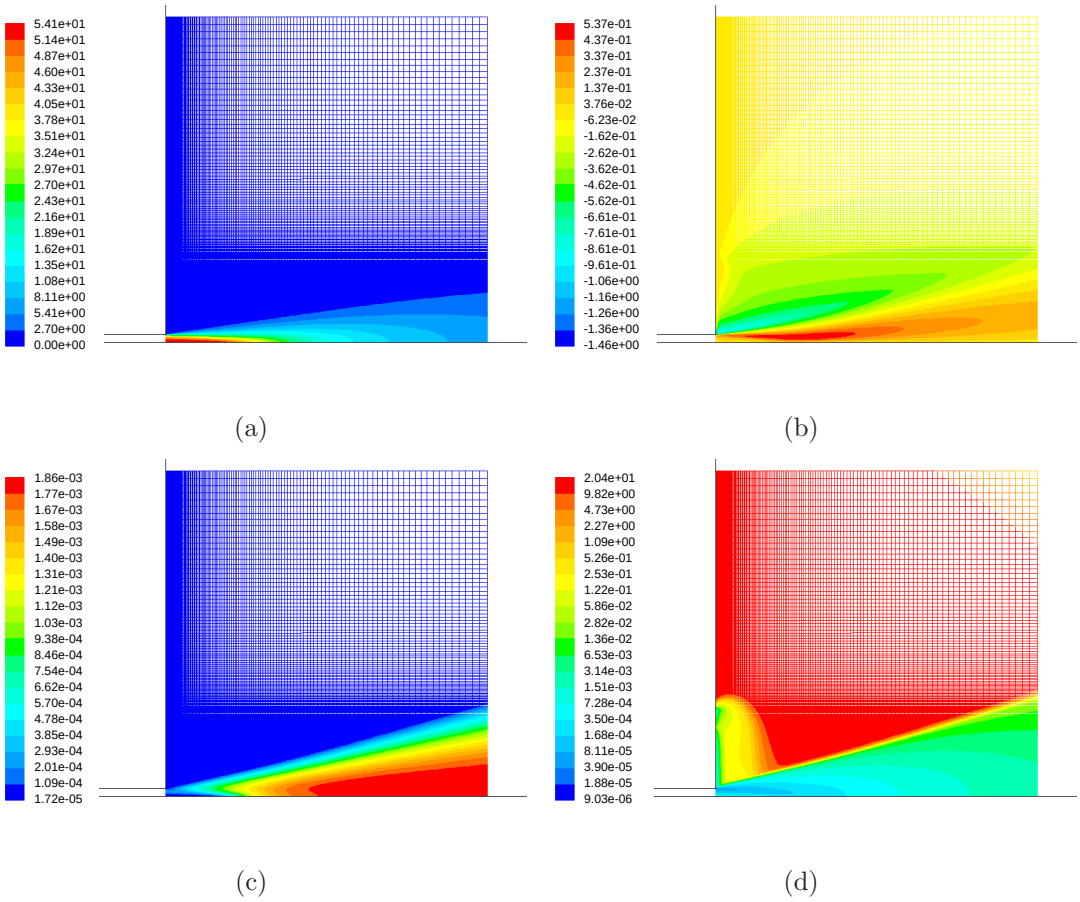

Figure 5.2: Velocity and turbulence fields used in SF aerosol nucleation calculations on an axisymmetric plane adjacent to the nozzle. (a) axial velocity [m s^{-1}]; (b) radial velocity [m s^{-1}]; (c) turbulent viscosity, ρK, [kg m^{-1} s^{-1}] and (d) turbulence timescale, T_{eddy}, [s].

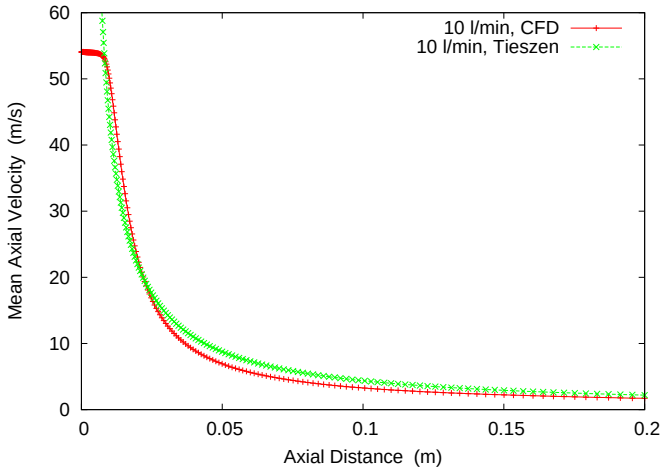

Figure 5.3: Mean axial velocity along the jet axis calculated by CFD solution and also using empirical expression [8].

5.3.4 Stochastic Fields Calculations

As mentioned previously the SF equation was solved on a 2cm by 2cm square grid. Two grid densities were used one had grid spacing of 1.0×10^{-4}m up to 3mm either side of the jet axis and 5.0×10^{-4}m outside this. The other grid had exactly half this resolution. The results, including variances, were found to be independent of the choice of grid and the finer grid was used unless stated. The axial distance step in the time-marching scheme was varied between 1.0×10^{-6}m and 1.0×10^{-4}m, it was again found that results were independent of this and therefore a value of 1.0×10^{-5}m was used unless stated. The micromixing term for vapour concentration and temperature was again carried out as a separate step to check that this caused no splitting errors. A total of 25 fields were used for the SF calculations unless stated and the method of Eq. (2.7) was again used for comparison to show the effect of including segregation.

An initial condition of a top hat profile was used for vapour concentration and temperature with the nozzle value for those nodes in a 0.235cm diameter circle and the background value for those outside. The three moments were set to low

values across all nodes. The method outlined above, including limiting the size of the random term for the scalars, proved to be very robust even for these top hat profiles.

5.4 Results

5.4.1 Inert Mixing

In order to test the time-marching Stochastic Fields scheme used in this chapter, results for the mean value of an inert scalar at various axial locations are compared with those obtained using the axisymmetric CFD solution used to produce the velocity and turbulence data. The inert scalar used is mixture fraction, i.e. a scalar which take a value of zero in the co-flow and one in the jet. The results are shown in Fig. 5.4. As will be the case throughout this chapter, the 2D SF solutions have been radially averaged to give a single radial profile at each axial location. This was done by taking the mean of all nodes whose radial distance to the centre line fell into the same size bin. The resolution of the size bins were equal to the grid spacing of the original grid.

Fig. 5.4 shows good agreement between the two solutions, meaning that the SF solution is producing the correct mean mixing behaviour within the constraints of the velocity and turbulence data provided by the CFD solution. It can also be seen that at 1cm downstream the mixing has just reached the centre-line, indicating that this is the end of the potential core.

5.4.2 Nucleation Only

By setting all B and C terms to zero in Eqs. 5.15 to 5.18 we are left with an aerosol mechanism where the only process is nucleation. Lesniewski [9] and Okuyama et al [109] found that classical theory (Eq. (5.4)) under-predicts nucleation rates of DBP droplets by several orders of magnitude. This has also been observed here. Using

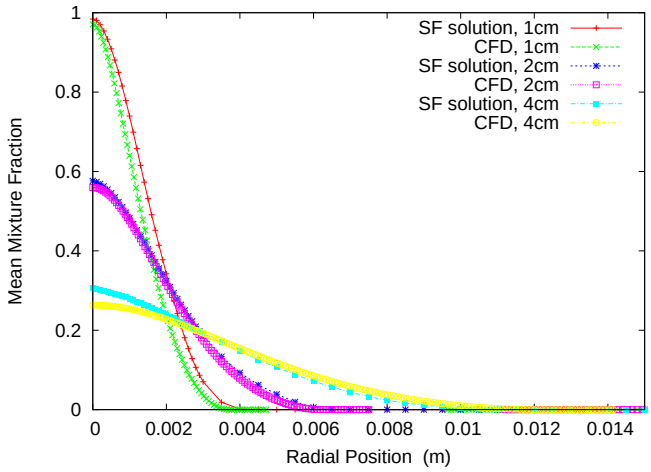

Figure 5.4: Radial profile of mean mixture fraction at 1cm, 2cm and 4cm downstream of the jet. Predictions by both CFD solution and by time-marched SF solution.

initial vapour mole fractions in the range used in the experiment, 100 - 500ppm (2.0×10^{15}molec cm^{-3} - 1.0×10^{16}molec cm^{-3}), negligible nucleation rates were observed. This illustrates the difficulties of using classical theory to predict nucleation rates in complex situations. Lesniewski [9] suggests the the results can be reconciled to the experimental observation by reducing the calculated surface tension by 10 - 15%. Following this, surface tension was reduced in subsequent calculations by 10%. This improved predictions considerably. Further tuning of the surface tension could have been attempted but this was not thought to be useful given the variability in experimentally measured data. Results presented from here onwards therefore use a surface tension that is reduced by 10% from that given in Table 5.1.

Results for inlet conditions of $T = 413$K and $X_{vap} = 6.0 \times 10^{15}$molec cm^{-3} are shown in Figs. 5.5 & 5.6 using both the SF method and a plain, non-stochastic method in order to show the effect of neglecting segregation in this process. In Fig. 5.5 the behaviour of the mean vapour concentration is shown to be the same as for the mixture fraction. This is as expected as the nucleation rate is so small compared to the vapour concentration that the latter should be virtually unchanged from inert

mixing values. As vapour concentration is effectively an inert scalar, the SF method should leave its mean value unchanged. Any deviation is the result of statistical error. Very little of such deviation is seen in Fig. 5.5 although this is partly due to the radial averaging used to produce the radial profile.

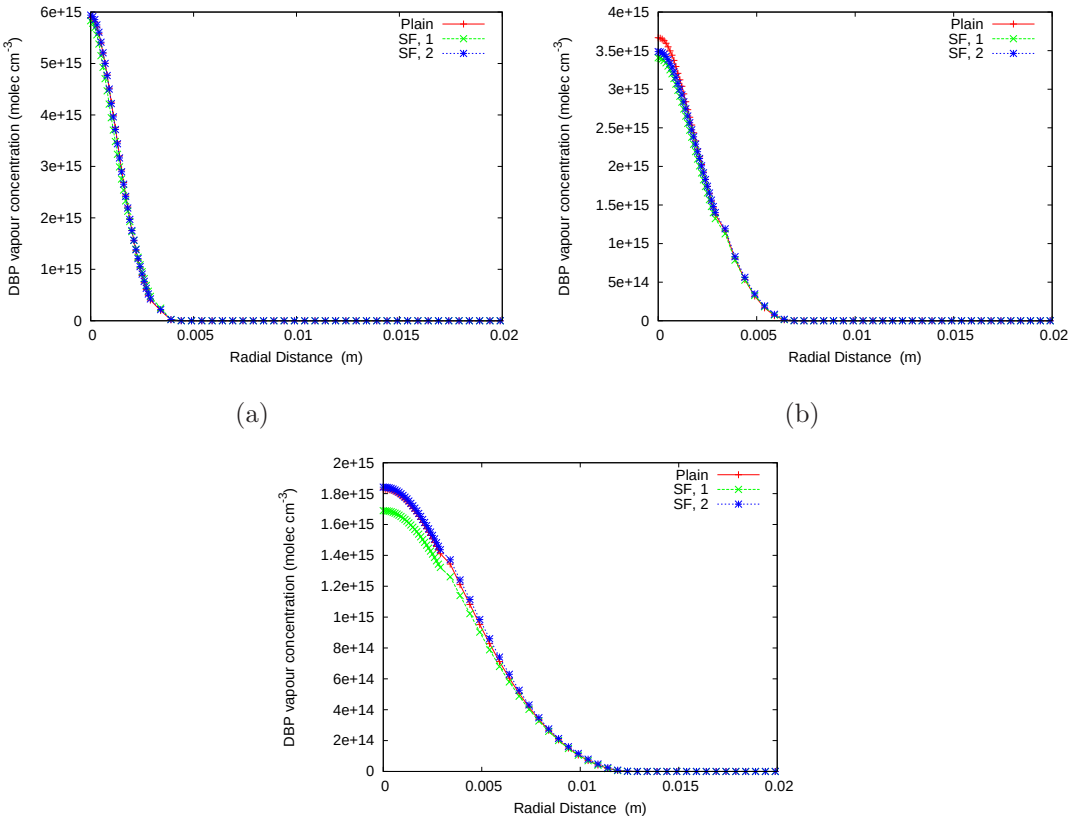

Figure 5.5: Radial profiles of mean vapour concentration at (a) 1cm; (b) 2cm and (c) 4cm downstream of the jet. Initial vapour concentration: 6.0×10^{15}molec cm^{-3}. Initial jet temperature: 413K. Calculations by both SF and plain advection-diffusion method.

In Fig. 5.6 the evolution of the mean particle number density is shown. The centre-line number density at 4cm downstream are of the same order of magnitude as the measurements given in [9] for similar conditions. For initial vapour concentration of 5.8×10^{15}molec cm^{-3} experimentally measured centre-line number densities at

4.7cm downstream of the nozzle ranged between 600 and 1300 # cm^{-3}. It can be seen that segregation does not have a great effect on centre-line number density where there are zero gradients for mean vapour concentration and temperature. However the peak in particle density around the edge of the jet is significantly reduced in the SF solution compared to the 'plain' solution. Experimental data for these radial profiles is not available.

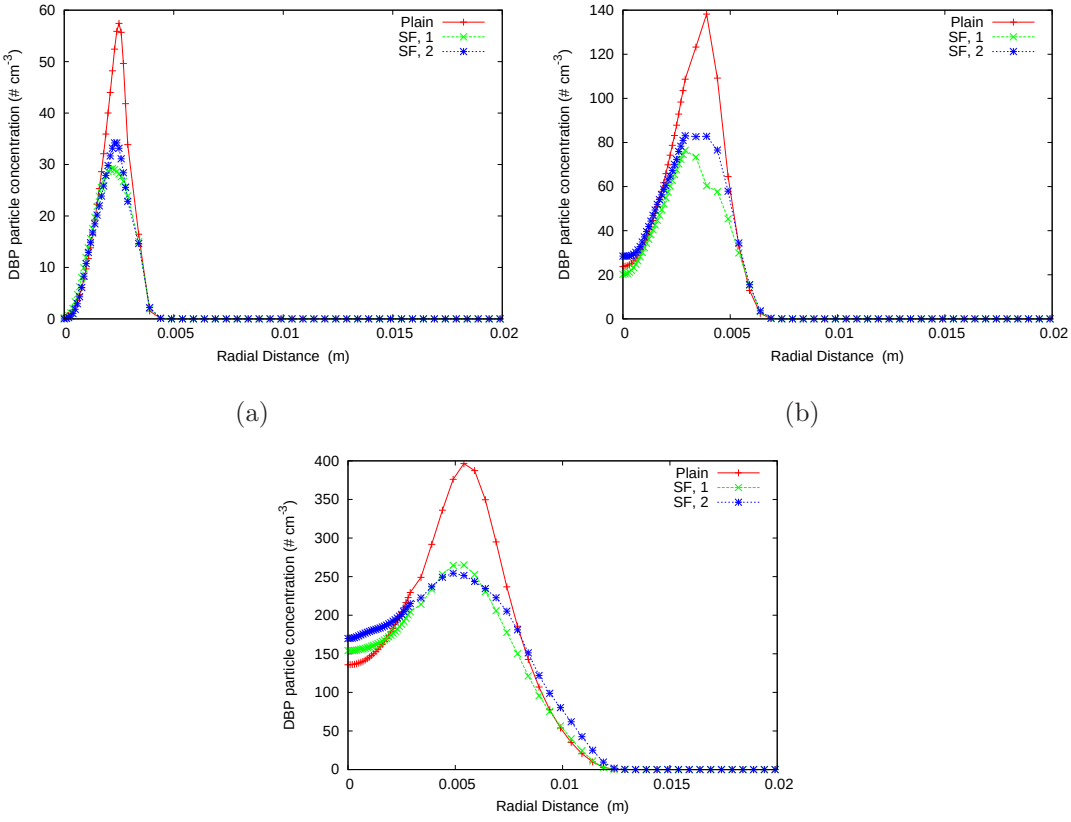

Figure 5.6: Radial profiles of mean particle number concentration at (a) 1cm; (b) 2cm and (c) 4cm downstream of the jet. Initial vapour concentration: 6.0×10^{15}molec cm^{-3}. Initial jet temperature: 413K. Calculations by both SF and plain advection-diffusion method. Nucleation only.

If a slightly larger initial vapour concentration of $X_{vap} = 8.5 \times 10^{15}$molec cm^{-3}

is used, the extreme sensitivity of nucleation rate to saturation ratio can be seen in Fig. 5.7. A 1.4 times increase in vapour concentration leads to an increase in particle number density of over 200 fold. Similar increases are seen in experimental results, as shown in Fig. 5.8. Here the experimentally measured [9] trend of number concentration with initial vapour concentration is compared with the results obtained numerically for the two cases above. It should be noted that the experimental results are taken at a point slightly further downstream. The predicted results show a slightly steeper trend with vapour concentration than experiment, but are of the same order of magnitude. The effect of including segregation in the simulation using a higher concentration is very similar to that seen for the smaller initial vapour concentration.

The effect of segregation can be further studied by considering the nucleation rate itself. The nucleation rate was calculated using both plain and SF methods. For the SF solution the nucleation rate was calculated in each field and then the mean was found at each grid node. This data was then radially averaged as before. Results of this are shown in Fig. 5.9 for 6.0×10^{15}molec cm^{-3} and 8.5×10^{15}molec cm^{-3}. The radial position has been offset by the radius of the nozzle and normalised by axial location in order to give η, which is a measure of the position in the shear layer.

$$\eta = \frac{r - d/2}{x_1} \tag{5.37}$$

where r is the radial position and d is the nozzle diameter. This is the same method as used in [99, 110].

The results obtained here using the SF method show very good agreement with Fig. 5.10, which is taken from Lesniewski [9]. This shows results found in Lesniewski and Friedlander's earlier paper [110]. In this they calculate reaction rate for one set of trial conditions, assuming unity Lewis number, in the shear layer using mean values and also by using measured PDF's for concentration and temperature from experimental data. They showed that nucleation rate is a function of position in

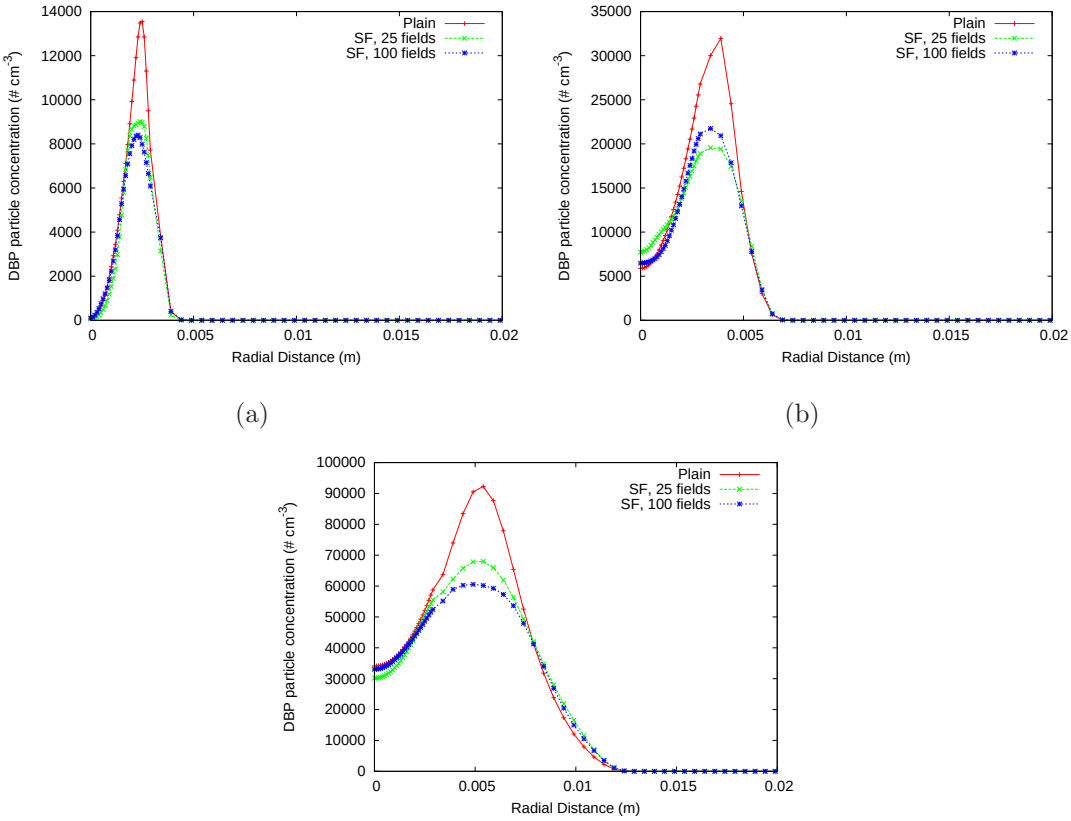

Figure 5.7: Radial profiles of mean particle number concentration at (a) 1cm; (b) 2cm and (c) 4cm downstream of the jet. Initial vapour concentration: 8.5×10^{15}molec cm^{-3}. Initial jet temperature: 413K. Calculations by both SF and plain advection-diffusion method. Nucleation only.

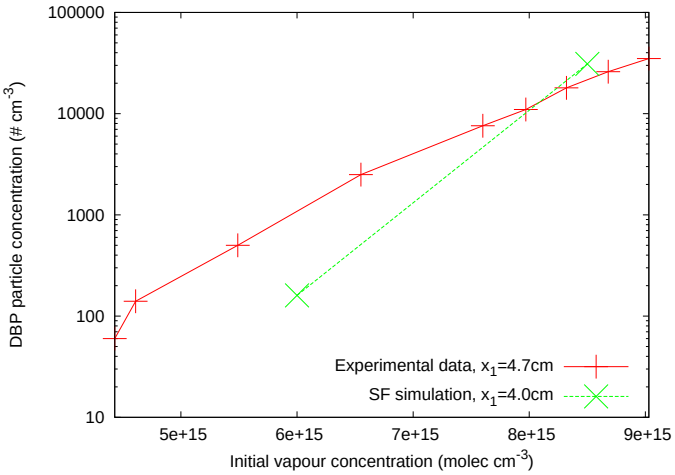

Figure 5.8: Measured and predicted variation of centre-line particle number concentration with initial jet vapour concentration. Experimental results taken from Trial 819, Appendix D of Lesniewski [9], for 4.7cm downstream of nozzle. SF predictions taken at 4.0cm downstream of nozzle.

the shear layer and also that, while using mean values to calculate the nucleation rate leads to a sharp high peak, correctly taking account of turbulence leads to a nucleation region that is wider and has a significantly lower peak. Lesniewski and Friedlander [99] suggests that nucleation should be quenched once beyond the shear layer, at around $x_1/d = 10$, for vapour concentrations lower than 6.2×10^{15}molec cm^{-3}, although the results presented in Figure 9 of [99] seem to suggest that nucleation occurs past $x_1/d = 20$ for vapour concentrations lower than their suggested cut-off value. As can be seen in Fig. 5.9, there is still significant nucleation occurring in plain and SF calculations at 4cm downstream or $x_1/d = 17$ at 6.0×10^{15}molec cm^{-3}.

If initial conditions in the jet of $x_v = 3.5 \times 10^{15}$molec cm^{-3} and $T = 350$K are used then the calculated nucleation rate and particle number density evolve downstream as shown in Fig. 5.11. No experimental results are available to compare with these results and they are included in order to explore the influence of jet temperature on

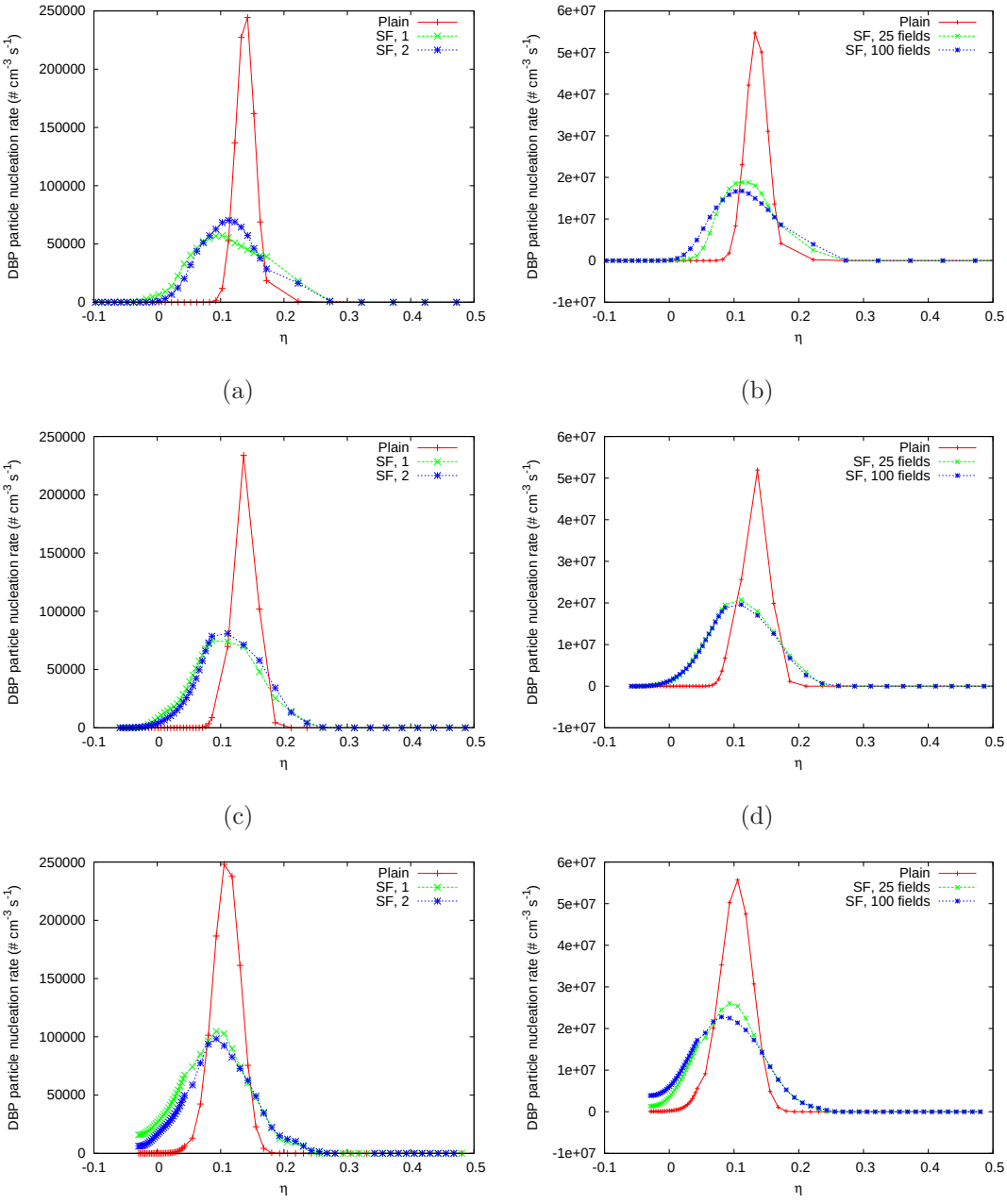

Figure 5.9: Radial profiles of mean nucleation rate at 1cm, 2cm and 4cm downstream. (a) $x_v = 6.0 \times 10^{15}$molec cm^{-3} at 1cm; (b) 8.5×10^{15}molec cm^{-3} at 1cm; (c) 6.0×10^{15}molec cm^{-3} at 2cm; (d) 8.5×10^{15}molec cm^{-3} at 2cm; (e) 6.0×10^{15}molec cm^{-3} at 4cm and (f) 8.5×10^{15}molec cm^{-3} at 4cm. Initial jet temperature: 413K. Calculations by both SF and plain advection-diffusion method.

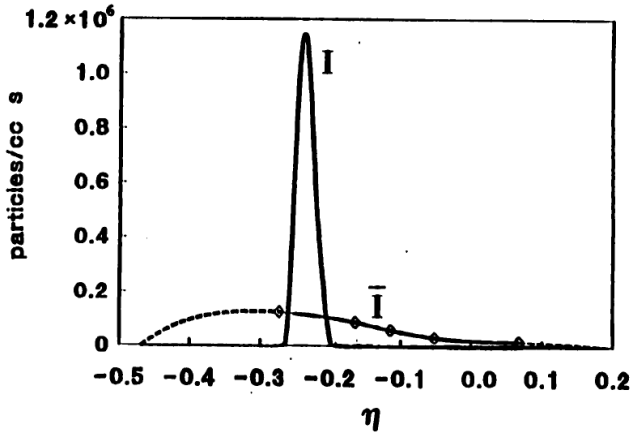

Figure 5.10: Calculated nucleation rate profiles in the shear layer. Figure taken from Lesniewski [9]. I is the rate calculated using local mean concentration and temperature. $\overline{I}$ is calculated taking fluctuations into account using experimentally measured PDF's. Dashed line represents extrapolation where PDF data not available. Note that η has been measured in opposite direction from centre-line compared to Fig. 5.9.

the nucleation predicted by this method. It can be seen in Fig. 5.11 that while in the early part of the plume, with $x_1 < 10d = 2.35$cm, a sharp peak is seen in the shear layer as was seen for the earlier results.

However further downstream the nucleation region has spread right across the plume, and the nucleation rate has started to decrease. Using the SF solution again shows a nucleation region that has a lower peak rate and is more spread out than that given by assuming mean conditions. The particle number density at 4cm has a lower centre-line value when the SF method is used but there is an increased value at the edge of the plume due to the spread in the nucleation region. Further downstream as conditions tend towards the background the rate will drop to effectively zero and particle formation would be quenched. However using either mean values only or a SF solution a nucleation region across the plume must be crossed before the jet reaches the quenched region.

In order to quantify the effect of segregation on predicted particle number density, integrated particle fluxes were calculated using

$$\dot{N}_T = \int N\boldsymbol{v} \cdot d\boldsymbol{A} \tag{5.38}$$

where N in this case in the number density equal to M_0. This was done for both plain and SF solutions and the percentage differences found between the two solutions, calculated as $(\dot{N}_{T,SF} - \dot{N}_{T,P})/\dot{N}_{T,SF}$, are presented in Table 5.3. Note that for seed 2 in the 8.5×10^{15}molec cm^{-3} results 100 fields were used rather than 25 in the other results and hence this results can be expected to have greater statistical accuracy. For the results with an initial jet temperature of 413K the percentage difference in the particle fluxes is approximately constant for all three locations. For the 350K jet, the difference in the particle fluxes is reduced to 1-5% by 4cm downstream. Fig. 5.11 shows that at this position with these conditions the centre-line particle concentration has been reduced but at larger radii the concentration has increased, explaining why the integrated flux for both solutions are closer together.

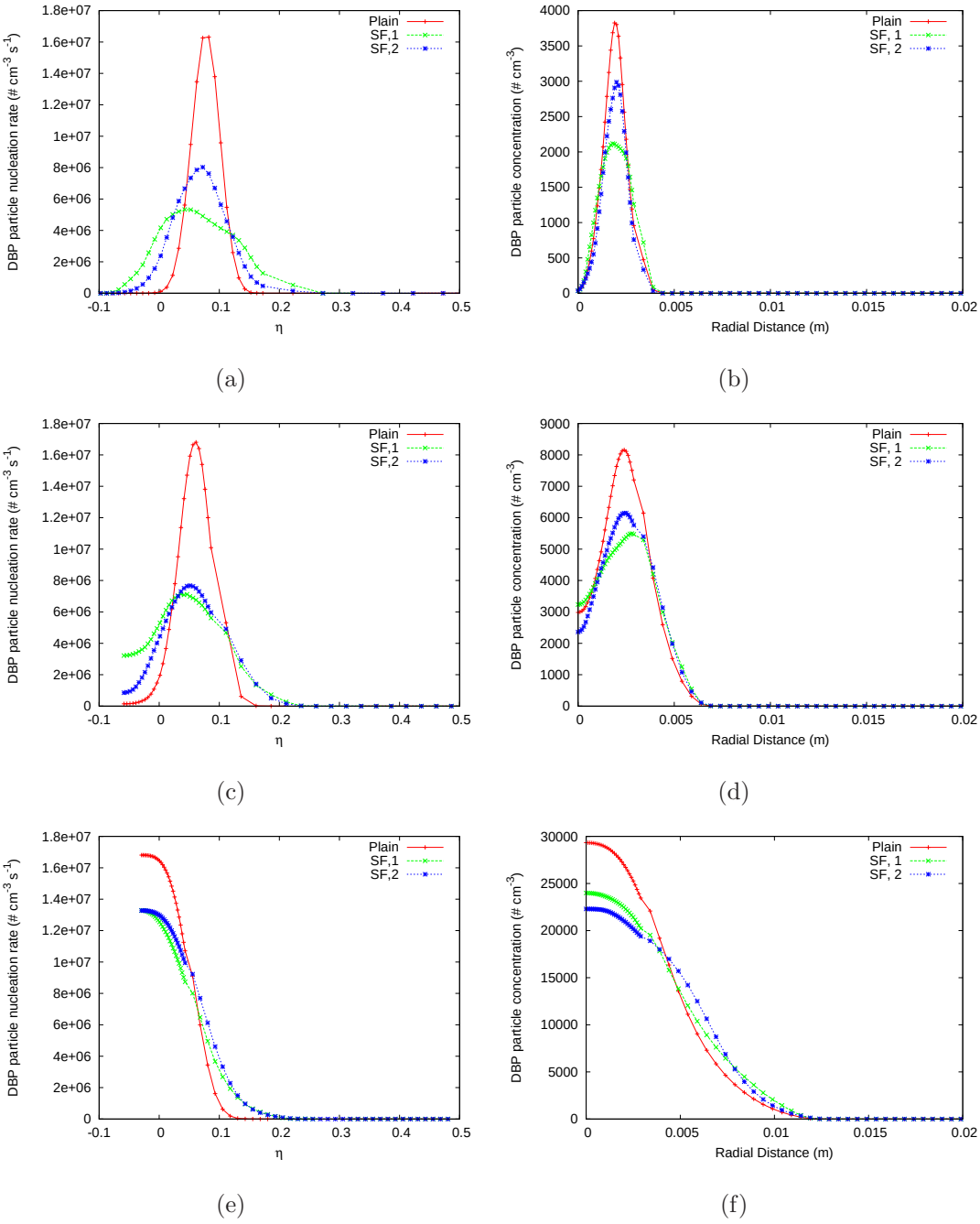

Figure 5.11: Radial profiles of nucleation rate and particle number density. (a) nucleation rate at 1cm; (b) number density at 1cm; (c) nucleation rate at 2cm; (d) number density at 2cm; (e) nucleation rate at 4cm and (f) number density at 4cm. Initial vapour concentration: 3.5×10^{15}molec cm^{-3}. Initial jet temperature: 350K. Calculations by both SF and plain advection-diffusion method.

Table 5.3: Normalised difference between particle fluxes with and without segregation effects at axial locations, x_1, downstream of Dibutyl Phthalate jet. $X_{vap,0}$ is jet vapour concentration and T_0 is the jet temperature.

$X_{vap,0}$ (molec cm^{-3})	T_0 (K)	x_1 (cm)	Normalised difference (%)	
			Seed 1	Seed 2
6.0×10^{15}	413	1.0	-25	-27
		2.0	-42	-24
		4.0	-27	-23
8.5×10^{15}	413	1.0	-28	-23
		2.0	-28	-26
		4.0	-17	-25
3.5×10^{15}	350	1.0	-29	-25
		2.0	-24	-18
		4.0	-5	-1

5.4.3 Aerosol Growth and Coagulation Results

The simulations using an initial vapour concentration of 6.0×10^{15}molec cm^{-3} were repeated using the full three moment method described in Section 5.3.2. This allows the effects of growth and coagulation on the aerosol size distribution to be modelled. If radially averaged number concentration profiles using the full method, shown in Fig. 5.12, are compared with those shown in Fig. 5.6 it can be seen that particle number concentration is unaffected by using the full method. This was confirmed by using Eq. (5.38) to calculate integrated particle fluxes which showed no difference either for plain or SF results. Therefore, in agreement the experiment which was designed to avoid coagulation, the effect of coagulation in the early part of the jet is negligible.

With the moment method employed here the first moment of the size distribution, M_0, is the particle number density and it is this that is plotted in Fig. 5.12. The

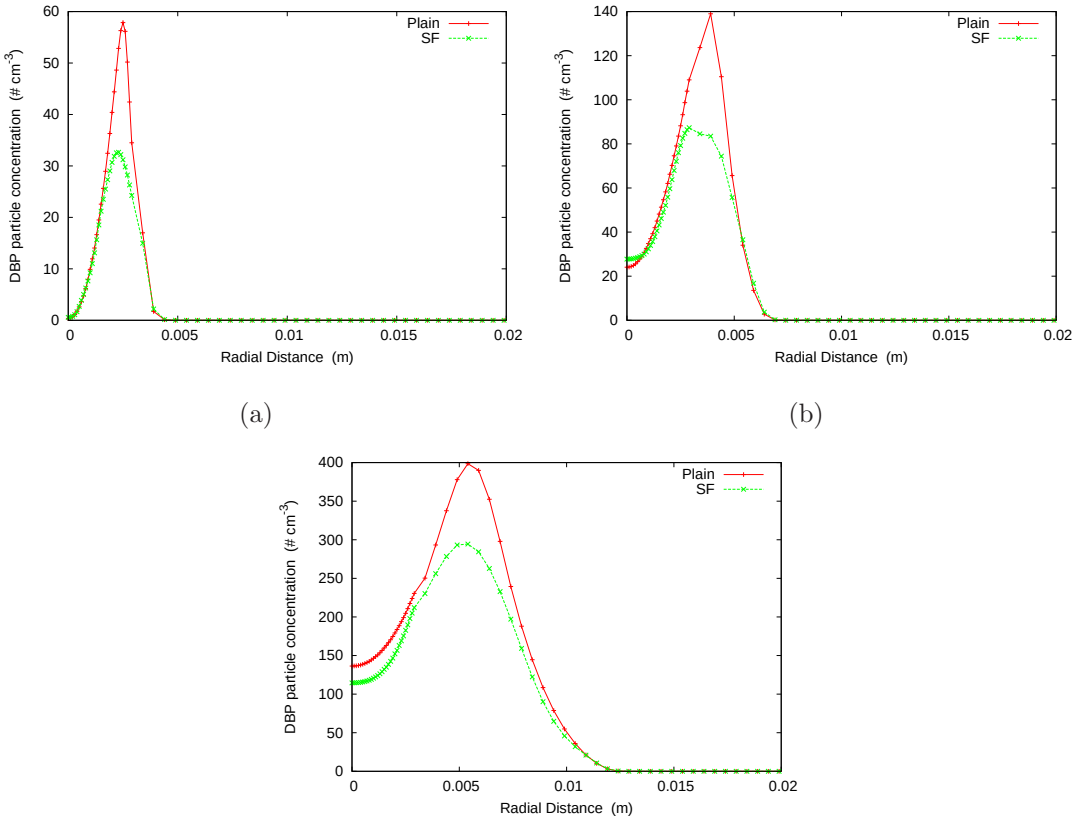

Figure 5.12: Radial profiles of mean particle number concentration at (a) 1cm; (b) 2cm and (c) 4cm downstream of the jet. Initial vapour concentration: 6.0×10^{15}molec cm^{-3}. Initial jet temperature: 413K. Calculations by both SF and plain advection-diffusion method using full three moment aerosol process system.

second moment, M_1, is total aerosol volume per unit volume of carrier gas. If only nucleation is considered then the development of the second moment will follow the first. When growth is considered the distribution of M_1 will evolve differently after particles have been nucleated. This is shown in Fig. 5.13. The volume radial profile at 1cm follows the same shape as the number profile at the same location, indicating that most of the increase in volume up to this point is due to the production of new particles. However, further downstream at 2cm and 4cm the profile take a different shape, showing that in this region volume is increasing due to existing particles growing, particularly close to the centre-line.

The influence of turbulence on volume concentration also seems to be different than on number concentration. For number concentration the effect of segregation was to reduce the peak around the edge of the jet but has left the centre-line values largely unchanged, perhaps because, with or without segregation the nucleation rate on the centre-line is relatively small. When volume concentration is considered, segregation reduces the centre-line value, but leads to increased values at the edge of the plume. This may be due to the turbulence mixing conditions which lead to slower particle growth towards the centre of the jet and conditions that lead to more rapid growth towards the edge.

Particles measured in the experimental work on the centre-line at $x_1/d = 20$ were found to range in size from approximately 0.3μm to 6.0μm, with the largest peak at around 2.0μm. Mass mean diameters ranged from 1.0μm to 3.0μm. With the moment method employed here the most convenient way to consider particle size is to divide the volume density by the number density in order to give a local mean particle volume. The results of applying this to the results presented above is shown in Fig. 5.14. The profiles are only shown up to a radial position corresponding with the edge of the particle number density plume, as results beyond this point have no physical meaning. Fig. 5.14 supports the conclusions drawn above that the influence of turbulence is to reduce particle size at the centre of the plume and increase it at the edge. By assuming these particles to be spherical a mean diameter

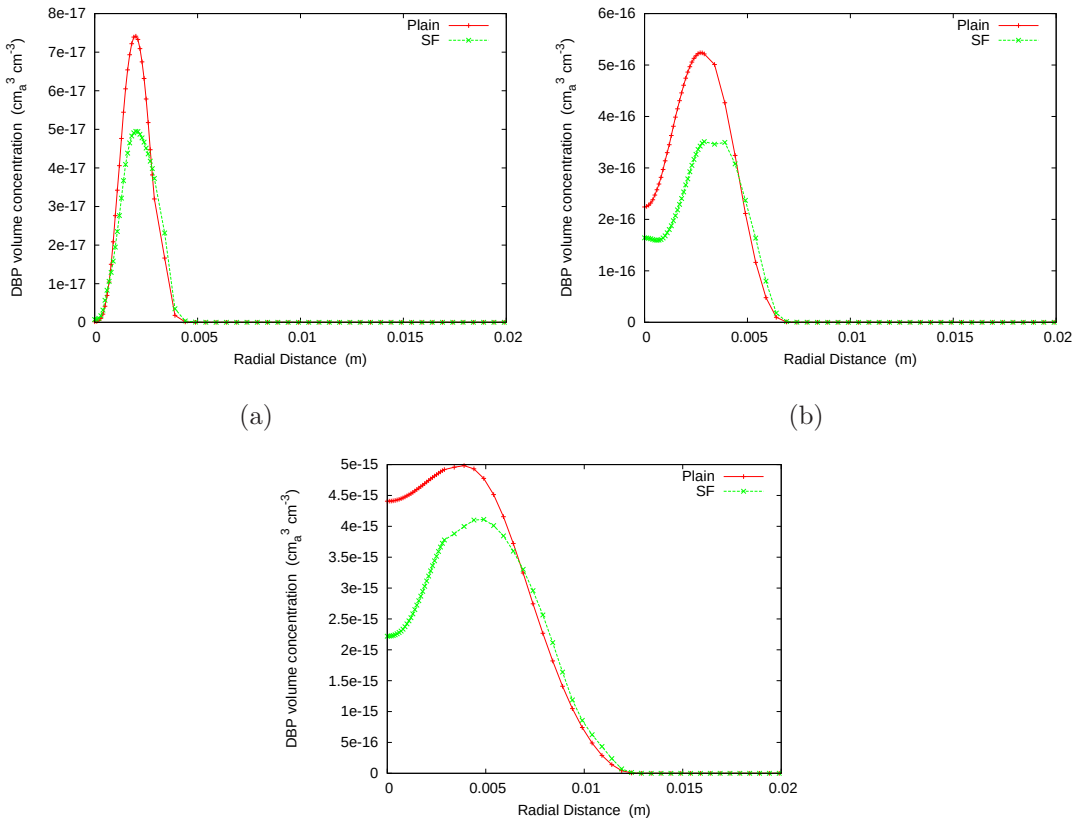

(a) (b)

(c)

Figure 5.13: Radial profiles of mean total aerosol volume concentration at (a) 1cm; (b) 2cm and (c) 4cm downstream of the jet. Initial vapour concentration: 6.0×10^{15}molec cm^{-3}. Initial jet temperature: 413K. Calculations by both SF and plain advection-diffusion method using full three moment aerosol process system.

can also be found, this will correspond to the volume mean diameter [101]. The mean particle diameter on the centre-line at 4cm is predicted as 3.9μm using the plain method and 3.3μm using the SF method. Hence the method employed here gives good predictions of particle growth for these conditions, with both plain and SF results falling in the size range found by experiment. Although both predicted values of volume mean diameter are higher than measured values of mass mean (which will be equivalent to volume mean given constant density), the result using the Stochastic Fields method is closer to the experimental values. This indicates the potential impact of considering the effect of turbulence on mean particle growth and also the usefulness of the SF method as a tool to deal with this.

Reduced Jet velocity

A second CFD solution was produced using a jet velocity equal to half that used in the above calculations. The velocity and turbulence data produced by this solution were used in a simulation using the same initial jet temperature and vapour concentration as used above; the initial vapour concentration was 6.0×10^{15}molec cm^{-3} and jet temperature was 413K. Results for these conditions at 4cm downstream of the jet are shown in Fig. 5.15. The nucleation rate is unchanged from the higher velocity jet, which agrees with the hypothesis described in [99] that nucleation rate is a function of position in the shear layer and jet vapour and temperature conditions but not a function of jet Reynolds number. The longer residence time leads to higher particle number concentrations, but the particle flux through a plane perpendicular to the jet will be unchanged. This trend with jet velocity agrees with experimental results for the turbulent jet. Reduction to laminar jet speeds in the experimental work [9] leads to a sharp increase in number density.

The slower jet has, however, led to a greater increase in volume concentration, which has increased by an order of magnitude at the same axial position. This is because the greater particle concentration implies more particles available for further

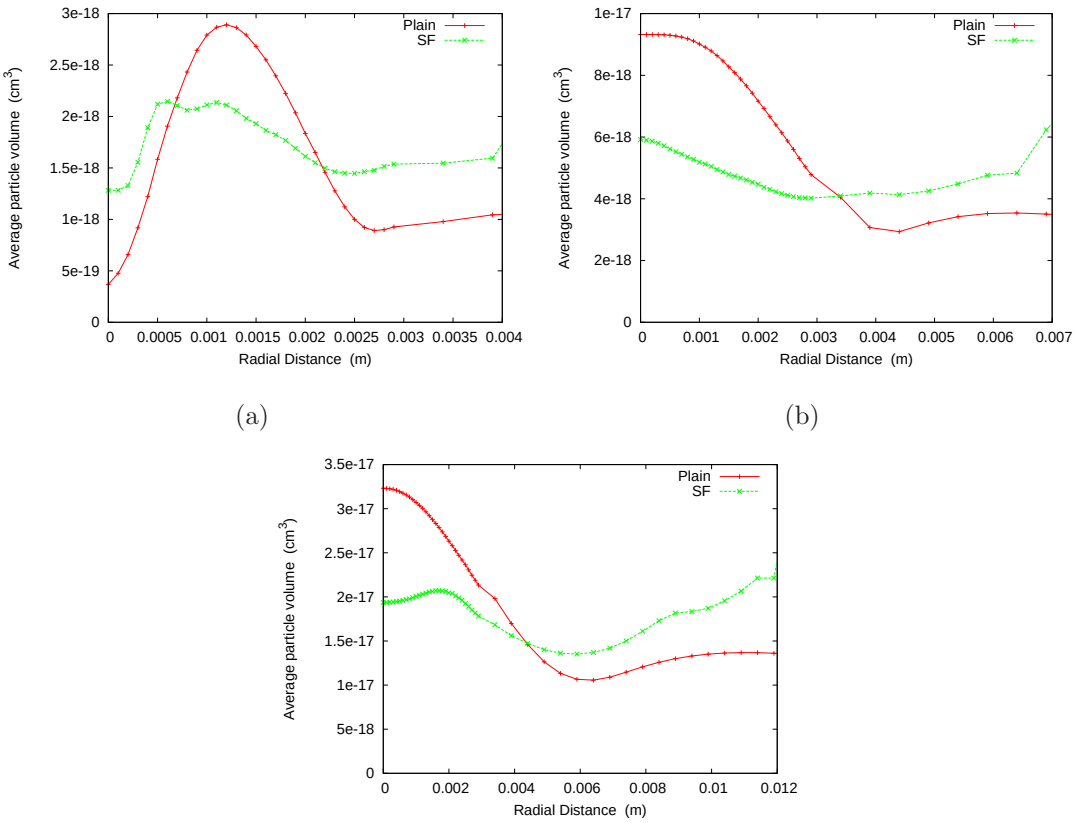

(a) (b)

(c)

Figure 5.14: Radial profiles of mean particle volume at (a) 1cm; (b) 2cm and (c) 4cm downstream of the jet. Initial vapour concentration: 6.0×10^{15}molec cm^{-3}. Initial jet temperature: 413K. Calculations by both SF and plain advection-diffusion method using full three moment aerosol process system.

growth in addition to allowing more time for growth to occur. The average particle volume has also increased significantly. The volume mean diameter at the centre-line is 4.6μm for the SF results. The limited experimental data [9] on particle size with jet speed does not show a clear trend. The changed turbulence conditions have not had a discernable influence on the segregation effects. The trends seen when turbulence is taken into account are much the same as those for the faster jet.

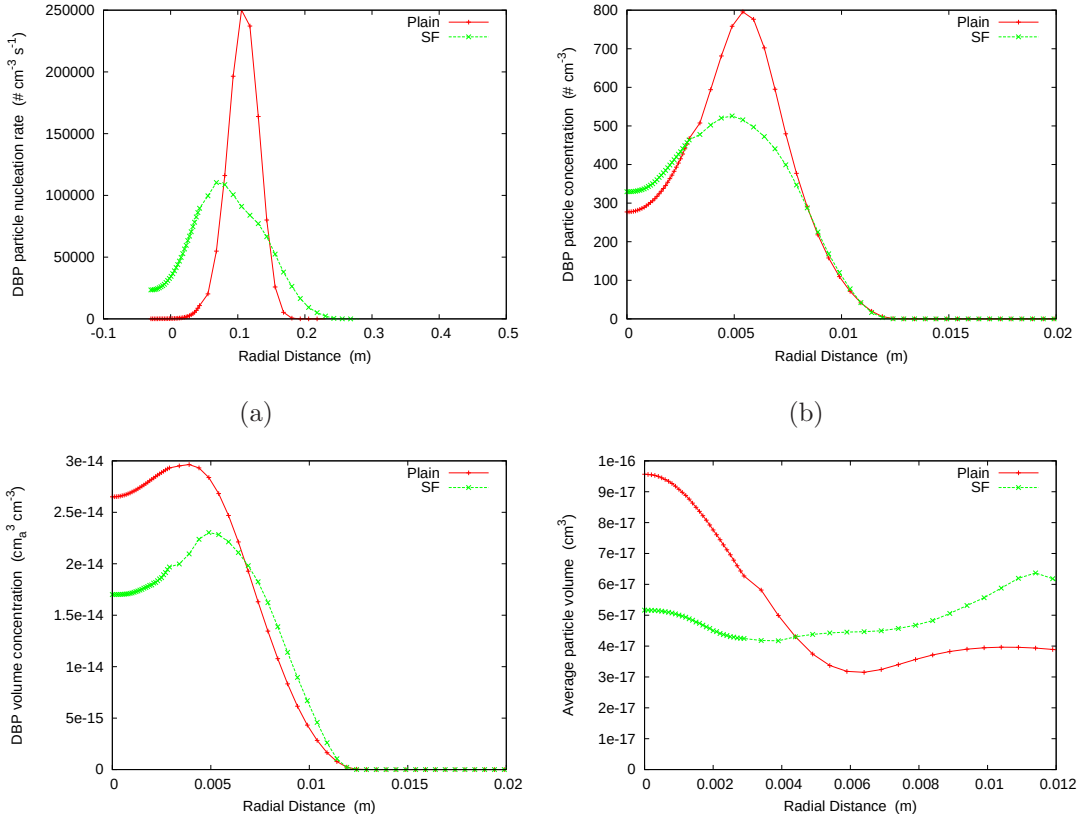

Figure 5.15: Radial profiles of (a) nucleation rate; (b) particle number density; (c) total volume density and (d) average particle volume, using slow jet. Initial vapour concentration: 6.0×10^{15}molec cm^{-3}. Initial jet temperature: 413K. Calculations by both SF and plain advection-diffusion method using full three moment aerosol process system.

Alternative Assumed Size Distribution

The moment method used so far in this chapter assumes that the particle size distribution takes a log-normal shape. As discussed in Section 5.2 this may not be appropriate with the small total number densities ($\sim$ 100) seen in the results so far. To investigate the sensitivity of the results to this assumption, calculations have been repeated using a less complex size distribution. As described in Section 5.3.2 this was done by assuming that all particles in a given location have the same volume, given by M_1/M_0. We assume that no coagulation takes place, which is supported by the results seen for the log-normal method and also in experimental results. The third moment, M_2, is no longer needed and the coagulation terms can be dropped from Eqs. 5.15 - 5.19. The growth terms are replaced by Eqs. 5.34 & 5.35, which are the same as Eqs. 5.30 & 5.31 in all respects other than the assumed distribution used to close the moment system.

This method was used with initial jet vapour concentration of 6.0×10^{15}molec cm^{-3} and temperature of 413K, using the higher velocity jet. As would be expected, due to neglecting coagulation results for particle number density are unchanged from the results using nucleation only or a log-normal distribution and are thus not presented here. Results for total volume concentration and average particle volume are presented in Fig. 5.16 for 1cm, 2cm and 4cm downstream of the jet.

The initial growth predicted by the simple method is greater than that using the full three moment method. At 1cm downstream the peak total volume concentration predicted by the simple method is 10% greater than that found using the log-normal method. Further downstream the difference is reduced. This indicates that close to the nozzle the effect of assuming that there are particles distributed either side of the mean particle volume is to slightly reduce the overall rate of condensation of vapour on to the particles, but that this effect is less important in the conditions encountered further from the nozzle.

The effect of including segregation on the average particle volume is qualitatively

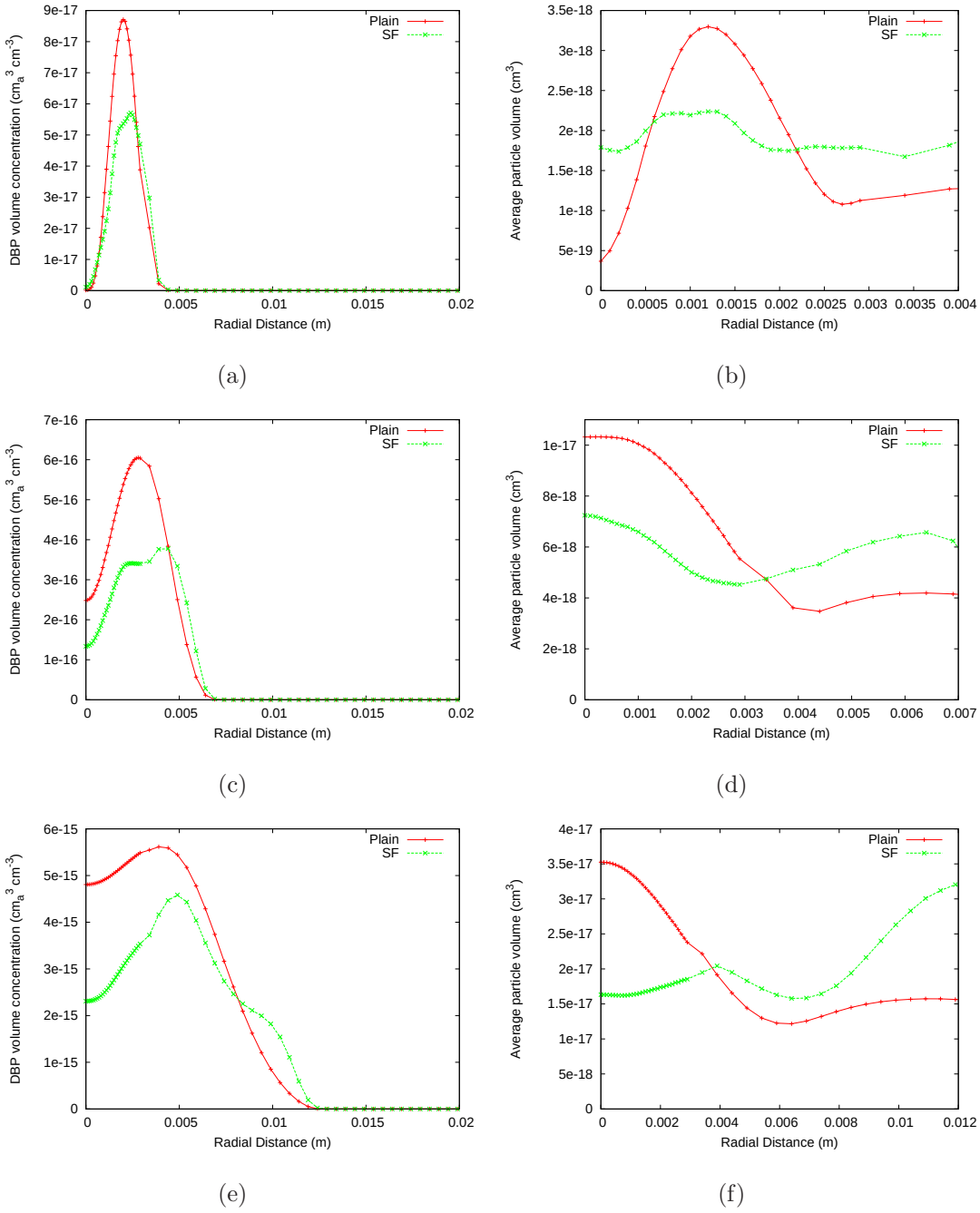

Figure 5.16: Radial profiles of total aerosol volume concentration and particle volume, assuming all particles have same volume locally. (a) volume concentration at 1cm; (b) particle volume at 1cm; (c) volume concentration at 2cm; (d) particle volume at 2cm; (e) volume concentration at 4cm and (f) particle volume at 4cm. Initial vapour concentration: 6.0×10^{15}molec cm^{-3}. Initial jet temperature: 413K. Calculations by both SF and plain advection-diffusion method.

the same as for the more complex moment system with particle size reduced near the centre of the plume and increased towards the edge when the SF method is used. This suggests that it may be the effect of turbulence on the vapour concentration and temperature that causes the difference rather than fluctuations in the moments. Quantitatively it appears that the reduction in particle size close to the centre of the plume, when segregation is included, is increased with the simple size distribution. The mean particle diameter on the centre-line, using the simple size distribution at 4cm is predicted as 4.1μm using the plain method and 3.1μm using the SF method.

5.5 Discussion

In the previous section the results of simulating nucleation and growth of Dibutyl Phthalate aerosol particles in a turbulent jet were presented. Using the Stochastic Fields method to take account of turbulent fluctuations of vapour concentration and temperature led to predictions of nucleation rate which, compared to assuming mean quantities in the nucleation rate expression, had a lower peak rate but which were effective over a greater area. This agrees with the work of Lesniewski and Friedlander [99]. The changed nucleation rate due to the turbulence led to reduced particle number densities. The extreme sensitivity of the nucleation rate expression, Eq. (5.4), to the vapour concentration and temperature as well as to the empirical expressions used for saturation vapour pressure and surface tension make accurate numerical predictions of exact number densities very difficult for this arrangement. Due to this, it is questionable how important the 25% reduction in total particle flux, found when using the SF method, is compared to the uncertainties already included in the modelling when attempting to simulate this experiment. However the effect of turbulence on nucleation is of wider importance and the SF method used here has been shown to be capable of revealing these differences.

With the modelled particle surface tension reduced by 10% as suggested by [99] it was possible to predict centre-line number densities in reasonable agreement with

experimental data. It was found that with a jet temperature of 413K, vapour concentrations that gave significant particle number densities (number densities greater than around $\sim$10 # cm^{-3}) still had fresh particle formation downstream of the shear layer. Lesniewski and Friedlander [99] report that at this temperature nucleation should cease by $x_1/d = 20$ for vapour concentrations below a cut-off value. By reducing jet temperature to 350K it was possible to reduce the axial extent of the nucleation zone.

Calculations including growth and coagulation were also performed. For the early part of the jet plume studied it was found that coagulation had a negligible affect. This agrees with experimental findings. Growth was included into the calculations by using moments of an assumed particle size distribution. Firstly, a log-normal distribution, which requires three moments to close the equations, was used [97]. For comparison an assumption of locally uniform particle size was used. Qualitatively both methods showed the same effect when the SF method was used to include turbulent fluctuations compared to using a plain, 'mean-value' method. Particle volume was reduced close to the centre of the plume, but was increased at the outer edge of the plume.

The particle volume calculated by assuming uniform size is around 10% bigger than the average volume found using a log-normal distribution at 1cm downstream of the jet and less than this by 4cm. This suggests that the presence of particles with volumes either side of the mean leads to a slight reduction in the total rate of condensation of vapour on to existing particles, particularly close to the jet nozzle. The log-normal distribution was derived as an assumed shape for a well-developed size distribution [97]. Figure 10 of [99] suggests that a log-normal distribution is a reasonable approximation to the measured size-distribution at 20 nozzle diameters downstream for low initial vapour concentrations. Note that the experimentally obtained distribution is thought to be produced by the growth of particles of varying ages rather than due to coagulation which will have an effect at higher particle number densities. Therefore at this axial location a log-normal distribution seems

a reasonable assumption to make. However, close to the nozzle all particles will be freshly nucleated and, according to classical theory, will have the same critical volume and it may be more appropriate in this region to assume uniform size.

Any assumed size distribution and moment method makes the implicit assumption that there will be a sufficient number of particles at a location for the assumed distribution to have any physical meaning. If only a small number of particles are present we cannot really assume that their sizes will always follow a particular shape. Many of the number densities predicted in this chapter are of the order of 100 # cm^{-3}, and this is perhaps too small to make assumptions of size distributions. The results for nucleation rate and hence total number density do not depend on the size distribution and so conclusions made about these quantities and the influence of turbulence upon them can be made with more confidence that those for aerosol volume. In order to better answer questions about how appropriate certain size distributions are in this setting, the simulations could be repeated using a discretised representation of the full size distribution in the manner suggested by Rigopoulos [30] and discussed in Section 5.2. This would be computationally more expensive but would give a useful insight into this problem.

5.6 Conclusions

In this chapter the Stochastic Fields method has been applied to Lesniewski and Friedlander's experiment modelling nucleation and growth of Dibutyl Phthalate aerosol particles in a hot turbulent jet mixing with ambient temperature background air [9, 99]. It was found that using the SF method to take account of turbulent fluctuations led to a reduction in overall nucleation rate and hence in predicted particle number density. This prediction agrees with experimental results. For a jet with initial temperature of 413K the total particle flux at 1cm, 2cm and 4cm downstream of the jet was found to be 25% less when the SF method was used. For a jet with initial temperature of 350K the reduction was again approximately 25% less at 1cm

and 12cm, but the change was reduced to around 1-5% at 4cm. Inspection of the radial profile of particle number density at this axial location shows that while the centre-line value is reduced, it is increased at the edge of the plume.

The first three moments of a log-normal size distribution were used to model growth and coagulation of the particles. In agreement with experimental data, it was observed that coagulation does not play a significant role in this situation due to relatively small particle number densities. The effect of turbulence on particle size via growth using this moment method was found to be a reduction in particle size close to the centre of the jet, but an increase in size at the edge of the plume. The volume mean diameters predicted on the centre-line fall within the measured size distribution from experimental data and are close to the value corresponding to the peak of the experimental size distribution. The same trend was found when a slower jet was used. For this slower jet total particle flux remains constant as particle concentration increases in proportion to residence time. The particle size increased by an order of magnitude as not only has the the residence time increased, but the number of particles for vapour to condense on has increased as well.

If a locally uniform particle volume is assumed then results of using the SF method on particle size is qualitatively the same as for the log-normal assumption, i.e. the particles reduce in size at the centre of the jet but increase at the edge. However the particle size predicted was slightly greater than that found using the log-normal distribution close to the nozzle. It may be the case that the log-normal assumption is not valid close to the jet where locally particles will be created at the same critical volume, according to classical theory. Further downstream there is some evidence that the log-normal distribution may be more appropriate. Further calculations using a full discretised size distribution could provide a further insight into what distributions, if any, would be more suitable.

Chapter 6

Conclusions

This thesis describes research undertaken into the effects of turbulence on chemical reactions and aerosol processes in local or urban scale atmospheric flows. This has been carried using an Eulerian formulation of the transported PDF equation, namely the Stochastic Fields (SF) or Field Monte Carlo method. The SF method has been derived from the modelled PDF transport equation in an Ito formulation by Valiño [49] and in a Stratonovich formulation by Sabel'nikov [50]. The two formulations are equivalent provided that the stochastic integrals contained in each are evaluated according to the correct calculus. The Stratonovich integral must be performed using an integrand evaluated at the midpoint of the step, meaning that iterative techniques such as a Runge-Kutta algorithm are appropriate. For Ito integrals the integrand must be independent of the random step, meaning that iterative schemes are not appropriate.

In Chapter 2 the SF method and its implementation in both forms was discussed and the results were using each were indeed shown to be equivalent when applied to a one dimensional numerical test case. The implementation of the Ito random step using a simple explicit Euler-Maruyama [55] step with a limit to prevent unbounded scalars or biasing the step away from the limit was found to be stable, in combination with an implicit scheme for the deterministic 'diffusion' term, and to give results

in good agreement with those obtained using a third order Runge-Kutta scheme for which no such limiting needed to be applied. Both methods gave the correct mean behaviour for the diffusion of an inert scalar for which an analytical solution could be used. As expected use of a smaller turbulent timescale leads to more rapid micromixing and hence lower variance of the scalars, this in turn leads to higher statistical accuracy when a smaller timescale is used, according to Eq. (2.19).

As much of the work in this thesis concerned systems with widely differing timescales, i.e. stiff systems [73], special solvers were required to integrate the chemistry or aerosol nucleation and growth terms. The solvers used were CHEMEQ2 which uses a predictor-corrector algorithm and also the VODPK backward multi-step solver, which is slower but more accurate. The VODPK solver was also used to integrate all deterministic terms for some calculations. Both these solvers are costly in terms of computational time and a large proportion of the total CPU time. This will be the case for either the Ito or Stratonovich interpretations and hence neither method will have a significant speed advantage over the other. A disadvantage of the SF method in terms of speed is that it appears that it is not possible to use an axisymmetric formulation, as it is unclear at present what boundary condition should be used on the axis. This is due to turbulent flows being axisymmetric in the mean but not if an instantaneous 'snapshot' is taken.

The Stochastic Fields method and the implementation used in this work were validated against experimental results in Chapter 3. The experimental results were for the one-way reaction of a plume of NO with background O_3 and were taken from Brown and Bilger's work [5]. It was found that the Ito code used here was more robust than the Stratonovich code. The latter required smoothed inlet profiles in order to give smooth accurate results. These smoothed initial profiles meant that steep initial gradients leading to scalar variance were not properly captured in the solution. Because of this the decision was made to carry out subsequent work using the Ito code.

Results for the mean and variance of an inert scalar in both the radial and ax-

ial direction were in excellent agreement with experimental results, thus validating the scheme used and also the values of turbulent diffusivity and timescale employed in the solution. The mean concentration of a reactive scalar, NO_2, was found to be within 5-10% of experimental measurements when using the Stochastic Fields method. When a plain advection-diffusion-reaction code, that does not take segregation into account, was used it overpredicted the NO_2 level by 30%. This agrees with values of segregation coefficient obtained both experimentally and here numerically that take values between -0.8 and -0.3, which indicates that reactant co-variance should retard the reaction rate. Predicted RMS values for NO_2 were found to be around 20% lower than measured values. This suggests that a different micromixing timescale may be needed for inert and reactive scalars [45].

6.1 Practical Reacting Flow Simulations

Simulations of a jet engine exhaust plume and a polluted street canyon were carried out using the SF method. To do this the SF method was coupled with a commercial CFD package, namely FLUENT. This allowed the use of FLUENT's grid generating and post-processing tools. It also gave the advantage that a separate calculation of the flow field was not necessary as the CFD was also carried out using the same grid. A disadvantage of this coupling is that the user has less control over the exact implementation of the transport terms in the SF equation, although for the applications here this was not found to be a problem. Other disadvantages are that, in the version of the CFD package used, there is a limit to the total number of scalars (number in mechanism multiplied by number of fields) and currently the turbulent diffusivity must be assumed to be the same in all three directions.

The conditions chosen for the jet exhaust were chosen to broadly approximate those that might be found in a 7kN rated turbofan at idle conditions on the ground. In agreement with earlier work [72] it was found that much of the chemistry took place in the jet potential core before the turbulent shear-layer. As such much fast

chemistry here is not affected by segregation because there is no scalar variance to cause this segregation. Outside of the potential core it was found that some species concentrations were affected by segregation. These were the radical species OH, HO_2, O, H, SO_3 and HSO_3, which were found to decay less quickly when segregation was taken into account. Other reactions, notably that of NO with background O_3, were found to be unaffected. Further investigation of the Damköhler number, as being characteristic of the speed of the chemical reaction compared to the speed of micromixing, revealed that it was the species with the highest Da that were affected by segregation, only when Da was greater than ~ 5 was an effect seen.

The ability of a PDF method to give information on more than just mean predicted concentrations allows further conclusions to be drawn. For instance it was found that in the plume the RMS fluctuations of sulphuric acid vapour, H_2SO_4, were around 10% of the mean. This could have significant consequences for the nucleation of binary water-sulphuric acid aerosols in the exhaust plume, as the nucleation rate is very sensitive to changes in H_2O and H_2SO_4 vapour concentration [88, 108].

For the street canyon a region high scalar variance was observed in the mixing region at the top of the canyon. The RMS in this region was found to be of the order of the mean quantities at the same position. Further investigation of the ensemble of fields at the top of the canyon revealed that there was a low kurtosis and that the PDF took a relatively flat shape rather than having a pronounced peak at the mean value. This shows that when taking an instantaneous sample of air in this region there is relatively high probability of finding a sample of air that is closer to the 'in canyon' or 'out of canyon' composition than the mean concentrations would suggest. This finding is supported by calculations of the mean photostationary state defect, δ_{ph}, which is measure of the local departure from chemical equilibrium. If the mean of δ_{ph} in each field is calculated rather than calculating δ_{ph} using mean concentrations, then the value found in the mixing layer is lower; indicating a composition closer to equilibrium as would be found outside the mixing region.

The results for the street canyon using the CBM-IV chemical mechanism [71] confirm those found for the jet exhaust using Kärcher's mechanism with regard to the correlation of Damköhler number with segregation effects. For the canyon it was again seen that only those species with a Da greater than ~ 5 are significantly affected by segregation. The seven species affected for this case are NO_3, OH, HO_2, C_2O_3, XO_2, XO_2N and PHO. Hence it appears that it may be possible, when Da is defined as in Section 4.2.3.3, to use $Da \cong 5$ as a cut-off value above which segregation must be taken into account when attempting to accurately predict mean concentrations of species.

6.2 Aerosol Nucleation and Growth Simulations

The Stochastic Fields method was extended to aerosol nucleation and growth in a turbulent jet. The experimental arrangement simulated was that of Lesniewski and Friedlander [9, 99], which uses Dibutyl Phthalate (DBP) vapour in a heated jet. DBP is a liquid at room temperature and hence nucleates aerosol droplets as the jet mixes out. Following previous work [97, 108] the aerosol size distribution was assumed to be of a log-normal shape and stochastic pde's were solved for the first three moments of the size distribution. The terms due to nucleation, particle growth and coagulation are all calculated by assuming them to be functions of local vapour concentration, local temperature and local size distribution. These assumptions seem to be fairly safe with regard to nucleation rate, but it is less clear whether they are valid for growth and coagulation. Assuming that there will be a particular distribution of particles at a point will not be physically realistic if only a small particle density is present. However these assumptions are implicit in the equations used to model the aerosol processes and will be present whether they are used in a PDF solution or one assuming mean quantities only. As the equations give local source terms they can be included in the PDF equation as source terms in the usual way.

Using the SF method it was found that proper inclusion of the effect of turbulence on the nucleation rate leads to a radial profile of nucleation rate in the shear-layer that has lower peak rate but shows nucleation over a larger area, i.e. it smears out the nucleation zone compared to using mean vapour concentration and temperature only. These results agree with Lesniewski and Friedlander's theoretical results for nucleation rate, they also agree in that nucleation rate is a function only of initial vapour concentration and temperature and radial position in the shear-layer. It was found here that changing the jet speed did not effect the nucleation rate and that total particle flux was unchanged. The particle number density predicted using the SF method was found to be reduced by around 25% compared to results using mean vapour concentration and temperature. The centre-line number densities predicted are of the same order of magnitude as those found experimentally and the trend with initial vapour concentration, where small increases lead to very large increases in number density, agrees with experiment. Further tuning of surface tension, as suggested by [99], may lead to more accurate results but due to the very large range seen naturally in the experimental results it was not thought necessary to do this. Based on these results it seems that the Stochastic Fields method as used here can be a useful tool in predicting aerosol nucleation.

The low number concentrations of particles led to negligible coagulation, again in agreement with experimental results, and hence use of the full three moment system did not affect number density. The SF method showed that the effect of turbulence on the growth of particles was to decrease the average particle size at the centre of the plume but to increase it at the edge, when compared to the non-SF solution. This is due to turbulent mixing causing conditions which promote growth to be mixed from the centre of the plume to the edge. For an initial vapour concentration of 6.0×10^{15}molec cm^{-3} the mean particle volume on the centre-line, 4cm downstream of the nozzle was found to be 40% lower when the SF method was used. The volume mean diameter on the centre-line at 4cm downstream found from these mean particle volumes is 3.9μm using the plain solution and 3.3μm using the

SF solution. Experimental measurements [99] have found particle diameter to range between approximately 0.3μm and 6.0μm, with mass mean diameters in the range 1.0 to 3.0μm. This is further evidence that the method used here can give reliable predictions of turbulent flows containing aerosol processes.

As a means of testing the sensitivity of the results to the assumed size distribution shape the calculations were repeated with a different distribution. This was a uniform distribution where locally all particles were assumed to have the same volume, which was equal to the volume mean diameter. With this distribution the initial growth rate was greater than that seen with the log-normal distribution. At 1cm downstream of the jet the peak volume concentration was 10% greater with uniform particle size. This indicates that the effect of assuming there are particles with volumes either side of the mean is to slightly reduce the overall growth rate. The centre-line volume mean diameters at this point were found to be 3.1μm with the SF method and 4.1μm with the plain method. These are both within the size range found in the experimental work of Lesniewski [99] and are close to the values obtained using the full three moment method. The uniform distribution gave the same trend in mean particle volume with radial position as the log-normal. It was also seen that the effect of turbulence, as revealed by the SF method, was the same for both distributions with particle size reduced at the centre of the jet but increased at the edge. This suggests that it is the effect of mixing on the vapour concentration and temperature that leads to the changed growth rate as the treatment of these that will remain the same when either distribution is used. This indicates that for this type of flow the error entailed in neglecting the effect of turbulence on growth rates is greater than that caused by the choice of size distribution.

6.3 Suggestions For Future Work

The application of turbulent reacting flow models for gas phase reactions or aerosol processes in atmospheric flows is a field of study in which an almost limitless amount

of future work could be undertaken. Only two practical flow situations, a jet exhaust plume and a street canyon, have been investigated in this work and there are clearly many more that could have been studied. However this final section will consider only immediately applicable extensions to the work presented in this thesis.

Throughout this work the only micromixing closure used has been the Interaction by Exchange with the Mean (IEM) model. This model has the advantage of simplicity and does not require conditional means which would, in turn, require a higher number of fields for statistical accuracy. To date, IEM has been used in all SF simulations and it was used in Chapter 3 of this work to correctly predict the RMS of an inert scalar. However, it was found to underpredict the RMS for a reactive scalar, which agrees with earlier research [45] that suggests that different mixing timescales are needed for inert and reactive scalars. This could be a highly useful area of future study, as could the implementation of alternatives to the IEM such as the Interaction by Exchange with the Conditional Mean.

The subject of micromixing closures for particles needs to be addressed. In this work it has been assumed that the destruction of fluctuations in particle number density by Brownian diffusion is negligible and therefore that an infinite micromixing timescale can be used. Further research needs to be conducted to establish whether this assumption is correct and if not what the correct mixing timescale to use actually is.

All the work on aerosols contained in this thesis have been performed using assumed shapes for particle size distribution. It was seen that the choice of shape can have an affect on growth, particularly in the early part of the flow. It may be that close to the jet nozzle, where particles are formed at the critical volume, it may be better to assume uniform size rather than a log-normal distribution. Also with the low number concentrations encountered in some of the results presented here the idea that particle sizes will fit a fixed shape of size distribution is unlikely to hold true. To investigate further the suitability of using size distributions the Stochastic Fields method could be employed using discretised size bins as the set

of scalars used. This would follow recent work by Rigopoulos [30] who has derived the PDF transport equation for the discretised size distribution. By doing this the source and sink terms due to growth and coagulation at a given particle size are considered directly.

The aerosol nucleation and growth considered in this work was for the nucleation of a single species. This work could be extended to binary nucleation such as that between water and sulphuric acid. This is a function of two vapour concentrations and this may lead to further effects due to turbulent fluctuations. This is of particular interest in the subject of contrails in exhaust plumes [83, 88, 108]. This could be combined with the gas phase reactions studied in Chapter 4 to understand the impact of turbulence on a combined system of gas phase and state-change reactions.

Appendix A

Summary of Numerical Methods

The following table summarises the combination Stochastic Fields formulation and solver used throughout this thesis.

Table A.1: Summary of numerical methods used for problems in this thesis.

Problem	SF Formulation	Solver	Chapter
1D diffusion	Ito	VODPK	2
1D diffusion	Stratonovich	Runge-Kutta	2
Grid plume	Ito	VODPK	3
Grid plume	Stratonovich	Runge-Kutta/VODPK	3
Jet exhaust	Ito	FLUENT/CHEMEQ2	4
Street Canyon	Ito	FLUENT/VODPK	4
Aerosol	Ito	VODPK	5

Bibliography

[1] A. Garmory, R. E. Britter, and E. Mastorakos. Simulation of the evolution of aircraft exhaust plumes including detailed chemistry and segregation. *To appear in Journal of Geophysical Research - Atmospheres*, 2007.

[2] A. Garmory, E. S. Richardson, and E. Mastorakos. Micromixing effects in a reacting flow by the Stochastic Fields method. *Atmospheric Environment*, 40:1078–1091, 2006.

[3] A. Garmory, I. S. Kim, R. E. Britter, and E. Mastorakos. Simulations of the dispersion of reactive pollutants in a street canyon, considering different chemical mechanisms and micromixing. In R. S. Sokhi and M. Neophytou, editors, *Urban Air Quality VI*. University of Hertfordshire, 2007.

[4] A. Garmory, E. S. Richardson, and E. Mastorakos. Micromixing effects in air pollution modelling. In C. A. Brebbia and F. Patania, editors, *Air Pollution XIII*, Southampton, 2005. WIT Press.

[5] R. J. Brown and R. W. Bilger. Experiments on a reacting plume - 1. conventional concentration statistics. *Atmospheric Environment*, 32:611–628, 1998.

[6] R. J. Brown and R. W. Bilger. Experiments on a reacting plume - 2. conditional concentration statistics. *Atmospheric Environment*, 32:629–646, 1998.

[7] C. D. Richards and W. M. Pitts. Global density effects on the self-preservation

behaviour of turbulent free jets. *Journal of Fluid Mechanics*, 254:417–435, 1993.

[8] S. R. Tieszen, D. W. Stamps, and T. J. O'Hern. A heuristic model of turbulent mixing applied to blowout of turbulent jet diffusion flames. *Combustion and Flame*, 106:442–466, 1996.

[9] T. K. Lesniewski. *Particle Nucleation and Growth in Turbulent Jets*. PhD Thesis, University of California, Los Angeles, 1997.

[10] Fluent Inc. *Fluent V6*.

[11] R. Britter and S. Hanna. Flow and dispersion in urban areas. *Annual Review of Fluid Mechanics*, 35:469–496, 2003.

[12] G. R. Hilst. Segregation and chemical reaction rates in air quality models. *Atmospheric Environment*, 32:3891–3895, 2000.

[13] J. H. Seinfeld and S. N. Pandis. *Atmospheric chemistry and physics*. John Wiley, New York, 1998.

[14] J. Liang and M. Z. Jacobson. Effects of subgrid segregation on ozone production efficiency in a chemical model. *Atmospheric Environment*, 34:2975–2982, 2000.

[15] M. Z. Jacobson. *Fundamentals of atmospheric modeling*. Cambridge University Press, Cambridge, 1999.

[16] J. Villa-Guerau de Arellano, A. Dosio, J.-F. Vinuesa, A.A.M. Holtslag, and S. Galmarini. The dispersion of chemically reactive species in the atmospheric boundary layer. *Meteorology and Atmospheric Physics*, 87:23–38, 2004.

[17] E. Mastorakos. The Conditional Moment Closure approach for atmospheric pollution problems. In C. A. Brebbia and F. Patania, editors, *Air Pollution XI*, pages 125–134, Southampton, 2003. WIT Press.

[18] W. R. Stockwell. Effects of turbulence on gas-phase atmospheric chemistry: calculation of the relationship between time scales for diffusion and chemical reaction. *Meteorology and Atmospheric Physics*, 57:159–171, 1995.

[19] M. Neophytou, D. A. Goussis, M. van Loon, and E. Mastorakos. Reduced chemical mechanisms for atmospheric pollution using Computational Singular Perturbation analysis. *Atmospheric Environment*, 38:3661–3673, 2004.

[20] J.-F. Vinuesa and J. Villa-Guerau de Arellano. Introducing effective reaction rates to account for the inefficient mixing of the convective boundary layer. *Atmospheric Environment*, 39:445–461, 2005.

[21] J. P. Meeder and F. T. M. Nieuwstadt. Large Eddy Simulation of the turbulent dispersion of a reactive plume from a point source into a neutral atmospheric boundary layer. *Atmospheric Environment*, 34:3563–3573, 2000.

[22] R. K. Srivastana, D. S. McRae, and M. T. Odman. Simulation of dispersion of a power plant plume using an adaptive grid algorithm. *Atmospheric Environment*, 35:4801–4818, 2001.

[23] S. K. Friedlander. *Smoke, Dust and Haze: Fundamentals of Aerosol Dynamics.* Oxford University Press, Oxford, second edition, 2000.

[24] C. A. Pope III. Review: Epidemiological basis for particulate air pollution health standards. *Aerosol Science and Technology*, 32:4–14, 2000.

[25] A. Seaton, W. MacNee, K. Donaldson, and D. Godden. Particulate air pollution and accute health effects. *The Lancet*, 345:176–176, 1995.

[26] K. Donaldson, X. Y. Li, and W. MacNee. Ultrafine (nanometer) particle mediated lung injury. *Journal of Aerosol Science*, 29:553–560, 1998.

[27] J. M. Samet, F. Dominici, F. C. Curriero, I. Coursac, and S. L. Zeger. Fine particulate air pollution and mortality in 20 U.S cities, 1987 - 1994. *The New England Journal of Medicine*, 343:1742–1749, 2000.

[28] J. P. Shi, A. A. Khan, and R. M. Harrison. Measurements of ultrafine particle concentration and size distribution in the urban atmosphere. *The Science of the Total Environment*, 235:51–64, 1999.

[29] H. Horvath. Atmospheric aerosols, atmospheric optics and visibility. *Journal of Aerosol Science*, 25:S23–S24, 1994.

[30] S. Rigopoulos. PDF method for population balance in turbulent reactive flow. *To appear in Chemical Engineering Science*, doi:10.1016/j.ces.2007.05.039, 2007.

[31] J. Baldyga and J. R. Bourne. *Turbulent mixing and chemical reactions*. John Wiley, Chichester, 1999.

[32] R. O. Fox. *Computational models for turbulent reacting flows*. Cambridge University Press, Cambridge, 2003.

[33] R. I. Sykes, S. F. Parker, D. S. Henn, and W. S. Lewellen. Turbulent mixing with chemical reaction in the planetary boundary layer. *Journal of Applied Meteorology*, 33:825–834, 1994.

[34] A. Y. Klimenko and R. W. Bilger. Conditional Moment Closure for turbulent combustion. *Progress in Energy and Combustion Science*, 25:595–687, 1999.

[35] R. W. Bilger. Turbulent flows with non-premixed reactants. In P. A. Libby and F. A. Williams, editors, *Turbulent Reacting Flows*, pages 65–113. Springer, Berlin, 1980.

[36] S. B. Pope. PDF methods for turbulent reacting flows. *Progress in Energy and Combustion Science*, 11:119–192, 1985.

[37] M. Gonzalez. Analysis of the effect of microscale turbulence on atmospheric chemical reactions by means of the PDF approach. *Atmospheric Environment*, 31:575–586, 1997.

[38] M. Cassiani, P. Franzese, and U. Giostra. A PDF micromixing model of dispersion for atmospheric flow. part i: development of the model, application to homogeneous turbulence and to neutral boundary layer. *Atmospheric Environment*, 39:1457–1469, 2005.

[39] H. Möbus, P. Gerlinger, and D. Brüggeman. Comparison of eulerian and lagrangian monte carlo PDF methods for turbulent diffusion flames. *Combustion and Flame*, 124:519–534, 2001.

[40] J. Xu and S. B. Pope. Assessment of numerical accuracy of PDF/Monte Carlo methods for turbulent reacting flows. *Journal of Computational Physics*, 152:192–230, 1999.

[41] J. H. Baerentsen and R. Berkowicz. Monte Carlo simulation of plume dispersion in the convective boundary layer. *Atmospheric Environment*, 18(4):701–712, 1984.

[42] A. K. Luhar and R. E. Britter. Random walk model for dispersion. *Atmospheric Environment*, 23(9):1911–1924, 1989.

[43] D. L. Ermak and J. S. Nasstrom. A lagrangian stochastic diffusion method for inhomogeneous turbulence. *Atmospheric Environment*, 34(7):1059–1068, 2000.

[44] C. V. Srinivas and R. Venkatesan. A simulation study of dispersion of air borne radionuclides from a nuclear power plant under a hypothetical accidental scenario at a tropical coastal site. *Atmospheric Environment*, 39(8):1497–1511, 2005.

[45] C.M. Cha and P. Trouillet. A model for the mixing time scale of a turbulent reacting scalar. *Physics of Fluids*, 15:1375–1380, 2003.

[46] R. O. Fox and P. K. Yeung. Improved Lagrangian mixing models for passive scalars in isotropic turbulence. *Physics of Fluids*, 15:961–985, 2003.

[47] T. L. Chan, G. Dong, C. S. Cheung, C. W. Leung, C. P. Wong, and W. T. Wung. A Monte Carlo simulation of nitrogen oxides dispersion from a vehicular exhaust plume and its sensitivity studies. *Atmospheric Environment*, 35:6117–6127, 2001.

[48] M.R.H. Sheikhi, T. G. Drozda, P. Givi, and S.B. Pope. Velocity-scalar filtered density function for large eddy simulation of turbulent flows. *Physics of Fluids*, 15:2321–2337, 2003.

[49] L. Valiño. A field Monte Carlo formulation for calculating the probability density function of a single scalar in a turbulent flow. *Flow Turbulence and Combustion*, 60:157–172, 1998.

[50] V. Sabel'nikov and O. Soulard. Rapidly decorrelating velocity-field model as a tool for solving one-point Fokker-Planck equations for probability density functions of turbulent reactive scalars. *Physical Review E*, 72(1):Article No. 016301, 2005.

[51] R. Mustata, L. Valiño, C. Jiménez, W. P. Jones, and S. Bondi. A Probability Density Function Eulerian Monte Carlo field method for Large-eddy simulations. Application to a turbulent piloted methane/air diffusion flame (Sandia D). *Combustion and Flame*, 145:88–104, 2006.

[52] V. Sabel'nikov and O. Soulard. Simulation of a turbulent premixed methane flame with an Eulerian Monte Carlo solver. In V. Dias and J. Vandooren, editors, *Proceedings of the European Combustion Meeting*, page E100, Louvain, 2005. Belgian Section of The Combustion Institute.

[53] D. B. Spalding. Multi-fluid models of turbulent combustion. In *CTAC95 Conference*, Melbourne, Australia, 1995.

[54] Y. Liu and J. Ducoste. Numerical simulation of chloramines formation in turbulent flow using a multi-fluid micromixing model. *Environmental Modelling and Software*, 21:1198–1213, 2006.

[55] C. W. Gardiner. *Handbook of stochastic methods*. Springer, Berlin, third edition, 2004.

[56] W. P. Jones. Personal communication. *Imperial College London*, 2007.

[57] R. L. Stratonovich. *Introduction to the Theory of Random Noise*. Gordon and Breach, New York, London, 1963.

[58] V. Sabel'nikov and O. Soulard. White in time scalar advection model as a tool for solving joint composition PDF equations. *Flow Turbulence and Combustion*, 77:333–357, 2006.

[59] S. B. Pope. Particle method for turbulent flows: integration of stochastic model equations. *Journal of Computational Physics*, 117:332–349, 1995.

[60] S. B. Pope. *Turbulent Flows*. Cambridge University Press, Cambridge, 2000.

[61] S. B. Pope. Lagrangian PDF methods for turbulent flows. *Annual Review of Fluid Mechanics*, 26:23–63, 1994.

[62] J. Y. Chen, R. W. Dibble, and R. W. Bilger. PDF modeling of turbulent nonpremixed $CO/H_2/N_2$ jet flames with reduced mechanisms. *Proceedings of the Combustion Institute*, 23:775–780, 1990.

[63] H. A. Wouters, P. A. Nooren, T. W. J. Peeters, and D. Roekaerts. Effects of micro-mixing in gas-phase turbulent jets. *International Journal of Heat and Fluid Flow*, 19:201–207, 1998.

[64] W. P. Jones and M. Kakhi. PDF modeling of finite-rate chemistry effects in turbulent nonpremixed jet flames. *Combustion and Flame*, 115:210–229, 1998.

[65] G. D. Byrne. Pragmatic experiments with Krylov methods in the stiff ODE setting. In J. Cash and I. Gladwell, editors, *Computational Ordinary Differential Equations*. Oxford University Press, 1992.

[66] I. S. Kim and E. Mastorakos. Simulations of turbulent lifted jet flames with two-dimensional Conditional Moment Closure. *Proceedings of the Combustion Institute*, 30:911–918, 2005.

[67] P. E. Kloeden and E. Platen. *Numerical Solution of Stochastic Differential Equations*. Springer, Berlin, corrected third printing edition, 1999.

[68] C. W. Shu and S. Osher. Efficient implementation of essentially non-oscillatory shock-capturing schemes. *Journal of Computational Physics*, 77:439–471, 1988.

[69] H. Tennekes and J. L. Lumley. *A first course in turbulence*. MIT Press, Massachusetts, 1972.

[70] R. G. Derwent, M. E. Jenkin, S. M. Saunders, and M. J. Pilling. Photochemical ozone creation potentials for organic compounds in Northwest Europe calculated with a Master Chemical Mechanism. *Atmospheric Environment*, 32(14/15):2429–2441, 1998.

[71] M. Gery, G. Witten, J. Killus, and M. Dodge. A photochemical kinetics mechanism for urban and regional scale computer modelling. *Journal of Geophysical Research*, 94(D10):12925–12956, 1989.

[72] B. Kärcher, M. M. Hirschberg, and P. Fabian. Small-scale chemical evolution of aircraft exhaust species at cruising altitudes. *Journal of Geophysical Research*, 101(D10):15,169–15,190, 1996.

[73] E. S. Oran and J. P. Boris. *Numerical Simulation of Reactive Flow*. Cambridge University Press, Cambridge, second edition, 2001.

[74] D. R. Mott and E. S. Oran. CHEMEQ2: A solver for stiff ordinary equations of chemical kinetics. *Naval Research Laboratory*, Technical Report 8553, 2001.

[75] R. J. Brown and R. W. Bilger. An experimental study of a reactive plume in grid turbulence. *Journal of Fluid Mechanics*, 312:373–407, 1996.

[76] C. Dopazo. Relaxation of initial probability density functions in the turbulent convection of scalar fields. *Physics of Fluids*, 22:20–30, 1979.

[77] O. Soulard, V. Sabel'nikov, and M. Gorokhovski. Stochastic scalar mixing models accounting for turbulent frequency multiscale fluctuations. *International Journal of Heat and Fluid Flow*, 25:875–883, 2004.

[78] Department For Transport. *The Future of Air Transport*. HM Stationary Office, 2003.

[79] Greener By Design. *Mitigating the Environmental Impact of Aviation: Opportunities and Priorities*. Royal Aeronautical Society, 2005.

[80] S. C. Herndon, J. H. Shorter, M. S. Zahniser, Jr. D. D. Nelson, J. Jayne, R. C. Brown, R. C. Miake-Lye, I. Waitz, P. Silva, T. Lanni, K. Demerjian, and C. E. Kolb. NO and NO_2 emission ratios measured from in-use commercial aircraft during taxi and takeoff. *Environmental Science and Technology*, 38:6078–6084, 2004.

[81] D. C. Lewellen and W. S. Lewellen. Effect of aircraft wake dynamics on measured and simulated NO_x and HO_x wake chemistry. *Journal of Geophysical Research*, 106(D21):27,661–27,672, 2001.

[82] M. E. Jenkin. Analysis of sources and partitioning of oxidant in the UK. Part 1: the NO_X - dependence of annual mean concentrations of nitrogen dioxide and ozone. *Atmospheric Environment*, 38:5117–5129, 2004.

[83] R. C. Brown, R. C. Miake-Lye, M. R. Anderson, C. E. Kolb, and T. J. Resch. Aerosol dynamics in near-field aircraft plumes. *Journal of Geophysical Research*, 101(D17):22,939–22,953, 1996.

[84] Z. Wang and J. Y. Chen. Modelling of microscale turbulence and chemistry interaction in near-field aircraft plumes. *Journal of Geophysical Research*, 102(D11):12,871–12,883, 1997.

[85] S. Menon and J. Wu. Effects of micro- and macroscale turbulent mixing on the chemical processes in engine exhaust plumes. *Journal of Applied Meteorology*, 37:639–654, 1998.

[86] C. Treviño and F. Méndez. Simplified model for the prediction of ozone generation in polluted urban areas with continuous precursor species emissions. *Atmospheric Environment*, 33:1103–1110, 1999.

[87] ICAO. *Engine Exhaust Emissions Data Bank. V2525-D5. Unique ID 1IA002.* 2004.

[88] J. Zhao and R. P. Turco. Nucleation simulations in the wake of a jet aircraft in stratospheric flight. *Journal of Aerosol Science*, 26(5):779–795, 1995.

[89] M. W. Rotach. Profiles of turbulent statistics in and above an urban street canyon. *Atmospheric Environment*, 29:1473–1486, 1995.

[90] F. Caton, R. E. Britter, and S. Dalziel. Dispersion mechanisms in a street canyon. *Atmospheric Environment*, 37:693–702, 2003.

[91] J-J. Baik J-J. Kim. On the escape of pollutants from urban street canyons. *Atmospheric Environment*, 36:527–536, 2002.

[92] S. J. Jeong and M. J. Andrews. Application of the $k - \epsilon$ turbulence model to the high Reynolds number skimming flow field of an urban street canyon. *Atmospheric Environment*, 36:1137–1145, 2002.

[93] D. Hamlyn and R. E. Britter. A numerical study of the flow field and exchange processes within a canopy of urban-type roughness. *Atmospheric Environment*, 39:3243–3254, 2005.

[94] J. Baker, H. L. Walker, and X. Cai. A study of the dispersion and transport of reactive pollutants in and above street canyons - a Large Eddy Simulation. *Atmospheric Environment*, 38:6883–6892, 2004.

[95] J-J. Baik, Y-S. Kang, and J-J. Kim. Modelling reactive pollutant dispersion in an urban street canyon. *Atmospheric Environment*, 41:934–949, 2007.

[96] L. J. Carpenter, K. C. Clemitshaw, R. A. Burgess, S. A. Penkett, J. N. Cape, and G. G. McFadyen. Investigation and evaluation of the NO_x/O_3 photochemical steady state. *Atmospheric Environment*, 32:3353–3365, 1998.

[97] S. E. Pratsinis. Simultaneous nucleation, condensation and coagulation in aerosol reactors. *Journal of Colloid and Interface Science*, 124(2):416–427, 1988.

[98] I. J. Ford, G. D. Hayman, and R. D. Kingdon. Plume and aerosol modelling for the POLINAT project. In U. Schuman, editor, *Pollution from Aircraft Emissions in the North Atlantic Flight Corridor (POLINAT)*, pages 258–279. 1996.

[99] T. K. Lesniewski and S. K. Friedlander. Particle nucleation and growth in a free turbulent jet. *Proceedings of the Royal Society, A*, 454:2477–2504, 1998.

[100] I. Kusaka, Z. -G. Wang, and J. H. Seinfeld. Binary nucleation of sulfuric acid-water: Monte Carlo simulation. *Journal of Chemical Physics*, 108(16):6829–6848, 1998.

[101] J. H. Seinfeld. *Atmospheric Chemistry and Physics of Air Pollution*. Wiley, New York, 1986.

[102] P. G. Saffman and J. S. Turner. On the collision of drops in turbulent clouds. *Journal of Fluid Mechanics*, 1:16–30, 1956.

[103] D. L. Marchisio and R. O. Fox. Solution of population balance equations using the direct quadrature method of moments. *Journal of Aerosol Science*, 36:43–73, 2005.

[104] W. T. Scott. Poisson statistics in distributions of coalescing droplets. *Journal of the Atmospheric Sciences*, 24:221–225, 1967.

[105] M. Warshaw. Cloud droplet coalescence: statistical foundations and a one-dimensional sedimentation model. *Journal of the Atmospheric Sciences*, 24:278–286, 1967.

[106] R. P. Lindstedt and S. A. Louloudi. Joint-scalar transported PDF modeling of soot formation and oxidation. *Proceedings of the Combustion Institute*, 30:775–783, 2005.

[107] D. Ramkrishna and J. D. Borwanker. A puristic analysis of population balance - I. *Chemical Engineering Science*, 28:1423–1435, 1973.

[108] J. Wu and S. Menon. Aerosol dynamics in the near field of engine exhaust plumes. *Journal of Applied Meteorology*, 40:795–809, 2001.

[109] K. Okuyama, Y. Kousaka, D. R. Warren, R. C. Flagan, and J. H. Seinfeld. Homogeneous nucleation by continuous mixing of high-temperature vapour by mixing with a cool gas. *Aerosol Science and Technology*, 6:15–27, 1987.

[110] T. K. Lesniewski and S. K. Friedlander. The effect of turbulence on rates of particle formation by homogeneous nucleation. *Aerosol Science and Technology*, 23:174–182, 1995.